Assessment of local land cover change on the streamflow dynamics in tropical montane cloud forest region,

Alta Verapaz, Guatemala

Master Thesis

Jolijn Hiemstra

Delft University of Technology

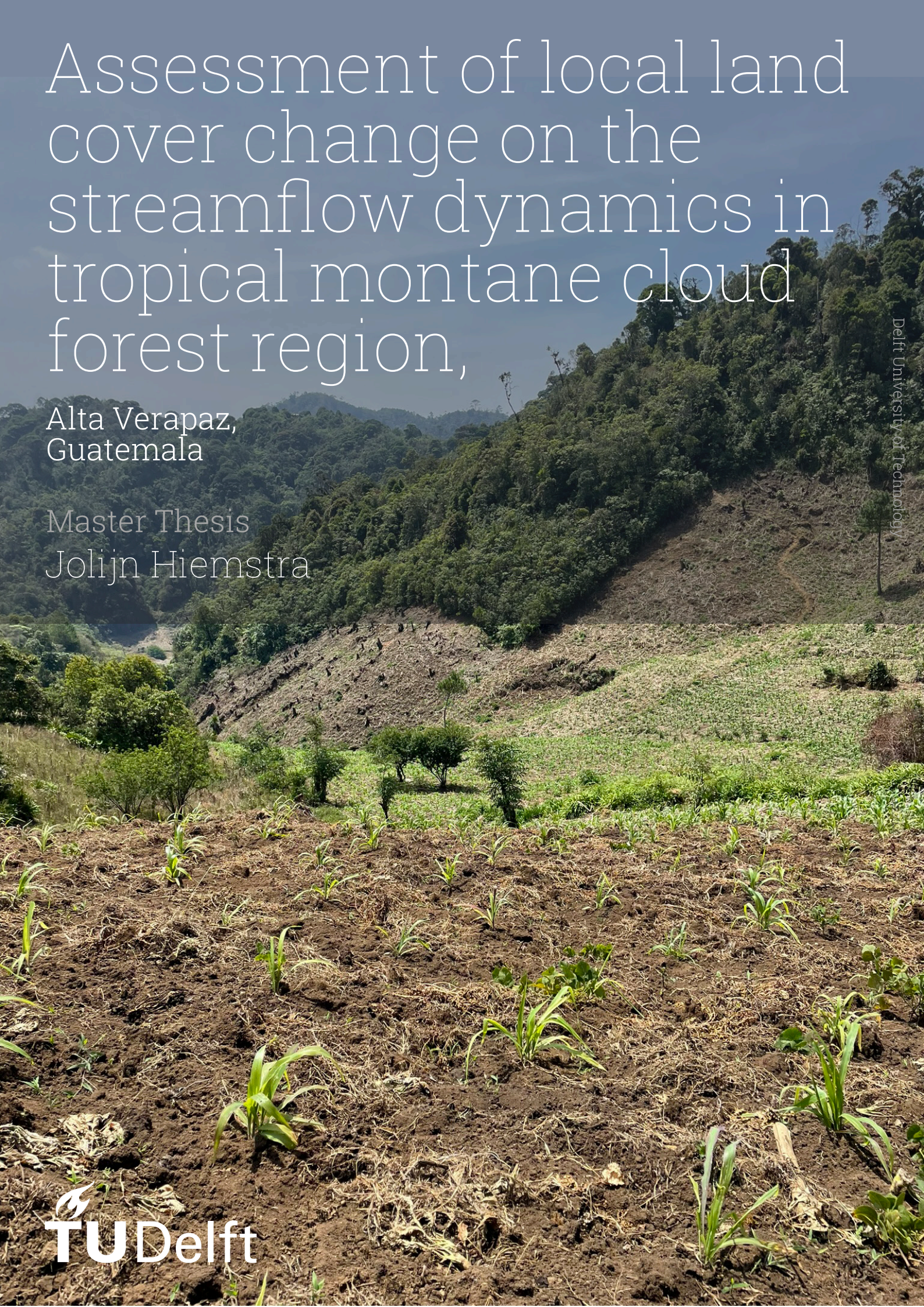

TU Delft

Assessment of local land cover change on the streamflow dynamics in tropical montane cloud forest region,

Alta Verapaz, Guatemala

by

Jolijn Hiemstra

Main supervisor:	Dr. S. Pande, TU Delft
Co-supervisor:	Dr. M. Hrachowitz, TU Delft
External supervisor:	Ir. L. Cahill, CCFC
Project Duration:	February, 2024 - October, 2024
Faculty:	Faculty of Civil Engineering and Geosciences, Delft

Cover: Land cover in Mestelá catchment

TU Delft

Preface

This research, titled "*Assessment of Local Land Cover Change on the Streamflow Dynamics in a Tropical Montane Cloud Forest Region*," was undertaken as part of the Master of Science degree in Environmental Engineering at the Technical University of Delft. It was conducted in collaboration with Community Cloud Forest Conservation (CCFC) and included a field study in the Alta Verapaz region of Guatemala.

I would like to extend my gratitude to my supervisors, Dr. Saket Pande and Dr. Markus Hrachowitz, for their guidance, constructive feedback, and support throughout this research. Special thanks to Linnaea Cahill, whose extensive knowledge of the study area and the research goals provided essential insight and direction, greatly helping shape the focus of this work.

The opportunity to conduct fieldwork in Alta Verapaz at CCFC was an invaluable experience, and I am deeply grateful to Tara and Rob Cahill for their hospitality, for showing me around the study area, and for sharing their local expertise. I also want to thank Nancy Guzman for her help, especially as a translator, without whom my interactions would have been far more challenging.

This field research would not have been possible without the financial support of the FAST Fund, Lamminga Fonds, Delft Global Initiative, and Kronendak. Their contributions made it feasible for me to conduct on-site research and gather valuable data.

Finally, I would like to express my appreciation to my family, friends, and especially my boyfriend, for their constant encouragement, support, and for engagin in discussions that provided new inspiration for this research.

Jolijn Hiemstra
Delft, October 2024

TU Delft | Global Initiative
Science for the benefit of people. All people. Worldwide.

FAST
TU Delft | University Fund

Abstract

The applicability of the FLEX-Topo and FIESTA models in simulating the impacts of land cover change on the streamflow dynamics in the tropical montane cloud forest of the Mestelá catchment, Alta Verapaz, Guatemala was investigated. Understanding these impacts is crucial for effective water resource management in regions vulnerable to deforestation, where cloud forests play a critical role in regulating hydrological processes, and in areas prone to flooding and droughts.

The FIESTA model was integrated to generate spatially distributed meteorological inputs, tailored to unique spatial characteristics of the tropical montane cloud forest region. These inputs informed the FLEX-Topo model, which was adapted to conceptualize the dominant hydrological processes in the study area for simulating streamflow in the Mestelá catchment. The model was calibrated to represent distinct land use classes within the catchment using multi-criteria calibration with different objective functions and constraints to account for parameter uncertainty. Scenario-based simulations, including deforestation, reforestation and the conversion of agricultural land to pine plantations, were conducted to quantify their effects on streamflow dynamics, water balance components and extreme hydrological events.

The integration of the FIESTA model provided spatially distributed inputs, however further evaluation is needed to assess the accuracy of this distribution. Its spatial variability enabled the inclusion of fog interception into the water balance, representing a key hydrological process in cloud forests. Calibration of the FLEX-Topo model was achieved by optimizing parameters for distinct land use classes and using dynamic land use fractions. Scenario analysis revealed that deforestation potentially increased peak flows by 18.5% ($\pm 1.4\%$), while restoring forest cover reduced extreme flows by 39.5% ($\pm 1.9\%$), highlighting the role of reforestation in flood mitigation. Replacing agriculture with pine trees on steep slopes also reduced extreme flows, while additionally addressing landslide risks.

The combined application of the FLEX-Topo and FIESTA models offers valuable insights into hydrological responses to land use changes, particularly in cloud forest regions, highlighting their potential for informing policy decisions related to land conservation and water management in tropical montane cloud forests.

Contents

List of Figures

List of Tables

1

Introduction

Cloud forests are among the rarest ecosystems in the world, covering only 0.26% of the earth's land surface in 2000 (Kapos et al., 2000). These unique ecosystems play a vital role in providing clean water sources, maintaining healthy soils and acting as carbon storage. Additionally, they provide food and shelter for a large percentage of the earth's plants and animals, with endemism rates surpassing any other forest type (Haber et al., 2000). However, cloud forests face increasing deforestation worldwide, primarily driven by land cover conversion like agricultural expansion, settlement growth and timber harvesting (Krasilnikov, 2020; Bruijnzeel and Mulligan, 2011).

Montane cloud forests, defined as forests occurring in areas of frequent or consistent wind-driven clouds, play a crucial hydrological role (Ray, 2013). Cloud water is directly intercepted by the vegetation surface as precipitation, a process called horizontal precipitation, which enhances net precipitation, leading to increasing streamflow volumes (Zadroga, 1981; Bruijnzeel, 2001). Due to reduced solar radiation and high atmospheric humidity, cloud forest vegetation uses a small amount of water (Jarvis and Mulligan, 2010). These two points and therefore the reduced evaporative losses contribute to a surplus in the watershed's water yield (Hamilton, 1995; Bruijnzeel and Mulligan, 2011). Therefore, deforestation of cloud forests would result in the loss of a crucial water supply function.

Another important function of a cloud forest is its water storage capacity, especially through epiphytes, a common plant present in cloud forests that absorbs and stores water in their tissues (Bruijnzeel, 2001). This stored water is gradually released over time (Ah-Peng et al., 2017). Also the storage of this water contributes to maintaining high humidity during dry periods. In the cloud forest, the stored water can evaporate into the air when there is no external atmospheric input, such as rainfall or fog, this is important for maintaining the unique micro-climates in cloud forests. (Wolf, 1993; Veneklaas et al., 1990).

In recent years, Guatemala has witnessed an increase in severe meteorological events, particularly impacting rural Indigenous communities. Examples of these are the tropical storms Julia and Lisa in 2022, which further intensified the devastation caused by the hurricanes Eta and Lota in 2020. These hurricanes produce an increase in heavy rainfall, which triggers extensive flooding and landslides across the nation (OMM, 2022). These events highlight how global climate change has intensified the oscillation between the wet El Niña and the dry El Niño phases, increasing the severity of both rainy seasons and droughts, which threatens agricultural productivity (OCHA, 2022).

Meanwhile, land use changes, such as deforestation, are altering the hydrological response to meteorological events, amplifying the severity of floods, droughts, landslides and water pollution (OCHA, 2023). The susceptibility of Guatemala's climate to land use change has been studied in context of the collapse of the ancient Maya civilization, it is hypothesized that droughts leading to the collapse has been a combination of natural climate conditions and human-induced effects by deforestation (Oglesby et al., 2010; Shaw, 2003), a pattern that could have devastating implications for Guatemala's future as deforestation continues. Given the country's topographic and geological conditions, population density and poverty levels, these climate disasters pose a threat to human life and livelihood. An alarming

indication of 5.3 million people, out of the total population of 17.3 million, will require humanitarian assistance in the year 2024, according to the United Nations Office for Coordination of Humanitarian Affairs, underscoring the urgent need for effective interventions (IOM, 2024; OCHA, 2023).

In the Guatemalan department of Alta Verapaz, home to the Sierra Yalijux Mountain range, the impacts of the disasters are strongly felt. The heavy rainfall during the hurricanes Eta and Lota in 2020 damaged and destroyed crops and harvest, which form a critical part of the livelihoods of many families in the area (Arroyo, 2023). Additionally, the region struggles with water shortages during the dry seasons. Community Cloud Forest Conservation (CCFC), located in the mountain range of the Sierra Yalijux, Guatemala, is one of the organisations striving to raise awareness about cloud forests and their importance for the local communities, aiming to help the native inhabitants of the region in understanding and improving their living environment (CCFC, 2020). The region is covered in small farming villages, populated by the rural Maya ethnic group, Q'eqchi. In these indigenous farming villages, there are high rates of poverty, lack of access to secondary education and antiquated agricultural practices, all contributing to deforestation (Vargas et al., 2016).

Additionally, the Q'eqchi inhabitants rely on freshwater springs as vital sources for drinking and household needs. However, residents have observed diminishing water availability. The effects of the replacing cloud forest with cornfields have been observed; increasing the severity of soil erosion (Pope et al., 2016). The only cloud forests remaining are located on the ridges and on the steep slopes. With land subdivision driven by population growth among native Q'eqchi inhabitants, deforestation persists as land is passed down through generations. Water scarcity is a known issue in the villages of Sierra Yalijux.

Although scientific studies are lacking, local indigenous knowledge suggests that reduced fog interception has led to greater irregularity in water availability from springs during the dry season (Alvarenga et al., 2016; Conservation, 2020b). These springs are essential for both local villages and the city of Cobán, the capital city of the Alta Verapaz department. Cobán, a city with 81,000 inhabitants, is heavily dependent on the water resources from the the rivers in Sierra Yalijux for both household purposes and drinking water. Given the increased intensity of meteorological events, it is essential to analyse the impacts of deforestation on the floods and droughts in the region.

The consequences of land cover change on the hydro-meteorological processes in Sierra Yalijux and the downstream streamflow dynamics need to be further researched. To evaluate the potential effects of deforestation on the streamflow in the mountain range of Sierra Yalijux, a hydrological model will be developed. It is hypothesized that conservation of cloud forests is important to maintain a good availability of water and quality of water.

2

Literature review

2.1. Research gap

Studies on the hydrological impacts of deforestation of cloud forests are still in the early stages. Despite their significance as vital ecosystems, there remains a substantial gap in understanding the impacts of loss of cloud forests, particularly in Guatemala. However, recent research efforts have been done on the influence of land cover change in tropical (cloud) forests on the streamflow using hydrological models. These models have demonstrated how factors such as topography, land cover, soil types and seasonal variations, collectively influence the spatial distribution of hydrological components within a watershed (Alvarenga et al., 2016).

Previous studies have researched the effects of deforestation and regeneration of forests on hydrological systems, through various land cover scenarios. Some of these scenarios include tropical montane cloud forests (TMCF), grazed pasture, cropland and agro-forestry systems such as coffee plantations (Alvarenga et al., 2016; Holwerda and Meesters, 2019; López-Ramírez et al., 2020; Thanapakpawin et al., 2007). It is well established that the hydrological consequences of land cover changes are significant; deforestation increases overland flow and total runoff, with a corresponding significant decrease in interception and evapo-transpiration (Alvarenga et al., 2016; Birkel et al., 2012; López-Ramírez et al., 2020). Therefore, deforestation of tropical forests results in an increase in daily high and low streamflow. Conversely, hydrological models indicate that conversion of agricultural land back to tropical forests can reverse these effects.

The research conducted by Birkel et. al. revealed that while land-use change had a minimal impact on the mean annual water yield, it significantly influenced streamflow dynamics. Specifically, alterations in land use were observed to affect frequency, timing and magnitude of discharge extremes within the watershed. Furthermore, Birkel et. al.'s study demonstrated the effective utility of hydrological modelling in assessing the impact of protection and reforestation efforts on ecosystem services (Birkel et al., 2012).

In Guatemala, it is also expected that in cloud forests, due to its low transpiration and fog interception, catchment streamflow decreases following deforestation to convert land to cropland or pasture. Not only due to the additional water capture capability of cloud forests from passing fog, also expected in cloud forests is a reduction in evaporative fluxes due to low radiation levels and high atmospheric humidity (Zadroga, 1981; Jarvis and Mulligan, 2010; Bruijnzeel, 2001).

Since grasses and crops typically have shallower roots than forest trees, the volume of water available for transpiration is usually greater in forests than in the agricultural land developed from them (Longman and Jenik, 1987). Surface soil structure is also altered by compaction, reducing infiltration of rainfall, and increasing runoff, ultimately decreasing soil moisture (Uhl et al., 1988). The general perception is that reforestation will lead to an increasing streamflow, due to tropical forests acting like sponges; groundwater recharge during the wet season and gradual release of the water during the dry season (Malmer et al., 2010). In contrast, when there is a mismanagement of the soil before reforestation,

often streamflow during the dry season seem to decline because forest trees typically use more water than the previous vegetation cover, such as grassland or crops (Bruijnzeel, 2001).

Another critical hydro-meteorological process influencing the hydrological system is precipitation. The distribution of precipitation is predominantly influenced by wind patterns. This implies that land-use decisions located upwind from catchment areas play a crucial role in determining water inputs, similar to the upstream land-use decisions affect water availability downstream (López-Ramírez et al., 2020).

Collaborations between researchers and CCFC has led to studies on the hydrological processes in the Alta Verapaz cloud forest ecosystem. In April 2023, a study identified the current regional situation by using available data and addressing the important hydrological processes in the cloud forest micro-climate (Agudelo et al., 2023). This study recommended further research on the development of regional-scale land-use scenarios, particularly deforestation scenarios, to assess the impact of land-use changes on the streamflow within the cloud forest ecosystem. In November 2023, another study highlighted the significance of cloud forest ecosystems for water security (Cilia et al., 2023). Furthermore, a conceptual FLEX-Topo model for the Mestelá catchment was developed, giving insight in the potentials and opportunities for improvement. Both of these studies were involved in the installation of permanent data collection setups, providing valuable data for both current and future research in the area. Building upon this research, this study aims to utilize the collected data to develop a hydrological model to identify the impact of different regional-scaled land-use scenarios on the streamflow in the Alta Verapaz region.

Most of hydrological modelling tools have been developed for temperate zones, research has been done on the applicability of popular models in tropical contexts (López-Ramírez et al., 2020). A study in the tropical rain forest of Brazil, used the HAND (Height Above Nearest Drainage) terrain model and DHSVM (Distributed Hydrology Soil Vegetation Model) to test the model's ability to represent processes at different spatial scales (Cuartas et al., 2012). The results from the DHSVM indicate that the model is applicable to tropical forests environments and the HAND terrain model is a useful tool for representing the spatial distributions of hydrological parameters. The study by Alvarenga et. al., also showed the DHSVM being a valid tool to compare hypothetical scenarios of land cover change and showing resulted change in streamflow (Alvarenga et al., 2016).

In the study by Birkel et. al. in the cloud forests of Costa Rica, the conceptual, semi-distributed HBVlight rainfall-runoff model was used to simulate daily streamflow developing several scenarios of forested and non-forested land use for different elevation zones and assigning different parameters to these scenarios (Birkel et al., 2012). The model showed that the HBV hydrological model is a good method to model the potential effects of land-use change on streamflow using a statistical analysis.

While the impacts of streamflow changes have been evident in recent years, there remains a lack of understanding how these processes are influenced by changes in land use in Alta Verapaz, Guatemala. Modelling scenarios could enhance our understanding of hydrological processes while also serving as a valuable tool for informing policy makers. By offering evidence-based projections on impacts of land-use scenarios, this study may help bridge the gap between scientific research and policy formulation.

To address these gaps in knowledge and build upon previous research, this study aims to investigate the potential impacts of land-use change on the streamflow dynamics in the tropical montane cloud forest of Alta Verapaz. This gap in knowledge also signifies a gap in information for policymakers, who rely on robust data and analyses to make informed decisions. By developing land-use scenarios of deforestation and regeneration of forests, this study seeks to clarify the role of hydrological processes in this vital ecosystem. Through hydrological modelling, this research aims to highlight the importance of the conservation of these tropical montane cloud forests for maintaining water resources.

2.2. Research question

The following research question has been formulated:

To what extent are the FLEX-Topo and FIESTA models applicable in simulating the influence of changes in land use, particularly local deforestation of the cloud forest within the tropical watershed of Sierra Yalijux, on streamflow dynamics, such as floods and droughts, in the Mestelá catchment?

Sub-questions:

- How can the FIESTA model be integrated to produce spatially distributed meteorological inputs for hydrological modeling in the Mestelá catchment?
- What are calibration and evaluation strategies for the FLEX-Topo hydrological model for simulation of streamflow dynamics in the Mestelá catchment?
- How can scenario-based land use simulations within the FIESTA and FLEX-Topo model framework be conducted to quantitatively assess the impacts of varying land use change scenarios (e.g. deforestation and reforestation) on streamflow dynamics?
- What methodologies can be employed to evaluate streamflow variability of different land use scenarios in the Mestelá catchment using outputs from the FLEX-Topo model?

2.3. Report structure

This report is organized as follows: Chapter 3 introduces and describes the study area, the Mestelá river catchment, focusing on the physical and environmental characteristics, climate and the surrounding community. Chapter 4 provides an overview of the data used in the study, detailing the sources and the types of data collected. Chapter 5 describes the land cover types and the hydrological features of the study area. In chapter 6, the methodologies applied in this research is outlined, including the development of spatially distributed meteorological data, the hydrological FLEX-Topo model framework, and the optimization approaches used to simulate streamflow. The methodology for conducting scenario runs is also explained. Chapter 7 presents the results of the study, including the meteorological data inputs for the FLEX-Topo model, streamflow predictions and scenario analysis. In Chapter 8 the results are interpreted and findings are discussed, considering potential study limitations. Finally, chapter 9 summarizes the key findings of the research questions and objectives.

3

Study area

This study focuses on the Mestelá river catchment, a region spanning from approximately 15°26'00.0"N 90°22'00.0"W to 15°24'00.0"N 90°15'00.0"W. The catchment is situated in the North-Central part of the Highlands of Guatemala, within the department Alta Verapaz.

This chapter will provide an overview of the Mestelá river catchment, detailing its topography, land cover, climate, and communities that inhabit the area.

3.1. Physical and Environmental characteristics

3.1.1. Topography

The Mestelá river catchment is located within the Cahabón river watershed, as illustrated in Figure 3.1. The Cahabón River flows through this watershed, with a length of 196 kilometres. The Mestelá catchment, highlighted in orange in the figure, stretches from the Sierra Yalijux mountain range to the capital city of the department Alta Verapaz, Cobán. The catchment outflow boundary is located near the water extraction point close to Cobán. The Mestelá river, a tributary of the Cahabón river, is 15 km long.

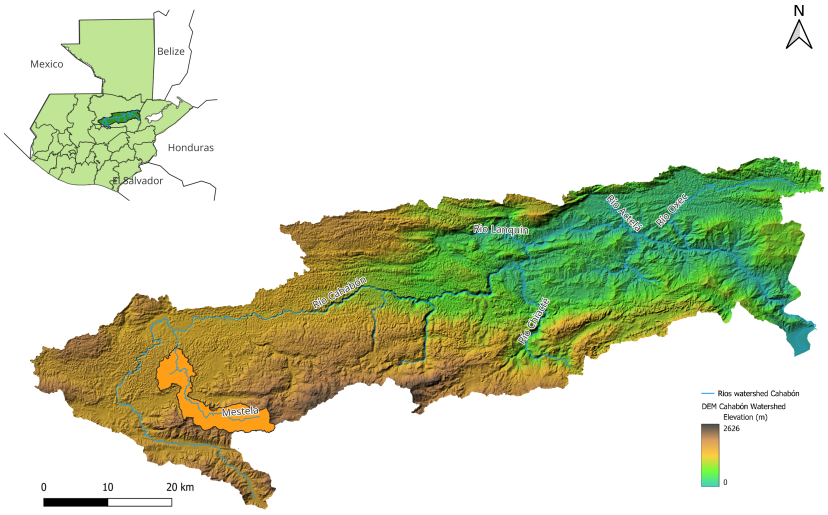

Figure 3.1: Cahabón river watershed, including the rivers, with the Mestelá river catchment highlighted in orange

The Mestelá catchment covers an area of 64.08 km^2. An elevation map is shown in Figure 3.2. This

part of the Sierra Yaluijx mountain range features several peaks with elevations ranging from 1,350 to just over 2,600 meters. The terrain is notably steep, with slopes reaching up to 60°.

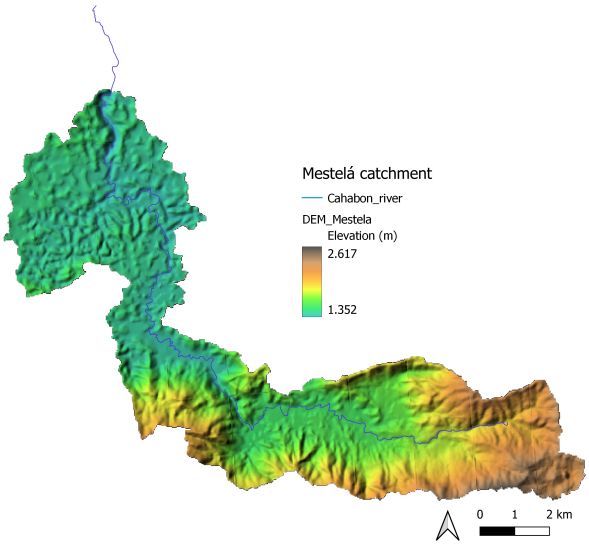

Figure 3.2: Mestelá catchment outline and elevation

Geology

The study area is located within the Sierra Yalijux mountain range, which extends from the top of the Mestelá river catchment towards the eastern part of the Cahabón river catchment. Within the catchment, Montaña Xucaneb is one of the prominent features. The outcropping rocks are from the Paleozoic and Mesozoic eras, with most formations consisting of shale and limestone (Walper, 1960). The thick limestone layer has developed a karst topography due to fractures and heavy rainfall events.

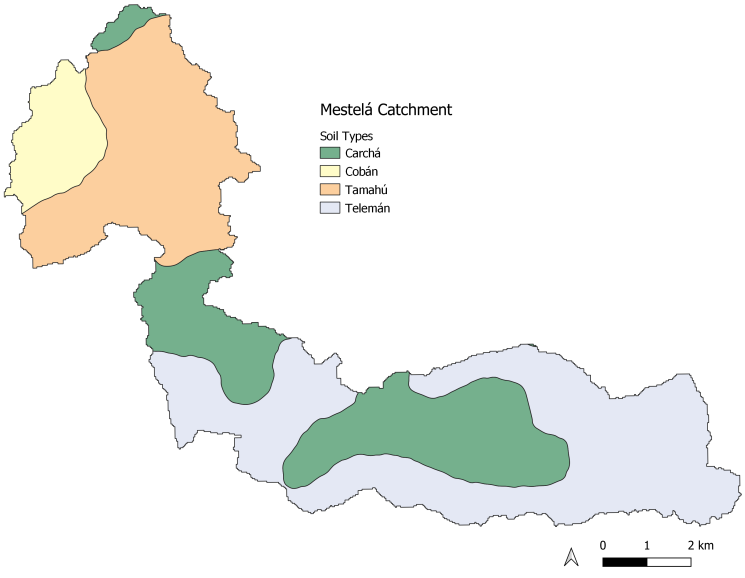

Figure 3.3: Soil types Mestelá Catchment

The Mestelá catchment is primarily composed of Mesozoic sedimentary rocks, with some areas containing volcanic rocks of varying ages. The distribution of different top soil types in the Mestelá catchment is illustrated in Figure 3.3. The soil types found in the region include limestone-dominated Cobán and

Tamahú, volcanic ash based Carchá, and a shale-rich Telemán (MAGA, 2024). The entire catchment is characterized by underlying karst formations, featuring outcrops above ground and systems of sinkholes and caves underground.

Karst formations lead to underground streams, caverns and springs, highly influencing the hydrology of the system. Most of the water transported within the catchment is through the karst aquifer. Precipitation will eventually infiltrate through the soil into the epikarst, which consists of many small fractures and conduits in the karst bedrock (Earle, 2024). The epikarst is a medium which can move and store water which is then gradually released into the subsurface groundwater system. Groundwater is primarily stored within fractures in the bedrock, caves and conduits. The water is eventually transported to springs, from which water will flow through mostly unknown paths and end up in the river. Karst rock enables fast infiltration of water from the surface to underground and often rapid flow over long distances compared to other aquifer types (Kuniansky et al., 2022).

Land cover

The study area features a variety of land uses or land covers, reflecting diverse ecological and human activities. Dense forests are prominent, especially on the high slopes of the Mestelá catchment. Cloud forests, in particular, are prominent at higher elevations, characterized by their unique moisture-rich environment.

The largest portion of the study area is dedicated to agriculture. These lands are mostly used for growing crops and some for livestock. Pine plantations are also a significant feature of the landscape, serving for mostly economic purposes. Additionally, rivers are distinctly present throughout the study area, serving as crucial sources of water for both ecological systems and human use. Built-up areas only occupy a small percentage of the land, consisting mainly of small villages. Figure 3.4 shows a landscape photo made at the top of the catchment giving an overview.

Figure 3.4: This photograph shows an overview of the Mestelá catchment taken during field study conducted in May 2024. The image highlights different land uses of the region.

3.2. Climate

In Alta Verapaz, where the Mestelá catchment is located, micro-climates emerge due to variations in altitude and topography. The higher elevated mountainous areas feature the cool highlands climate, while the city Cobán, downstream from the catchment, has an oceanic climate (Merkel, 2021a). Overall, Alta Verapaz can generally be classified as tropical, characterized by consistently high temperatures and precipitation throughout the year. According to the Holdridge classification the region is characterized by a bmh-MBT ecosystem, a very humid lower montane tropical forest (Holdridge, 1978; Hijmans, 2005). However, due to the impacts of climate change, it is projected that by 2080, the area will shift to a bh-PBT ecosystem, a humid pre-montane tropical forest, according to IARNA (Gálvez et al., 2011).

The region's monthly average temperatures range from 16 to 21°C for elevations below 1,500 meters and from 10 to 16 °C for elevations above 1,500 meters. Historical precipitation data for Alta Verapaz indicate that February is the driest month, with 101 mm of rainfall per month, while June is the wettest, with an average rainfall of 428 mm per month for (Merkel, 2021b). At around 1350 meters elevation, annual precipitation can reach up to 3052 mm/year. The higher altitudes receive more precipitation due to orographic lift, as moisture-laden winds are funneled through the Cahabón and Polochich valleys by North East winds, impacting both sides of the Sierra Yaluijx (Ray et al., 2006). Relative humidity in the region also varies seasonally, peaking at around 90% in September and dropping to approximately 80% in April.

3.2.1. Seasonality

Alta Verapaz experiences distinct dry and wet seasons, contributing to the seasonal variability of water availability. The dry season generally spans from December to April, while the wet season occurs from May to October (OCHA, 2000). The country's climate is influenced by the interactions of the atmospheric circulation within the region's mountain ranges. Rainfall seasonality and inter-annual variability are primarily driven by the the North-South movement of the Intertropical Convergence Zone (ITCZ), as well as the effects of El Niño and La Niña phenomena. These climatic variations, additional to climate change, can lead to anomalies in rainfall patterns, impacting streamflow, and consequently freshwater supplies, agriculture and food production (Magrin et al., 2014).

The well-defined rainy season follows the annual migration of the the Intertropical Convergence Zone (ITCZ), which ends the rainy season in October as it moves south. The ITCZ is a band of low pressure encircling the Earth, typically positioned near the equator. It can be identified as a tropical belt of clouds that delivers maximum precipitation (Schneider et al., 2014). Warm and moist winds near the surface feed this zone, playing a critical role in determining seasonal weather patterns and influencing regional climate.

The oscillation between warm El Niño and cold La Niña also affects Guatemala's climate. El Niño events cause droughts in the eastern part of the country, while La Niña events result in significant increases in rainfall. The ITCZ generally migrates towards the warming hemisphere, areas transitioning from La Niña to El Niño conditions (Schneider et al., 2014). Strong El Niño events in combination of warming of the Earth cause the ITCZ to shift more dramatically to the North, leading to more intense rainfall events. La Niña is associated with more hurricanes, due to less shear winds removing a brake on the hurricanes (Klotzbach, 2008).

Additional to the La Niña to El Niño phenomena affecting the climatic patterns, climate change is also causing anomalies in meteorological patterns. In the study area, observations of lower humidity, heavier rainfall events, longer droughts, higher temperatures and shifting and extension of wet and dry seasons have been made (Field Discussion, 2024).

Overall, the climate of the Sierra Yaluijx mountain range plays a significant role in shaping the hydrological processes and ecosystems, including various micro-climates that must be considered. Understanding climate patterns and dynamics is crucial for conservation efforts, land management practices and assessing the impacts of climate change on this ecologically important area.

3.2.2. Streamflow

Figure 3.5b shows a photograph of the Mestelá river. Streamflow in the Mestelá river catchment is highly influenced by the region's precipitation patterns. The area is prone to both floods and droughts,

reflecting the extremes of its climatic conditions and the changes of it. The last most extreme flooding occurred in 2020, with massive increase in streamflow of at least two months. In 2023 a significant increase in rainfall with an extended raining season has been observed, causing increase in streamflow.

Droughts are also a reoccurring challenge, with a notable shift in the rainy season there is an extended period of no rain leading to droughts. These conditions have led to parts of the river drying up in the upper catchment, as shown in Figure 3.5a.

(a) Mestelá river in upper catchment without water, photograph taken in the village Sebob

(b) Mestelá river downstream in the catchment at the location CCFC campus

Figure 3.5: Photographs of the Mestelá river taken during field study in May 2024

3.3. Community

The central highlands are bordered by small, high-elevation mountain villages, primarily inhabited by the Q'eqchi' Maya. Historically, the Q'echi' have maintained a deep connection to the land, relying on traditional practices and community-driven land management.

In recent years, Guatemala has experienced significant population growth. An even larger population increase is projected for the municipality of Cobán, with an expected 10 % rise by 2030 (INE, 2019). Large families are common in the area, leading to an increased need for food and also distribution of land parcels. These mentioned factors are the main drivers of land use change in the area, leading to forests being cut down to create cropland.

The Highland Q'eqchi' agriculture rely on their annual harvest of rainfed corn and beans, primarily focused on meeting the needs of the family rather than external markets. Traditionally, corn fields were poly cultures that included edible weeds, banana plants and various squashed and pumpkins. Today, these polycultural practices are in decline, and corn fields have largely become monocrops, which has negatively impacted both the family economy and nutrition. Historically, secondary vegetation on the agricultural lands was cleared using slash-and-burn practices (Pope et al., 2015). All agricultural activities such as clearing and burning, planting and cultivating, and harvesting and storing are all done with ritual significance. However, since 2015 the introduction of the cash crop broccoli by outside organization has led to the heavy use of pesticides (CCFC, 2020).

In addition to agriculture, the Q'eqchi depend on timber cutting for fuel and building materials (Pope

et al., 2015), leading to deforestation in the region.

3.3.1. Water collection in the catchment

The cloud forest in Alta Verapaz is a crucial water source for local communities and the agriculture. The rivers and streams originating in the cloud forest provide water for drinking, household use and water for agricultural crops. Figure 3.6 highlights the river's role in supporting community livelihoods. Most residents in the catchment collect water originating from springs near their homes, as shown in Figure 3.6. While a few villages have access to piped water systems, there is no water treatment in the catchment, and storage infrastructure remains limited.

(a) Local use of Mestelá river for washing clothes and daily activities.

(b) Community collecting water from a natural spring.

Figure 3.6: Water usage and collection within the Mestelá catchment. Photographs taken during field study in May 2024

Downstream, the city of Cobán depends on the Mestelá River, which serves as the water collection point for the cities water supply. A photograph of the water collection point is shown in Figure 3.7a. Cobán water system is a piped water system with water treatment plants and storage tanks, also shown in Figure 3.7a.

(a) Water collection point for Cobán city water supply

(b) Piped system Cobán water supply system

Figure 3.7: Cobán water collection system, photographs taken in May 2024

Increasingly dry conditions lead to challenges for many people in the region, especially those who depend on agriculture. In the upper areas of the Mestelá catchment, springs are dried up during the dry season, leading to dry rivers and lack of water for inhabitants. This impact is also felt downstream, where for example in the period of May 2024, families in Cobán were only able to access water in their homes for three hours a day due to the drought.

3.3.2. Conservation efforts

Organizations such as Community Cloud Forest Conservation (CCFC) are actively engaged in conservation and reforestation efforts in the cloud forest. Their initiatives focus on forest restoration using native trees and woody plant species, as well as fast-growing, fine wood trees.

Besides reforestation efforts, CCFC encourages families who depend on agricultural food production to establish agro-forest parcels. These parcels face multiple specific socio-economic challenges in rural Guatemala, including extreme poverty, chronic malnutrition, food insecurity in a changing climate, landscape degradation, deforestation, livelihood issues, opportunities and economic marginalization (CCFC, 2020). Agro-forestry parcels combine a variety of crops and trees, offering several benefits that address these challenges.

Agro-forestry parcels shield crops from heavy rain and strong winds, filtering rainfall and increasing soil percolation, which protects from minor droughts. The shade from tall trees also helps retain soil carbon and nutrients, creating a cooler micro-climate compared to open fields. The variety of species in these parcels promotes deeper root systems, enhancing water storage capacity and preventing soil erosion (Dixon-Sullivan, 2024). Families benefit from complementary greens, fruits, and vegetables, providing a more balanced diet and year-round food security (CCFC, 2020).

Through these comprehensive conservation strategies, CCFC is making significant strides in promoting environmental sustainability and improving the livelihoods of the Q'echqi' Maya communities.

4

Data availability and pre-processing

This chapter explains the data available and used for developing the hydrological model. In this chapter another catchment is introduced, the Upper Cahabon catchment. Both the Mestelá catchment and the Upper Cahabon catchment are studied, however for discussion of the influence of land use change scenarios on streamflow dynamics only the Mestelá catchment is discussed. Since streamflow data for the Mestelá catchment is not available and is available for the Upper Cahabon catchment, the Upper Cahabon catchment is used for calibration of the hydrological model. The catchments are located next to each other and have similar characteristics.

In this chapter, first the available meteorological data is explained. Secondly, the streamflow data is elaborated on. Lastly, the spatial data is explained, for both the Mestelá and the Upper Cahabon catchment. Figure 4.1 shows the locations of the measurement stations used in this study and the outlines of both the Mestelá river catchment and the Upper Cahabon river catchment. The streamflow data is obtained from Santa Cruz Verapaz and the metereological data is measured in Cobán. CCFC has an additional data station with meterological measurements with a shorter timeseries.

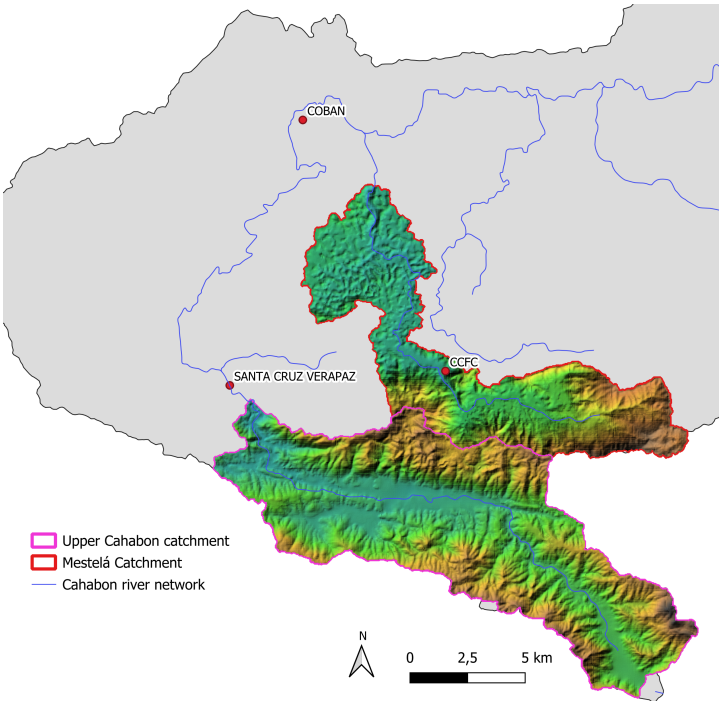

Figure 4.1: Upper Cahabon and Mestelá river catchments, including location of meteorological data measurement station in Cóban and streamflow data measured in Santa Cruz Verapaz

4.1. Meteorological data

Meteorological data is obtained from Instituto Nacional de Sismología, Vulcanología, Meteorología e Hidrologia (INSIVUMEH) (INSIVUMEH, 2024) of the station located in Coban: IOCBN2 (Lat: 15.46°and Lon: -90.41°, Elevation: 1320 m). This data is available from 25-09-1970 to 13-03-2024. This data includes includes minimum, maximum and average temperature (°C), precipitation (mm/day), relative humidity (%), solar radiation index (-), cloudiness index (-), wind direction (°), wind velocity (m/s), and atmospheric pressure (hPa). A summary of the dataset is shown in Table 4.1.

Table 4.1: Summary of meteorological data statistics for station Cobán (1997 - 2024)

Description		Units	Cobán
Precipitation	Mean	mm/year	2189
	Trend	mm/year	+0.02
Temperature	Min average	°C	13.2
	Max average	°C	25.2
	Mean	°C	18.8
	Trend	°C/year	+0.07
Wind speed	Mean	m/s	4.6
Wind direction	Most occuring	°	0
Relative humidity	Mean	%	84
Atmospheric pressure	Mean	mb	870

A visualization of the obtained data is shown in Figure 4.2. The monthly averages of precipitation, temperature with minimum and maximum range, and relative humidity with minimum and maximum ranges of the entire timeseries is plotted in Figure 4.2a. Figure 4.2b shows the seasonality of the data, by plotting the average value per month of the year.

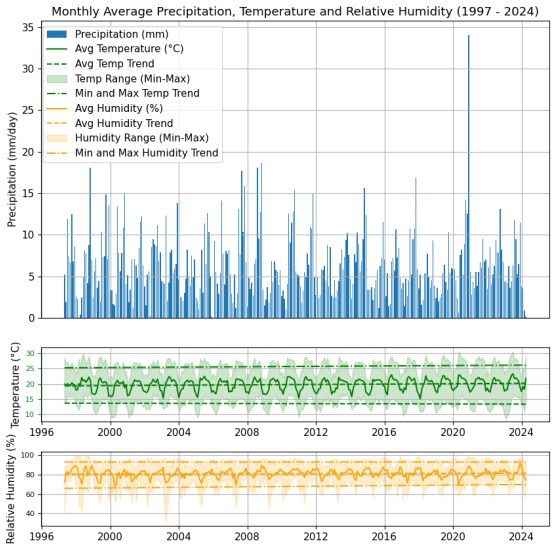

(a) Monthly average of precipitation, temperature and relative humidity per day

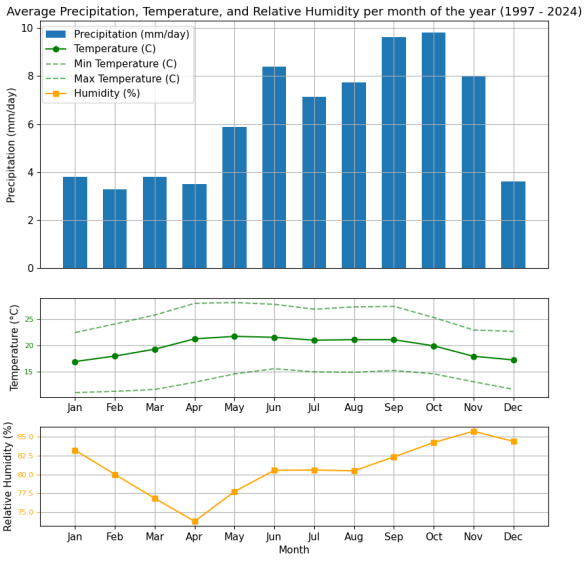

(b) Precipitation, temperature and relative humidity by showing average value per month of the year

Figure 4.2: Precipitation, temperature and relative humidity data from the meteorological measurement station located in Cobán for the years 1997-2024

4.1.1. Pre-processing Data

Missing Data

The data from the station in Cobán is missing data for some days in the year 1998 and missing data for the month May in 2018. Linear interpolation is used for the missing data in 1998. For the month May in 2018, the data from the May in the year 2019 is used, considering this year accurately represents the trend in most years. Other missing variables throughout the timeseries are also determined using linear interpolation.

Solar radiation

Solar radiation from the location Tactic (Lat: 15.306159, Long:-090.346106. Elev: 1634m) is obtained from the Global Solar Atlas $[Wh/m^2]$ (Solargis, 2024). These values are given for each hour of the day for each month of the year. Four hours of the day are included in the dataset: 0-1, 6-7, 12-14, 18-19.

Atmospheric Pressure

It is mentioned in the study of Agudelo et. al., which uses the same dataset, that the atmospheric data shows a systematic bias (Agudelo et al., 2023). Likely to be there due to human error in reporting pressure at different times of the day, since pressures between 635 and 670 mb and for other periods between 850 - 900 mb are observed. The same correction in this study has been made as in the study mentioned; the values in the first range are shifted by the difference between the averages of each set of measurements.

4.2. Streamflow

Stream flow data is available from November 2011 to February 2024 from the INSIVUMEH gauge in the Cahabón River in Santa Cruz Verapaz $[m^3/s]$ (Lat: 15.221949, Long: -90.261770), see Figure 4.3. There is an average flow of 4 m^3/s over the entire timeseries, without considering the peak flow. The highest flow occurs in the month November, with the most peak flows also occurring in this month. The lowest flows occur on average in the months March and May.

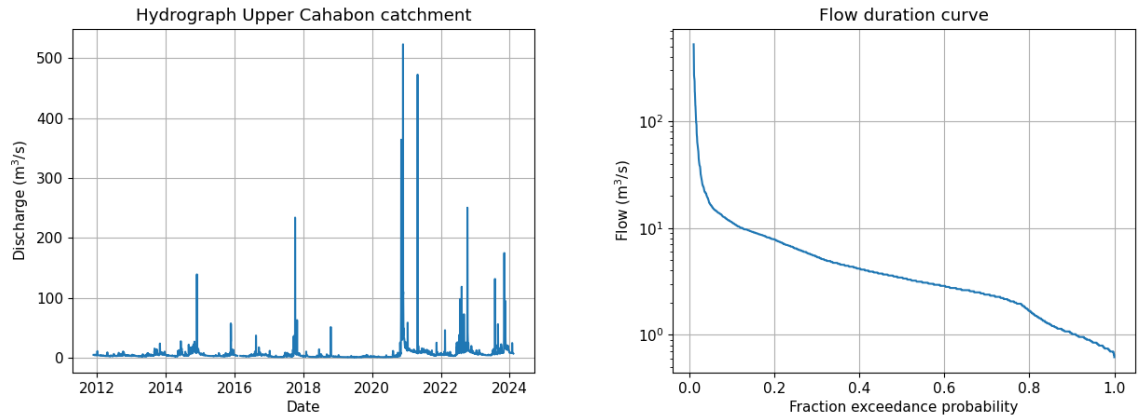

(a) Hydrograph of Upper Cahabon Catchment

(b) Flow Duration Curve

Figure 4.3: Measured discharge of the Cahabón River in Santa Cruz Verapaz

Four times during the day the water height [m] of the river is measured, with an accuracy of two decimals. Using the rating curve shown in Equation 4.1, the streamflow is calculated. The average water height of the four times of the day is taken to determine the daily average streamflow $[m^3/s]$ for each day of the year.

$$Q = 4.9545 * (H + 0.32275)^4 \tag{4.1}$$

4.3. Spatial data

From the Ministry of Agriculture, Livestock and Food (MAGA) the Digital Elevation Model (DEM) and a map of the soil types is obtained (MAGA, 2024). The DEM is of pixel size 20x20 m. Using the DEM, the slopes and aspects of both the catchments are obtained, seen in the Figure 4.4 below. Table 4.2 shows a summary of the spatial characteristics of both of the catchments.

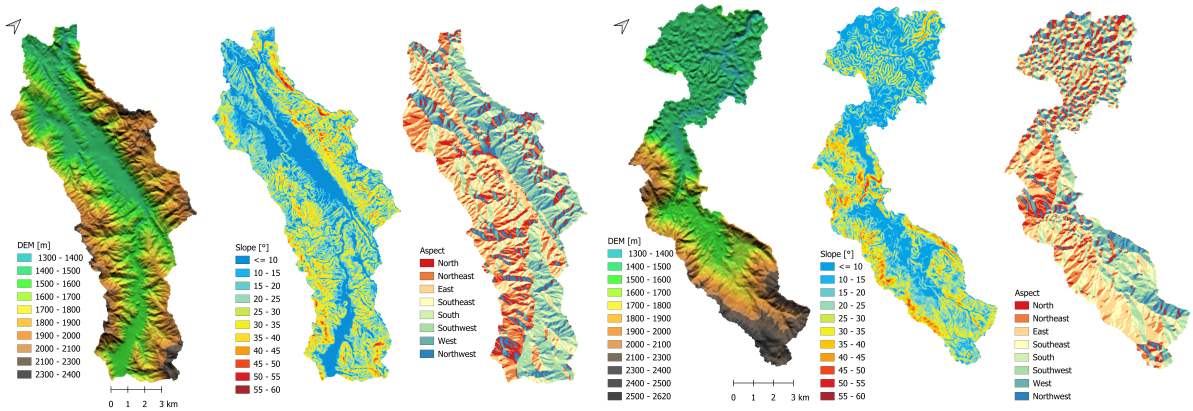

(a) Upper Cahabon catchment spatial characteristics

(b) Mestelá catchment spatial characteristics

Figure 4.4: Spatial maps of catchment characteristics: DEM, slope and aspect

Table 4.2: Summary of catchment spatial characteristics

Description		Units	Upper Cahabon	Mestelà
Area	Total	km^2	107.97	64.08
Elevation	Min	m	1393	1352
	Max	m	2345	2617
	Mean	m	1697	1683
Slope	Mean	°	20.5	19.5
River slope index		m/km	8.2	24.3
Geology	Volcanic ash	%	35.1	26.7
	Shale	%	34.6	40.8
	Limestone	%	26.5	32.5
	Valley soils	%	3.8	0
Land cover 2014	Pine plantation	%	25.8	8.6
	Agriculture	%	33	34.3
	Forest	%	41.2	57.1
Land cover 2023	Pine plantation	%	20.4	13.3
	Agriculture	%	51.7	46.9
	Forest	%	27.9	39.8

Figure 4.5 presents the land cover maps for the Upper Cahabon and Mestelá catchments. Land cover maps for the years 2014, 2019 and 2023 were created using Landsat 8 imagery. The land cover maps for the Upper Cahabon catchment are sourced from an unpublished study by Taslimi (2024). For the Mestelá catchment, land cover maps are developed using supervised classification techniques, specifically employing the Semi-Automatic Classification Plugin (SCP) in QGIS. The classification process involves developing training data through various band combinations from the remote sensing images. Spectral analysis is used to define land use classes such as forest, pine plantation and agriculture by grouping pixels with uniform values across several spectral bands (NASA, 2022).

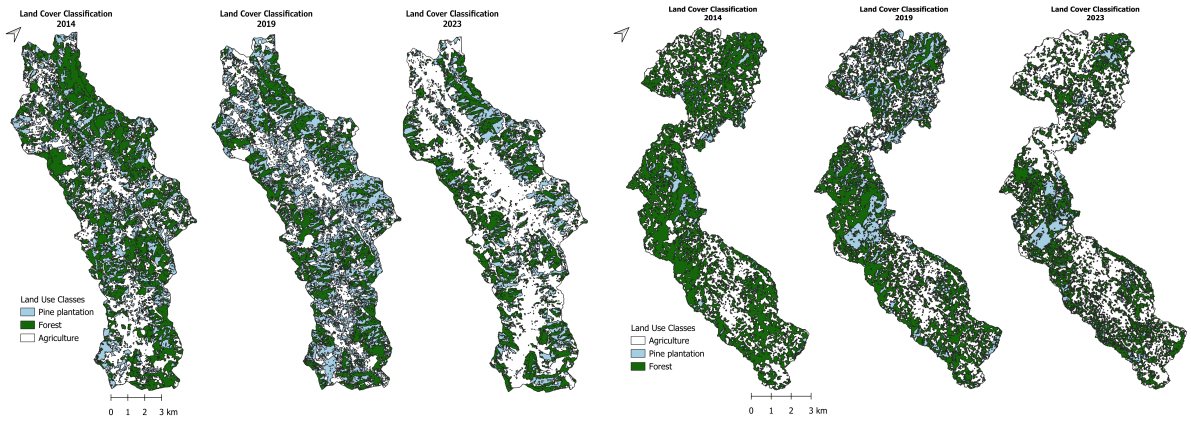

(a) Land cover classification maps of the Upper Cahabon catchment

(b) Land cover classification maps of the Mestelá catchment

Figure 4.5: Land Use classification maps of the Upper Cahabon catchment and the Mestelá catchment for the years 2014, 2019 and 2023. Showing the land cover classes Forest, Pine plantation and Agriculture.

Figure 4.6 presents the bar plots of the total land use areas of each land cover class in the Mestelá catchment and the Upper Cahabon catchment, for the three land use classification map years 2014, 2019, 2023. The figures highlight the changing land cover over the years.

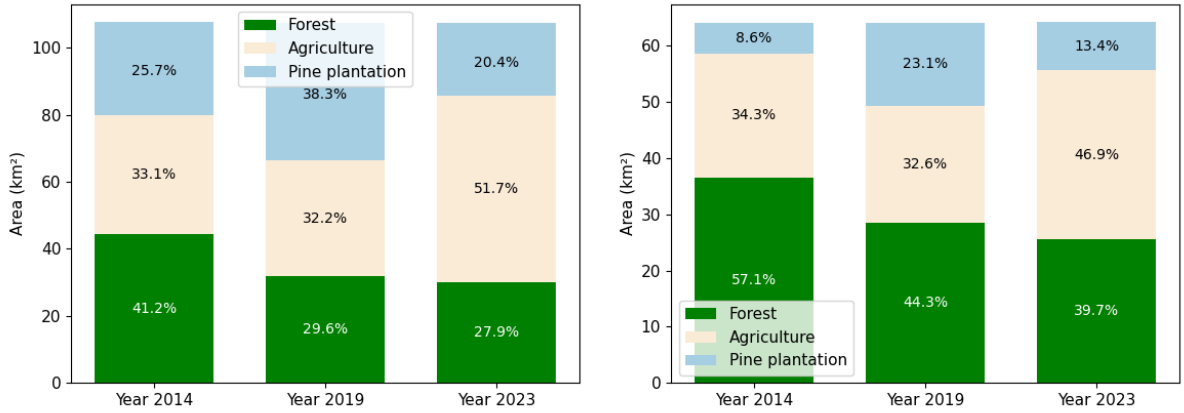

(a) Bar plot showing the total land-use classes areas and their changes over time in the Upper Cahabon catchment

(b) Bar plot showing the total land-use classes areas and their changes over time in the Mestelá catchment

Figure 4.6: Bar plots showing the total land-use classes areas and their changes over time with percentages of total land uses in the catchments

5

Land cover and perceptual hydrological models

To better understand the relationship between land cover and streamflow in the Mestelá catchment, a field study has been conducted during May 2024. This study focused on the Upper Cahabon and the Mestelá catchments, which are located in the rugged, mountainous terrain of Alta Verapaz, Guatemala. This area is known for its rich biodiversity and large variety of ecosystems. Over the course of three weeks, four major land cover types were identified: forest, pine plantation, agriculture and wetland. Figure 5.1 provides a visual representation of three of these land use classes. At the bottom of the image, corn and bean crops illustrate the agricultural land. The middle and top-left sections of the photo show a pine plantation, with noticeable differences in tree height; the right side of the image features recently planted, smaller pine trees. In the background, a transitioning forest is visible, highlighting the variety of tree types and density.

Figure 5.1: Overview land use classes. Bottom: agriculture, middle: pine plantation and right top: forest, photograph taken during field study conducted in May 2024.

These land cover classes are based on their hydrological processes including vegetation interception, soil infiltration, evaporation rates and runoff characteristics. Fieldwork included visiting various landscapes, noting vegetation types and assessing changes in land use. This on-the-ground data provided insights into the interactions between these land covers and the local hydrology.

In this chapter, each land cover type is discussed in detail, with an emphasis on its hydrological characteristics and its influence on streamflow. Additionally, the chapter addresses recent land use changes and their potential impacts on water resources in the Mestelá catchment. Insights gained from discussions with local experts at CCFC further informed this analysis, enhancing the understanding of specific hydrological processes across different landscape types.

5.1. Forest

In the Mestelá catchment, the cloud forest stands out as one of the most important ecosystems. Cloud forests are identified as forested areas where wind-driven clouds play a crucial hydrological role, this occurs at a certain elevation dependent on the meteorological conditions. They are predominantly found between an elevation of 1000 to 3000 m, the exact elevation is based on the temperature, humidity and atmospheric pressure. Within the catchment, cloud forests are complemented by tropical forests, which do not intercept fog. Most of the forest present in the catchment occurs on high slopes and the higher range of elevations of the study area.

Cloud forests are valuable ecosystems due to their high biodiversity, housing numerous endemic species (Haber et al., 2000). They contribute significantly to carbon sequestration and climate regulation through cooling via evapo-transpiration (Bruijnzeel, 2001). Situated mostly on high slopes, cloud forests also play a crucial role in erosion control (Pope et al., 2016; Bruijnzeel, 2004). Importantly for local hydrology, they regulate and maintain water sources such as streams and rivers, which are vital for downstream communities' freshwater supply.

Both tropical and Cloud forest in the Mestelá catchment primarily consist of broad-leaf trees such as the oak, with additional species like pine, cedar and cypress present. These forests have dense vegetation, structured into several layers including forest floor vegetation, understory plants, a dense canopy with compact crowns, and emergent trees.

The high moisture levels in cloud forests promote the growth of epiphytes, such as ferns, lichens, mosses, bromeliads and orchids. These plants act as sponges, absorbing and storing water in their tissues and releasing it slowly. This is also one of the contributors of making the forest very compact and densely vegetated. Epiphytes are contribution to the high number of endemic plants in cloud forests (of Encyclopaedia Britannica, 2022).

(a) Forest floor and understory vegetation of (cloud-) forest

(b) Forest crown with clouds

Figure 5.2: Characteristics photos of land use class forest. Photos taken by drone in the Mestelá catchment by R. Cahill in February 2024.

The high density of vegetation of forest contributes to a high capacity of interception of rainfall and atmospheric moisture. The tree crowns and emergent trees are especially important for capturing wind-driven fog. The deep root systems of various types of vegetation promote infiltration in the root-zone of the soil following rainfall as well as creating a large storage capacity of water in the unsaturated

root-zone. As mentioned, the epiphytes promote additional water storage of fog and precipitation interception and slowly releasing it over time during times of no precipitation as evaporation, to regulate the micro-climate.

In this study both tropical forest and cloud forest are included in the class forest, however the separation has been made that only the cloud forest intercepts fog.

5.2. Pine Plantation

In the Mestelá catchment, pine plantations represent a significant land cover type. Unlike the diverse ecosystems of tropical and cloud forests, pine plantations are predominantly mono-cultures with sparse undergrowth. These plantations are established for wood production, typically in a 25 year cycle with a thinning every 5 year. This results in a bare soil after each cycle. The understory of the pine trees is removed during maintenance, leaving large areas of bare soil. Figure 5.3 shows a picture of the most common pine plantation, showing the Pinus Maximinoi. These plantations are found at all slopes and elevations within the study area.

Pine plantations do no not provide the complex ecosystem services provided by natural forests such as cloud forest. They lack the characteristic dense vegetation layers and biodiversity associated with natural forests. The needle-like leaves of pine trees are less effective in interception water compared to to broad-leaf trees and there is less epiphitic growth, resulting in an expectation of less rainfall interception and storage.

Figure 5.3: Pine plantation in the Mestelá catchment, photograph taken during field study in May 2024.

Due to the sparse undergrowth, it has been observed that pine plantations have a compacted soil structure, reducing their ability to absorb water. This compaction limits infiltration rates and leads to overland flow in pine plantations after heavy rainfall events. Additionally, their mono-cultural nature expects to lead to a smaller root-zone and further limiting water storage capacity in the soil.

5.3. Agriculture

In the Mestelá catchment, agricultural activities play a significant role, primarily focusing on the cultivation of rain-fed crops such as corn and beans, shown in Figure 5.5a. These crops are cultivated extensively throughout the region, often employing traditional techniques such as slash and burn. Due to the growing stages of crops and planting seasons, fields are left bare for extended periods, which contributes to increased soil temperatures and evaporation rates. The agricultural land cover class also includes areas dedicated to pastures and horticulture.

Recent agricultural trends have introduced cash crops such as broccoli and avocados, which led to intensified pesticide use (Figure 5.4a). This widespread application of pesticides poses several environmental challenges. Firstly, pesticides hinder the growth of deep roots and contribute to soil compaction, reducing the soil's ability to absorb water and increasing surface runoff. Moreover, pesticides do not allow the living of beneficial insects such as worms, which would otherwise improve soil structure and enhancing water infiltration through the creation of micro-pores (Local discussions with CCFC staff, May 2024). An example of soil degradation in the Mestelá catchment is shown in Figure 5.4b). Additionally, the continuous application of pesticides depletes soil nutrients, resulting in diminished vegetation cover and further exacerbating erosion risks.

(a) Pesticides application on avocado trees

(b) Degraded agricultural soils in an avocado plantation

Figure 5.4: Pesticide application on the land use class agriculture. Photographs taken during field study conducted in May 2024.

Consequently, considering all these agricultural practices, there is little interception capacity of vegetation due to the absence of vegetation. The soil is compacted and has often been burned, leading to exceedance of infiltration capacity during intense rainfall events, resulting in significant surface runoff (DeBano, 1990). The constructed ditches in the agricultural field, as seen in Figure 5.4b, serve as evidence of efforts to redirect overland flow water outside of the fields.

Most of the agricultural fields in the study area can be found on lower slopes and lower elevation. However, due to the need of more corn cultivation, the agricultural fields have expanded to the higher elevations and higher slopes, by cutting down natural forest. This increases vulnerability to erosion and runoff due to steeper terrain and reduced natural vegetation cover, see figure 5.5b.

(a) photograph showing agricultural field with alternating corn and bean crops.

(b) Corn fields on steep slopes, showcasing the agricultural use of high-elevation terrain

Figure 5.5: Photographs taken May 2024 of agricultural fields.

The mentioned agricultural practices collectively contribute to soil degradation, erosion, reduced water quality and increased runoff, presenting significant obstacles for sustainable agriculture and effective water resource management in the region.

5.4. Wetland

Wetland areas in the Mestelá catchment are defined as regions situated near the groundwater table, typically within floodplains of the river. These areas are often characterized by abundant vegetation and low slopes, which play a significant role in moderating streamflow and providing important habitats for diverse flora and fauna.

Vegetation within wetlands is particularly vital due to its proximity to the river. The dense vegetation helps stabilize soil, reducing erosion and sedimentation in adjacent water. Moreover, this vegetation acts as a natural filter, trapping pollutants and sediments, and thereby improving water quality as it flows through the wetland. During periods of flooding, the root systems of wetland vegetation absorb excess water and slows down floodwater, thereby mitigating flood peaks downstream and reducing the risk of downstream flood damage, however this is dependent on the location of the wetland (Wu et al., 2023).

In Guatemala, a law passed in 1997 prohibits the cutting down of trees within 25 meters of a river to prevent soil erosion and water contamination (Knorr-Evans et al., 2019). However, enforcement of this regulation is inconsistent, and in many areas, agricultural fields and pastures are located in wetlands next to rivers. Agricultural activities in these areas can introduce pesticides directly in the water, bypassing natural filtration processes and compromising water quality downstream. Figure 5.6a illustrates a wetland area with intact vegetation, while Figure 5.6b depicts a pasture situated within a wetland area.

Additionally, the absence of vegetation in wetland areas may lead to reduction in interception, infiltration, and water storage capacity, leading to increased runoff into rivers. This further exacerbates flood risks and reduces the ability of wetlands to regulate water flow effectively. Vegetation in wetlands is essential for maintaining the ecological functions of wetlands, safeguarding water sources and supporting biodiversity in the Mestelá catchment.

(a) Wetland with natural vegetation **(b)** Pasture located within wetland area

Figure 5.6: Different types of wetlands encountered in the Mestelá catchment.

5.5. Land use change

In recent years, significant changes in land use have been observed, as illustrated in Figure 4.5b. The most profound changes have occurred since the introduction of cash crops in 2015, just after the starting point for the land use maps.

The land cover maps reveal an increase in agricultural activities, accompanied by widespread deforestation for both agricultural expansion and timber extraction. Also, an increase in pine plantations is observed, see Figure 4.6b. Particularly alarming is the expansion of agricultural fields onto higher slopes and elevations, driven by limited space on lower terrain, shown in Figure 5.7. This encroachment is gradually erasing the last cloud forest present in the catchment, altering the landscape irreversibly.

Figure 5.7: Agriculture encroaching onto the high slopes in the Mestelá catchment

The decline in forest cover and the expansion of agricultural areas are primarily driven by the increasing demand for food and economic opportunities. Climate change has also played a role, with rising temperatures leading to more frequent floods and drought, which in turn threaten crop yields and necessitate further land clearance.

6

Methodology

To assess the applicability of the FLEX-Topo and FIESTA models in simulating the influence of land cover on streamflow in the Mestelá catchment, a detailed methodological framework was implemented, involving the simulation and calibration of hydrological models. Firstly, the FIESTA model was employed to generate forcing data, including precipitation, fog and potential evaporation. This model provides spatially distributed climatic data based on topographic, vegetation and climatic variables. The output from the FIESTA model serves as input for the FLEX-Topo model.

The next step involves developing the conceptual model for the FLEX-Topo model and then calibrating the model using observed streamflow data of the Upper Cahabon catchment to ensure accurate representation of the hydrological processes within the catchment.

Once calibrated, the FLEX-Topo model is run for the Mestelá catchment and is utilized to run simulations under various land use scenarios. This process enables the evaluation of how different land cover types affect streamflow dynamics. Given that forcing data characteristics are influenced by land use, the integration of FIESTA-generated data is crucial for both calibration and scenario analysis.

6.1. FIESTA model

The Fog Interception for the Enhancement of Streamflow in Tropical Areas (FIESTA) model calculates the water balance by quantifying fog inputs, rainfall, and the outputs of evapo-transpiration according to spatially variable topographic, climatic and vegetation properties (Mulligan and Burke, 2005).

The model is primarily used to estimate meteorological inputs for which there is no direct data: potential evaporation, wind-driven precipitation and fog interception. Given that the meteorological data in this study is sourced from a station located in Cóban, outside the study area, and considering the presence of various micro-climates within the area, the FIESTA model is useful for adjusting the meteorological data input using spatial data.

The model simulates various cloud and radiation processes, including fog and cloud formation, solar radiation, and atmospheric heating and cooling. It considers factors like cloud condensation nuclei, aerosols, and the interaction between radiation and surface features. The model focuses on simulating the above-ground components of the hydrological cycle, for which good spatial data can be accessed (Mulligan and Burke, 2005).

Once run, the various outputs of the FIESTA model are used to model the hydrological processes in the catchment; fog interception, wind-adjusted precipitation and potential evaporation, spatially distributed in the catchment. Other output variables include adjusted temperature, cloud cover, fog duration, cloud elevation.

The FIESTA model does not account for baseflows, changes in local storage and associated time lags, therefore it is only used to estimate the outputs mentioned and not the streamflow. Additionally, the

model does not simulate infiltration and runoff generation due to the lack of detailed soil and subsurface data, which cannot be remotely sensed.

6.1.1. Data collection and pre-processing

Meteorological data from the Cóban INSIVUMEH station for the study period of 11 April 1997 to 12 March 2024 is used as input for the FIESTA model. The following data variables are used; minimum temperature [°C], maximum temperature [°C], mean temperature [°C], relative humidity [%], cloud coverage [-], wind speed [m/s], wind direction [°], atmospheric pressure [mb] and precipitation [mm]. Extraterrestrial solar radiation data for four specific hours of the day [wh/m^2], 24:00, 06:00, 12:00 and 18:00, is taken from the Global Solar Atlas for the location Tactic.

The FIESTA model utilizes spatial data of the Upper Cahabón catchment, obtained through remote sensing. Elevation [m], slope [°], aspect [°] of pixel size 20x20 and land cover classification of pixel size 30x30 m.

The Fiesta model is run for both the Upper Cahabon catchment and for the Mestelá catchment.

Pre-processing

The catchment is divided into different spatial classes based on elevation, slope and aspect classes of certain ranges. Table 6.1 shows the average value of each of these classes for the Upper Cahabon catchment and Table 6.2 shows the average value of each of these classes for the Mestelá catchment. Each spatial class in the catchment represents one of the possible combinations of the elevations, slope and aspect, resulting in 48 different classes, with different cell areas. For each of these spatial classes the model is run, developing spatially distributed meteorological data.

Table 6.1: Spatial classes used to determine cells as input for the FIESTA model for the Upper Cahabon catchment

Classes				
Elevation [m]	1510	1760	2000	2250
Slope [°]	10	30	50	
Aspect [°]	North	East	South	West

Table 6.2: Spatial classes used to determine cells as input for the FIESTA model for the Mestelá Catchment

Classes				
Elevation [m]	1515	1840	2165	2540
Slope [°]	10	30	50	
Aspect [°]	North	East	South	West

These cell areas, which are the planimetric surface areas, are converted to 3D areas using the average slope of each cell, shown by the following equation: $Area3D = \frac{Pixelarea}{cos(slope)}$. This transformation is important for mountainous areas since the true surface area can be significantly larger than the planimetric surface area.

For each of these cells the fraction of land cover covering the cell is determined using the land cover maps of the Upper Cahabón and the Mestelá catchment. This is done in Python by developing a map of the catchment for each of the spatial classes, providing the location in the catchment where the spatial class is true and not true, an example of an spatial cell of the Mestelá catchment is shown in Figure 6.1. All of the spatial maps are resized to a pixel size of 30x30 m. Using the land cover maps, the amount of pixels for each of the land use classes are counted where the spatial class is true. Finally, using the total amount of pixels of the spatial class, the fraction of land cover for the classes agriculture, pine plantation and forest are calculated.

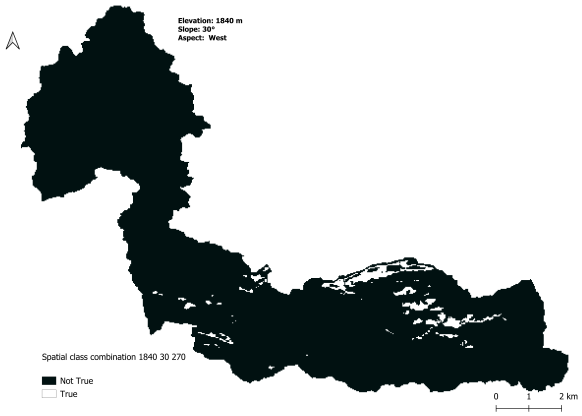

Figure 6.1: Example of spatial class location in the Mestelá catchment of elevation range 1840m, slope 30° and aspect 270°, where white represents the locations where the these combinations are true.

Constants

The FIESTA model incorporates several physical constants to run the model. Table 6.3 shows the constants used in this model, which are based on literature and field observations.

For the fog droplet size, the model uses the values provided in the original FIESTA model by Mulligan and Burke, which represent the mean particle size of fog droplets. The terminal velocity of a raindrop varies depending on its diameter, increasing with height until it reaches a maximum threshold of 9 m/s at around 20 meters above ground level, beyond which it remains constant. (Serio et al., 2019). In the FIESTA model, an average terminal velocity of raindrops is used as a constant parameter.

The fractional trapping areas, which represents the proportion of vegetation which captures fog droplets, is also based on the study done by Mulligan and Burke. This parameter accounts for the effects of leaf self-shading and is assumed to be the same across all land cover classes. The mean height values for forest, emergent trees above the canopy, and vegetation in agricultural fields are based on field observations.

The Leaf Area Index (LAI) is defined as the one-sided green leaf area per unit ground surface area. An average value of the LAI for each land use class is used. For tropical mountane forests, the average LAI is measured to be around 5.5 (Grubb, 1977), considering there are many different height layers in forests. The LAI for the class agriculture, which includes agricultural fields and pastures, varies depending on crop type and growth stage. Field observations indicate that agricultural fields are often sparsely vegetated, with approximately one meter of bare soil between seedlings. Consequently, an average LAI for agricultural fields of 0.7 is used, consistent with studies on the LAI of corn fields (Hosseini et al., 2015; Yang et al., 2012).

The LAI for Pine plantations is estimated to be 2.0, considering factors such as needle density and litter fall (Peduzzi et al., 2010; López-Serrano et al., 2000). It is important to note, that in pine plantations observed in the study area, understory vegetation is often removed, and litter fall is minimized through management practices such as thinning.

Table 6.3: Physcial constants used in FIESTA model

Item	Category	Unit	Value	Source
Fog droplet size		μm	7.5	(Mulligan and Burke, 2005)
Average terminal velocity of raindrop v_{term}		m/s	9	(Serio et al., 2019)
Fractional trapping areas	All land covers	-	0.8	(Mulligan and Burke, 2005)
Mean height	Forest edges ($H_{f_{edge}}$)	m	10	(Field observation, 2024)
	Emergent trees ($H_{f_{emergent}}$)	m	2	(Field observation, 2024)
	Agricultural vegetation (H_{agr})	m	0.5	(Field observation, 2024)
LAI	Cloud Forest	-	5.5	(Grubb, 1977)
	Agriculture	-	0.7	(Hosseini et al., 2015)
	Pine plantation	-	2.0	(Peduzzi et al., 2010)

6.1.2. Model implementation

This section describes the FIESTA model implementation, which is divided into three main processes: precipitation, fog interception, and evaporation. The equations used are adaptations from the FIESTA model by Mulligan and Burke (Mulligan and Burke, 2005) and from the implementation of the FIESTA model in Python by (Agudelo et al., 2023). Adjustments are made to fit the study area, available data and the Python programming environment. The equations which are used from the original FIESTA model are shown in Appendix A. Only the adaptations are shown in this chapter.

Precipitation

Available precipitation data is collected outside of the Upper Cahabón catchment near the city Cóban, as mentioned in the previous chapter. Due to the high spatial variability of precipitation, estimating this variable can be challenging. Given the mountainous nature of the study area, accounting for the influence of topography on precipitation is crucial. On the windward side, the forced lifting of approaching air masses cause the release of rainfall, increasing precipitation with elevation (Smith, 1979). Conversely, on the leeward side, precipitation decreases due to reduced wind speed influenced by the mountain's aspect and slope (Johansson and Chen, 2003).

The FIESTA model adjusts measured precipitation for wind-driven effects by considering the topography. This adjustment involves factors such as wind direction, wind speed, aspect and slope, all of which are explained in detail in the following sections. Although Humidity is known to influence precipitation, it is not included in the FIESTA model.

Adjusted wind speed and adjusted wind direction The wind direction varies significantly with local topography. The model deflects the assumed horizontal wind by topography based on local slope and aspect. When wind travels toward a slope with an aspect facing left or right from the wind direction, it deflects accordingly depending on the slope gradient, with a maximum deflection at the highest slope. No deflection occurs when the slope faces away from the wind direction. The topographical adjusted wind is the original wind direction in addition to the deflection.

Wind speed is adjusted based on the mountain's aspect and wind direction. A reduction in wind speed occurs when the mountain blocks the wind, Equation 6.1 shows the developed equation. The use of the cosine function and the absolute value creates symmetry around the mountain. This method does not consider the topography of surrounding cells, unlike the FIESTA model, to avoid complexity.

$$W_{s_{adj}} = W_s * abs(cos(\frac{\text{Aspect} - W_d}{2})) \tag{6.1}$$

Where, W_s [m/s] is the wind speed, $W_{s_{adj}}$ [m/s] the adjusted wind speed and W_d [rad] is the wind direction. The aspect is also used in radians.

Wind-adjusted precipitation Precipitation is adjusted for wind-driven effects using Equation 15 of the study by Mulligan and Burke (2005). If rainfall occurs, the dataset's precipitation is multiplied by a wind slope correction factor, based on the wind speed, wind direction, slope and aspect.

Fog interception

Fog interception by vegetation is quantified through the deposition (vertical) and impaction (horizontal) processes for each land use class and corresponding vegetation type.

The actual fog interception is determined by the the volume of water passing by the representative surface area, the fraction of surface area that will intercept fog and the proportions of the flux that are horizontal and vertical. These factors depend on the horizontal wind, temperature, relative humidity and atmospheric pressure. The volume of water passing is dependent on elevation, as fog only occurs above Lifting Condensation Level (LCL). The total interception in mm is determined considering the cloud frequency and the elevation.

All the specific steps of calculating fog interception are detailed in the following sections. First, meteorological inputs are adjusted considering the topography to facilitate accurate calculations.

Temperature Adjustments The input data temperature [◦C] is adjusted based on elevation, time of the day and land cover. The elevation adjustment is -0.6 ◦C per 100m elevation increase. Forest presence reduces temperature by by 1 ◦C proportional to the forest fraction in each cell. Diurnal temperature variations are considered using four daily time steps, using the same method used in FIESTA model, Equation 6.

Mean Sea Level Pressure (MSLP) Atmospheric pressure at the measurements station's elevation is converted to mean sea level pressure for meteorological comparisons. Corrections are applied for temperature, humidity, earth's asphericity, and gravitational acceleration variation (Scott, 2011). The following equation 6.2 is used to convert the atmospheric pressure to mean sea level pressure [mb], using the formula of Laplace (WMO, 1954).

$$Z_p = K * (a + \alpha * T_{mean}) * (\frac{1}{1 - 0.378 * \frac{E}{b}}) * (\frac{1}{1 - k * cos(2\varphi)}) * (1 + \frac{Z_p}{r}) * log(\frac{P_0}{P_s}) \quad (6.2)$$

Where, Z_p [m] is the geometric altitude, K is the hypsometric constant (18400m), α is thermal expansion coefficient of air (0.0037), T_{mean} is the mean temperature [°C], E [mb] is the vapour pressure explained in A.8, b [mb] is the mean barometric pressure of the air column, k is the earth's figure constant (0.00259), φ [degrees] is the latitude of the meteorological station, r is the earth's mean radius (6367324 m), and P_0 and P_s [mb] are the atmospheric pressures at the mean sea level and the station, respectively.

Lifting condensation level The Lifting Condensation Level (LCL) [m] is determined to identify fog presence, as fog interception only occurs when fog is present at a certain elevation. In order to calculate the LCL first the dewpoint temperature [°C] is calculated using vapour pressure [mb] and relative humidity [%]. The dewpoint temperature (Td), is the temperature when the air is saturated with water vapour and cloud formation starts. The LCL is calculated in mb and then converted to meters above sea level. Fog occurs when the elevation in the cell is greater than the LCL, if not there is no fog interception.

Fog Impaction flux Fog impaction flux is calculated using the FIESTA model's Equation 16. The impaction flux determines the amount if water passing through several vegetation types: agricultural fields and forest, specifically emergent trees and forest edges, considering. Forest edges are significant due to their exposure to horizontal wind-driven precipitation and fog and are represented as catching surfaces. In order to determine the impaction flux at forest edges and emergent trees, the sizes of these areas need to be determined (see Appendix A.2).

The impaction is influenced by the wind flux and Liquid Water Content (LWC) of clouds. The LWC is proportional to absolute atmospheric humidity, calculated using vapour pressure and temperature.

The wind flux is determined considering the wind speed and a reduction factor for vegetation frictional losses considering the sizes of the vegetation types considered.

Fog deposition flux The fog deposition flux, or in other words; the settling flux, is calculated using Equation 17 from the FIESTA model. The settling flux is calculated with the LWC and the gravity flux, determined by fog settling velocity according to Equation 2 of the FIESTA model.

Proportion of impaction and deposition The total fog interception is a sum of the deposition interception and the impaction interception. Proportions of deposition and impaction depend on the cosine of the fog inclination angle over vegetation fractions. The fog inclination angle is different for trees and agricultural fields, due to different frictional loss factors.

Surface area fog impaction and deposition To calculate the total amount of impaction and deposition which has occurred in the study area, the surface area available for fog impaction and deposition needs to be determined. The deposition surface area is calculated for forest, pine plantations, and agriculture, dependent on the fractional trapping area, the fractional land covers and the Leaf Area Index (LAI).

The impaction surface area depends on the leaf area density of the vegetation and the angle of incoming fog relative to the leaves.

Total fog interception The total fog interception is calculated as the proportion of deposition multiplied by the deposition flux and the deposition fraction area, added to the proportion of impaction multiplied by the impaction flux and the impaction surface area fraction. Fog only occurs when the elevation is greater than the LCL.

The total fog interception is calculated in $kg/m^2/hr$. To convert to millimeters, the fog interception is divided by the true area of the grid cell and multiplied by the factor of cloud fraction, accounting for the amount of fog present during the day. Since fog interception is calculated for four times per day, each time step is multiplied by six to give the total daily fog interception [mm/day].

Evaporation

Evaporation is calculated based on the available energy and atmospheric demand, combining these factors to determine the potential evaporation. The actual evaporation is then adjusted according to vegetation types, cover, and climatic conditions.

Solar radiation The obtained solar radiation for the four hours of the day is adjusted using a Solar Radiation Index (SRI) to consider for the aspect and the slope, using the method in the study by Keating and Gogan (2010), shown in Equation 6.3. The initial measured solar radiation is multiplied by the SRI to obtain the adjusted value used for further calculations.

$$SRI = cos(latitude) * cos(slope) + sin(latitude) * sin(slope) * sin(180 - aspect) \tag{6.3}$$

Net radiation Net radiation serves as the main energy source of evaporation, and therefore needs to be determined in order to calculate the amount of potential evaporation. Firstly, the input meteorological data solar radiation $[Wh/m^2]$ is used to calculate the effective solar radiation accounting for transmission losses due to fog and clouds (Equation 12 FIESTA model). Secondly, net radiation is determined using a linear relationship between solar and net radiation for forest and field sites, established by Mulligan and Burke (2005) using sensors above forest and pasture covers (Equation 13 FIESTA model).

The total net radiation for an area is calculated by summing the net radiations of forest, pine plantations and agricultural areas, weighted by their land cover fractions within the cell. Given that input solar radiation data is available for four hours of the day, net radiation and subsequent evaporation calculations are performed four times daily.

Potential evaporation Both potential evaporation (Ep) and actual evaporation (Ea) are calculated using the slope of the saturation vapor pressure curve, based on current temperatures.

Actual evaporation Actual evaporation is derived from potential evaporation, factoring in the non self shaded surface area available for the interception of evaporation water. This calculation reflects vegetation cover and climatic conditions.

The assumption is made that water availability is less significant in determining the evapo-transpiration than the energy available. Intercepted energy fractions of land covers are determined using the Leaf Area Index and the fraction of land class in the cell. Given the coarse spatial and temporal scale of the FIESTA model, plant processes and aerodynamic are considered negligible. Actual evaporation is then calculated as the sum of energy intercepted by tree leaves, pine needles and agricultural crops. The difference of actual evaporation between forest and agriculture is primarily due to the radiation intercepted by the canopy (Mulligan and Burke, 2005).

The daily fog interception [mm], daily potential evaporation [mm] and the daily wind-adjusted precipitation [mm] per cell of the catchment are used as meteorological data input for the FLEX-Topo model.

6.2. FLEX-Topo model

The FLEX-Topo model is a conceptual hydrological model framework driven by topography to simulate water flow and storage for the Upper Cahabón and the Mestelá catchment. The model is structured around landscape classes primarily determined by topography, but it also incorporates geological, geomorphological, and land-use classifications (Savenije, 2010).

To reflect the diverse hydrological behavior of the study area, four landscape classes are defined: hillslope forest, hillslope pine plantation, hillslope agriculture and wetland, consistent with the perceptual model described in Chapter 5. Each landscape class is associated with an unique model structure, developed in this study to simulate its dominant hydrological processes. Furthermore, the FLEX-Topo model framework is adapted to the Upper Cahabón and Mestelá catchment by reflecting the study area's landscape characteristics.

The FLEX-Topo model was initially calibrated for the Upper Cahabon catchment. The calibrated model was then transferred to the Mestelá catchment, applying the same parameter set across both catchments due to their similar spatial characteristics and proximity. The model can then be applied for comparison of streamflow dynamics using different land-use scenarios in the Mestelá catchment.

The following sections provide an explanation of the model structure and landscape classifications, followed by a description of the conceptual model used to represent each landscape class. Finally, the parameter calibration and model evaluation strategies are discussed.

6.2.1. Spatial distribution in FLEX-Topo

The catchment is subdivided in the 48 cells based on elevation, slope, and aspect, as detailed in Section 6.1.1. The subdivision accounts for the spatial variability in precipitation, fog interception and evaporation driven by diverse micro-climates within in the system. Each cell contains distinct landscape fractions and input data for precipitation, fog interception and potential evaporation, as outlined in Chapter 6. While each cell features its own fluxes and states, model parameters are defined per landscape class.

The FLEX-Topo model's distributed conceptual approach uses a approach similar to that of Fenicia et al. (2008), which demonstrated improved model performance with spatially distributed rainfall and storage reservoirs. In this study, the model runs the four landscape classes in parallel for each subdivided catchment cell, with the exception of the groundwater reservoir, which is treated as a unified system. The model integrates the states and fluxes of each landscape class within each cell, using the specific landscape fractions, to calculate the total output for each cell. The final streamflow of the catchment is obtained by summing the weighted outputs of all cells and applying a filtering process. The model is run on a daily timestep.

6.2.2. Landscape classification

Given the catchment's steep topography, the model distinguishes two topographic classes: hillslope and wetland (Savenije, 2010). The hillslope category is further divided based on land use, as derived from remote sensing data, into three specific classes: hillslope forest, hillslope agriculture and hillslope plantation.

Wetlands are identified using the Height Above Nearest Drainage (HAND) method (Rennó et al., 2008). Areas within six meters of height above the nearest river point are classified as wetlands. This classification is superimposed on the land cover maps derived from satellite imagery.

Table 6.4 summarizes the proportions of different landscape classes used as inputs for the FLEX-Topo model for both the Upper Cahabon and the Mestelá catchments. The model operates with time series data of landscape classification, applying linear interpolation between the years 2013, 2019, and 2023. For the years prior to 2013, the land use is assumed to be consistent with 2013, while for the years beyond 2023, the land use is held constant at the 2023 values.

Figure 6.2 illustrates the final landscape maps for the years 2014, 2019 and 2023 for the Mestelá catchment. These maps provide the landscape class distributions used in the FLEX-Topo model.

Table 6.4: Landscape classification percentage input FLEX-Topo model of total catchment Upper Cahabon and Mestelá

	Hillslope Forest (%)	Hillslope Pine plantation (%)	Hillslope Agriculture (%)	Wetland (%)
Upper Cahabon - 2014	41	22	32	5
Upper Cahabon - 2019	30	35	30	5
Upper Cahabon - 2023	28	20	47	5
Mestelá - 2014	55	8	33	4
Mestelá - 2019	43	22	31	4
Mestelá - 2023	38	13	45	4

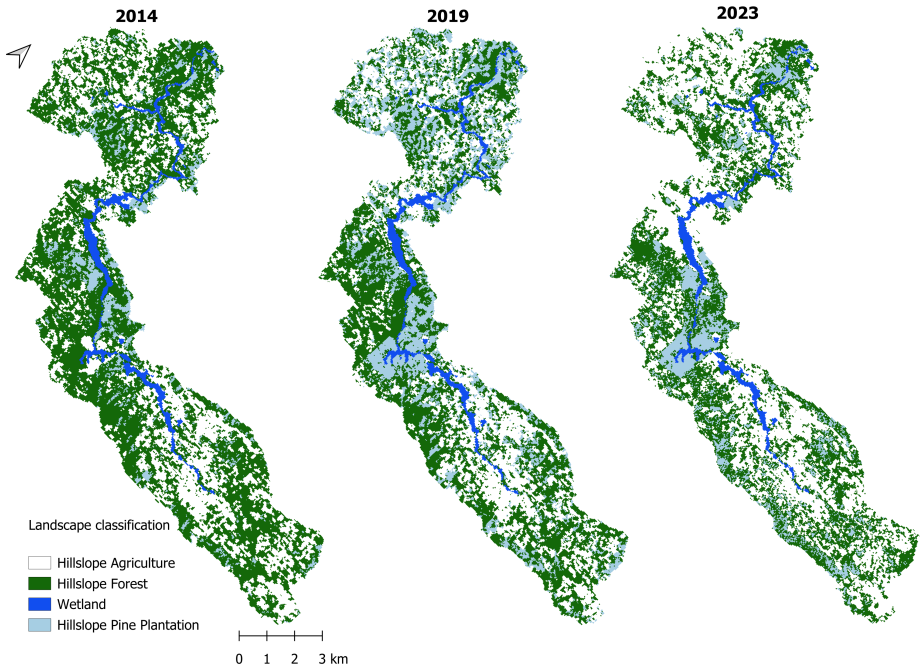

Figure 6.2: Landscape classification TOPO-Flex for the Mestelá catchment

6.2.3. Conceptual model description

The FLEX-Topo model represents hydrological processes through reservoirs, connection elements and lag functions, using the SUPERFLEX flexible modelling framework. It builds on earlier applications of the FLEX model (Fenicia et al., 2008, 2011; Gao et al., 2014).

Each landscape class has its own conceptual model structure, based on the perceptual model, described in Chapter 5 and shown in Figure 6.3. For the hillslope classes, storage excess subsurface flow is the dominant runoff mechanism, while in the wetland class, saturation excess overland flow prevails when then groundwater level is close to the surface (Savenije, 2010). The conceptual models for the hillslope classes have a similar structure but differ in characteristics that reflect land use. Figure 6.4 shows the model structures for each landscape class. The total streamflow is modelled using a combination of this model structure for each spatial cell.

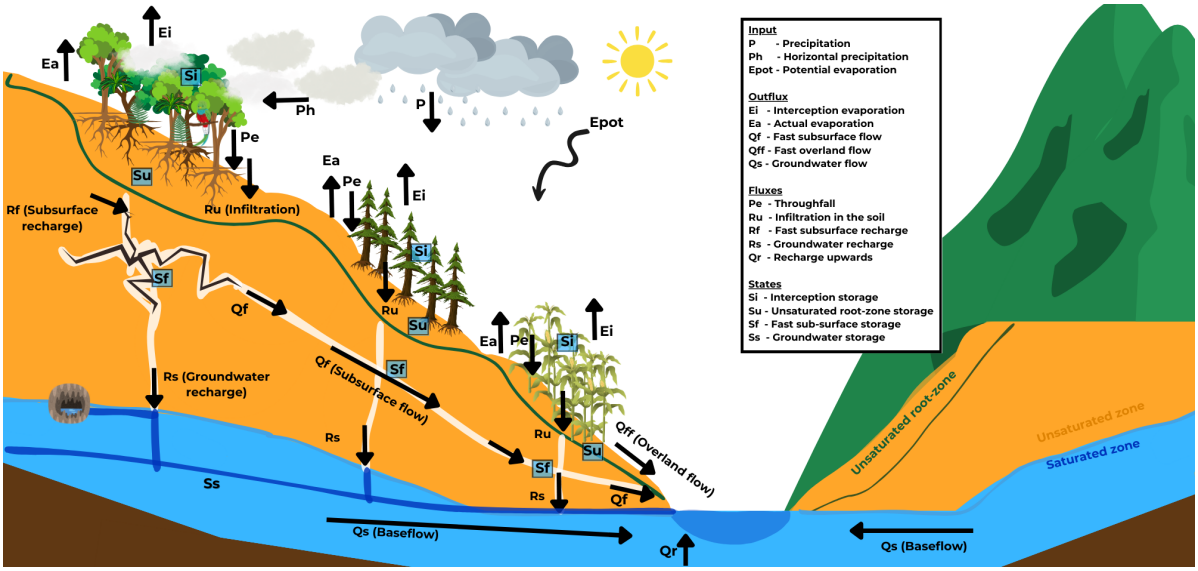

Figure 6.3: Perceptual model of all landscape class, showing all dominant water fluxes and storage components of each landscape model structure.

The model incorporates four storage components: the interception storage reservoir (S_i), the unsaturated soil storage reservoir (S_u), the fast reacting reservoir (S_f) and the slow reacting reservoir (S_s). Inflows and outflows define the dynamics of these storage components, with precipitation (P) and fog interception (P_h) being the inflows. Outflows include interception evaporation (E_i), actual evaporation (E_a) and the three runoff processes: fast overland runoff (Q_{ff}), fast runoff (Q_f) and slow runoff (Q_s). The model determines the total runoff using lag functions and includes 23 parameters to characterize storage capacities and storage-outflow relationships.

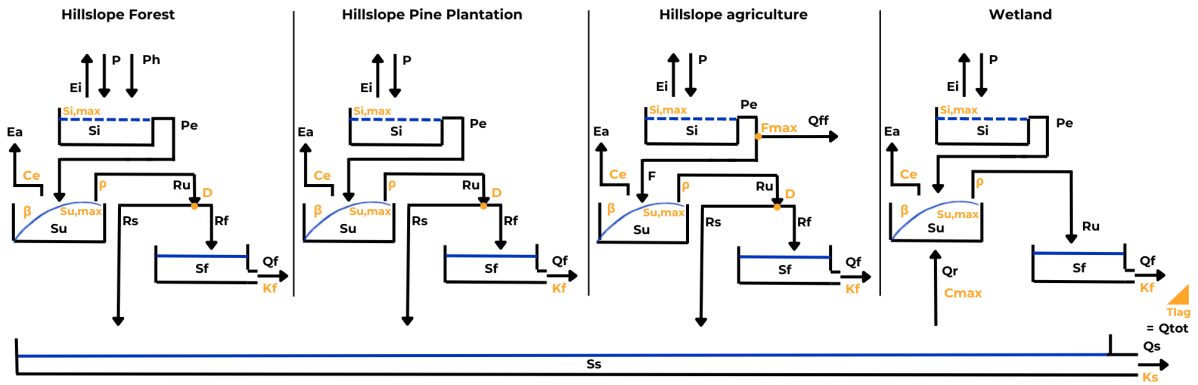

Figure 6.4: Conceptual FLEX-Topo model structure comprising four parallel components representing landscape classes and a shared groundwater storage component. Parameters are shown in orange, states represented with blue lines and fluxes shown with arrows.

Interception reservoir

When rainfall occurs, a considerable amount of the (vertical) rainfall P [mm/d] is intercepted by the canopy of the forest and stored in the interception storage reservoir S_i [mm]. Some of this intercepted precipitation evaporates back into the atmosphere as interception evaporation E_i [mm/d]. The amount of interception evaporation is constrained by the potential evaporation E_p [mm/d] and the daily storage capacity of the interception reservoir $S_{i,max}$ [mm], and it only occurs in the absence of rainfall (Equation 6.4). Water that exceeds the maximum storage capacity $S_{i,max}$, is released as throughfall or effective precipitation P_e [mm/d] (Equation 6.5).

$$E_i = \begin{cases} E_p, & S_i > E_p \\ S_i, & S_i < E_p \\ 0, & P > 0 \end{cases} \tag{6.4}$$

$$P_e = \begin{cases} 0, & S_i < S_{i,max} \\ S_i - S_{i,max}, & S_I > S_{i,max} \end{cases} \tag{6.5}$$

The total water balance of the interception reservoir is given by:

$$\frac{dS_i}{dt} = P - E_i - P_e \tag{6.6}$$

Horizontal precipitation interception of Hillslope Forest In cloud forests, fog interception adds an additional influx of horizontal precipitation P_h [mm/day], which is applied only where cloud forests are present in the class forest. Horizontal precipitation is determined by the FIESTA model, see Chapter 6. The water balance for hillslope forests becomes:

$$\frac{dS_I}{dt} = P_v + P_h - E_i - P_e \tag{6.7}$$

Unsaturated soil storage

It is assumed that all throughfall P_E infiltrates soil in the unsaturated root-zone storage reservoir S_u [mm], expect for agriculture, where overland runoff occurs. The amount of throughfall stored in the unsaturated root-zone storage reservoir S_u [mm] depends on the soil moisture. S_u has a maximum storage capacity $S_{u,max}$ [mm], representing the water stored between field capacity and the Permanent Wilting Point within the reach of vegetation roots. From the proportion of incoming effective rainfall that cannot be stored, runoff is generated. The beta function of the Xinanjiang model (Zhao, 1992) is used to determine the amount of rainfall, shown in Equation 6.8. This is represented using a probabilistic approach using the concept of a runoff coefficient ρ [-], characterized by the spatial heterogeneity of $S_{u,max}$ represented by the parameter β [-]. Here, ρ is the fraction of the soil with a storage capacity smaller than or equal to the amount of water present in the unsaturated root-zone storage. The runoff generated according to the parabolic manner of the runoff coefficient is calculated according to Equation 6.9.

$$\rho = 1 - (1 - \frac{Su}{Su,max})^{\beta} \tag{6.8}$$

$$R_u = \rho * P_E \tag{6.9}$$

Transpiration and soil evaporation from the S_u is represented by actual evaporation E_a [mm/d]. E_a depends on the available energy after interception evaporation ($E_{P,t} = E_P - E_I$), the water available in S_U and the parameter relative soil moisture when vegetation starts to experience water stress C_e [-] (Equation 6.10). The actual evaporation is constrained by the amount of water present in S_u and the potential evaporation E_p.

$$Ea = min(E_{P,t} * min(\frac{S_U}{S_{Umax} * C_e}, 1), S_u) \tag{6.10}$$

This process results in a non-linear response: what comes in is partially drained away and partially evaporated, with the water balance given by:

$$\frac{dS_U}{dt} = P_e - R_u - E_a \tag{6.11}$$

Overland flow of Hillslope Agriculture In agriculture, compacted soils and burned soils with low infiltration capacity produce overland flow (Q_{ff}) during heavy rainfall events. When the throughfall P_e exceeds the infiltration capacity F_{max} [mm/day] of the soil, overland flow is generated. The overland flow Q_{ff} [mm/d] is assumed to reach the river the same day, shown in Equation 6.12. The flow capable of infiltrating the soil is represented by F [mm/d].

$$Q_{ff} = \begin{cases} 0, & P_e < F_{max} \\ (P_e - F), & P_e > F_{max} \end{cases} \tag{6.12}$$

Recharge of Wetlands Wetlands experience upwelling groundwater fluxes Q_r [mm/d] due to groundwater head differences. These fluxes can sustain high level of soil moisture during dry periods in S_u. Q_r can be calculated as a constant fraction of Q_s, the groundwater flow, see section 6.2.3 below. This fraction is defined by C_{max} [-] and the upwelling groundwater fluxes depend on the unsaturated storage, see equation 6.13.

$$Q_r = (1 - \frac{S_U}{S_{Umax}}) * C_{max} \tag{6.13}$$

Thus, the water balance for wetland becomes:

$$\frac{dS_U}{dt} = P_e + Q_r - R_u - E_a \tag{6.14}$$

Fast and slow reacting reservoir

Water that cannot be stored in S_u according to the runoff coefficient ρ, is then released and separated into two recharge flows according to splitter D [-]. The first flow, fast subsurface recharge R_f [mm/d], occurs over preferential flow paths such as soil cracks or macro-pores and is stored in the fast subsurface water storage S_f. The second flow, percolation to the groundwater R_s [mm/d] through macro-pores such as caves, represents water stored in the slow reacting groundwater storage reservoir S_S. The distribution of these flows according to splitter D is shown in equation 6.15 and 6.16, where sub-surface flow and its distribution is determined by the soil types and soil textures.

$$R_f = \rho * (1 - D) * P_E \tag{6.15}$$

$$R_s = \rho * D * P_E \tag{6.16}$$

Fast reacting reservoir

Water stored in the fast reacting storage S_f eventually becomes shallow subsurface flow towards the stream, denoted as Q_f. This flow is determined using a storage coefficient k_f [/d], also known as the fast flow recession coefficient. The water balance of the fast reacting storage is represented in equation 6.18.

$$Q_f = S_F * k_f \tag{6.17}$$

$$\frac{dS_F}{dt} = R_f - Q_F \tag{6.18}$$

Slow reacting reservoir

Percolation R_s [mm/d] recharges the groundwater storage, also called the slow reacting storage S_s [mm]. The slow reacting storage S_s is one reservoir shared by all the landscape classes and cells, where the flow R_s of each of the landscape classes contribute to the total storage amount in the groundwater based on their landscape fraction. The groundwater S_s then releases water as groundwater flow Q_s [mm/d]. This flow follows a linear relationship with S_s and a storage coefficient k_s [/d], shown in equation 6.19. The water balance then leads to the following shown in equation 6.20.

$$Q_s = \sum (S_s * f_L) * k_s \tag{6.19}$$

Where f_L represents the fraction of the landscape class present in the subcatchment.

$$\frac{dS_S}{dt} = R_s - Q_s \tag{6.20}$$

Wetland In wetlands, the dynamics of fast and slow reacting reservoirs differ from those in the hillslope classes. Consequently to the groundwater level being close to the surface, any throughfall that does not infiltrate the unsaturated root-zone storage is released as saturation overland flow, which drains into the stream as Q_f. This flow is routed through a storage equivalent of k_f. Saturation overland flow results from shallow groundwater tables with limited pore space, causing even small precipitation events to trigger fast flow responses. This contrasts with hillslopes, where groundwater tables are deeper.

Total streamflow

The overall water balance for the system, accounting for all inflows and outflow, is described by:

$$\frac{dS}{dt} = P_v + P_h - E_I - E_a - Q_f - Q_s - Q_{ff} + Q_r \tag{6.21}$$

The total streamflow at each timestep is computed as the sum of both fast and slow flows, weighted by the area of each spatial cell, as shown in Equation 6.22. Fast-responding reservoirs primarily contribute to peak flows via preferential flow paths and overland flow, while slow-responding groundwater reservoirs provide base flow contributions.

$$Q_{tot}(t) = \sum_{i=0}^{N_{\text{cells}}} f_i * (Q_{s,i}(t) + Q_{f,i}(t) + Q_{ff,i}(t)) \tag{6.22}$$

Where:

$$f_i = \frac{A_i}{A_{tot}} \tag{6.23}$$

Here, i represents the cell number and N_{cells} is the total number of spatial cells, f_i is the fraction of the total catchment area A_{tot} occupied by cell i and $Q_{s,i}(t)$ $Q_{f,i}(t)$ and $Q_{ff,i}(t)$ represent slow, fast, and overland flows, respectively. t represents the timestep.

To account for the lag in streamflow as water moves through the catchment, a lag function is applied. The final modelled streamflow is adjusted using a triangular smoothing function defined by the parameter T_{lag}, which represents the time it takes for water to travel from a specific point in the catchment to the outlet. This process is described in Equation 6.24.

$$Q_{\text{m}}(t) = \sum_{i=0}^{T_{\text{lag}}} Q_{tot}(t-i) \cdot w_i \tag{6.24}$$

Here, w_i are the smoothing weights. These weights, generated by the triangular transfer function, ensure that recent values have a stronger influence on the smoothed streamflow, while older values contribute less, effectively creating a lagged effect in the streamflow data. This helps reduce noise in the timeseries and emphasize underlying trends in streamflow behaviour.

6.2.4. Parameters

The FLEX-Topo model includes variety of parameters representing distinct aspects of the hydrological processes and storage components, tailored for each landscape class. Depending on the landscape's hydrological characteristics, not all parameters are applicable to every class. Below is an overview of the key parameters used in the model.

Interception storage parameters

- I_{max} [mm]: The maximum daily storage capacity of the interception reservoir, representing the canopy's ability to hold water. Present in landscape classes: I_{max} hillslope forest, I_{max} hillslope plantation, I_{max} hillslope agriculture and I_{max} wetland.

Soil and Root zone parameters

- $S_{u,max}$ [mm]: The maximum storage capacity of the unsaturated root-zone storage reservoir representing the volume of water that can be stored between the field capacity and the permanent wilting point of the root depth. Present for the landscape classes: $S_{u,max}$ hillslope forest, $S_{u,max}$ hillslope plantation, $S_{u,max}$ hillslope agriculture and $S_{u,max}$ wetland.
- C_e [-]: Evaporation coefficient, which is based on the relative soil moisture at which vegetation starts to experience water stress, affecting the actual evaporation rate. Present for all landscape classes and set equal to 0.5, as previously suggested by Savenije (1997).
- F_{max} [mm]: The maximum infiltration capacity of the soil, beyond which overland flow occurs. Only present for the landscape class hillslope agriculture.

Distribution parameters

- β [-]: The shape factor for throughfall distribution, representing the spatial heterogeneity of $S_{u,max}$. Present for the landscape classes: β hillslope forest, β hillslope plantation, β hillslope agriculture and β wetland.
- D [-]: Splitter parameter that controls the distribution of excess water between the fast subsurface recharge (R_f) and the groundwater recharge (R_s), dependent on the soil texture. Present for the landscape classes: D hillslope forest, D hillslope pine plantation, and D hillslope agriculture.

Flow Parameters

- C_{max} [-]: The recharge coefficient, the maximum fraction of upwelling groundwater flux (Q_r) that contributes to the unsaturated root-zone storage. Only present in the landscape class wetland.
- k_f [/d]: The fast flow recession coefficient, determining the rate at which water stored in the fast reacting reservoir is released as shallow subsurface flow. It characterizes the recession of streamflow following a precipitation event or runoff generation period. The recession coefficient helps understand how quickly excess water from precipitation is routed through the catchment and into the stream network. Present for the landscape classes: k_f hillslope forest, k_f hillslope plantation, k_f hillslope agriculture and k_f wetland.
- k_s [/d]: The slow recession coefficient, defining the rate at which groundwater is released from the slow reacting storage reservoir. k_s is assumed to be the same for each landscape class.
- T_{lag} [d]: Travel time through catchment to reach streamflow outlet. Characterized by the catchment sub-cells and not the landscape classes.

These parameters need to be calibrated to ensure accurate representation of the system's behaviour.

6.2.5. Disinformation

When analysing the water balance, inconsistencies were observed in the dataset, indicating that the data does not always satisfy the water balance equation. This suggests that the hydrological data may not consistently provide accurate information, potentially due to poor extrapolations or measurement errors (Beven and Westerberg, 2011). Since precipitation is measured outside the catchment, not all precipitation events occurring within the catchment are captured, leading to missing water inputs during streamflow simulations. Consequently, certain events in the hydrological dataset are identified as disinformative to prevent introducing errors in the model calibration process (Beven, 2024). Including such disinformative events can cause the model to adjust parameters to fit erroneous trends instead of actual hydrological behavior, leading to incorrect peak fitting and reduced accuracy.

Following a method similar to Beven and Smith (2013), disinformative data is identified by categorizing the hydrological data into distinct events. For each event, the runoff coefficient is calculated, and if this coefficient exceeds 1.1, the event is marked as disinformative. Events are defined based on the timing of precipitation and discharge: a new event begins when the previous day had no precipitation,

discharge was below a threshold of 6.5 mm/day, and the current day registers precipitation. During model calibration, events with a runoff coefficient greater than 1.1 are excluded to prevent inaccuracies in the calibration process.

6.2.6. Model Calibration and evaluation

Calibration is performed using the split-record method, which divides the available streamflow data into two distinct periods: 2012-2017 for calibration and 2018-2024 for validation. A spin-up period of 1.25 years, starting with a dry period to stabilize the model, is used.

To capture different stramflow characteristics, a multi-objective optimization approach is employed (Gupta et al., 1998). Nash-Cluttclif Efficiency (NSE) of the hydrograph is used to evaluate the model performance for the peak flows, the NSE of the logarithmic flow (logNSE) evaluates the performance of the baseflow and the third objective function is the NSE of the flow duration curve (FDC) (Nash and Sutcliffe, 1970) to asses overall flow variability, the equation for NSE is provided in Equation 6.25. Since these objectives are often in conflict, Pareto optimal solutions are used to identify the best trade-offs between competing objectives (Zitzler and L.Thiele, 1999).

$$NSE = 1 - \frac{\sum_{i=1}^{N}(Q_o - Q_m)^2}{\sum_{i=1}^{N}(Q_o - \overline{Q_o})^2} \tag{6.25}$$

The Non-dominated Genetic Algorithm II (NSGA-II) is used for the multi-objective optimization calibration process (Deb et al., 2002). This algorithm identifies an optimal solution set of parameters that balance multiple conflicting objectives. NSGA-II sorts solutions using non-dominated sorting, where one solution dominates another if it performs better in at least one objective without performing worse in others.

To ensure a diverse solution set, NSGA-II applies a crowding distance metric, preventing clustering of solutions and encouraging exploration of the objective space. Solutions are generated through standard genetic operations: crossover (combining parts of two solutions) and mutation (introducing small random changes). Latin Hypercube Sampling (LHS) is employed to ensure that the samples are equally distributed along the parameter space.

Table 6.5 presents the range of the parameters used for calibration for the 23 parameters, excluding C_e which is fixed at 0.5. These ranges are based on assumptions, literature, field observations and iterative testing.

Table 6.5: Parameter ranges for calibration FLEX-Topo Model, presented for the different landscape classes or for the catchment

Parameter	Unit	Wetland		Agriculture		Forest		Plantation		Catchment	
		Min	Max	Min	Max	Min	Max	Min	Max	Min	Max
I_{max}	[mm]	0.001	10	0.0001	10	2	10	1	10	-	
$S_{u,max}$	[mm]	10	1000	30	300	100	1000	50	800	-	
β	[-]	0.1	5	0.1	5	0.1	5	0.1	5	-	
C_e	[-]	0.5		0.5		0.5		0.5		-	
C_{max}	[-]	0.01	4	-		-		-		-	
D	[-]	-		0.1	0.99	0.1	1	0.1	1	-	
F_{max}	[mm]	-		5	300	-		-		-	
k_f	[1/d]	0.1	0.9	0.05	1	0.05	1	0.05	1	-	
k_s	[1/d]	-		-		-		-		0.0005	0.15
T_{lag}	[d]	-		-		-		-		0.0001	8

Parameter and process constraints

In developing parameter and process constraints, a comprehensive understanding of the study area, as detailed in Chapter 5, was utilized. The constraints developed, informed by previous studies (Gharari et al., 2015; Gao et al., 2014), aim to minimize unrealistic parameter combinations and reduce predictive

uncertainty. Any parameter set or simulation violating these constraints is classified as non-behavioral and excluded.

Forests are assumed to have the highest interception capacity (I_{max}), followed by pine plantations, then agricultural land.

$$I_{max_{Forest}} > I_{max_{Plantation}} > I_{max_{Agriculture}} \tag{6.26}$$

The unsaturated zone of a wetland is expected to have a shallower water table and therefore less maximum soil moisture capacity (Su_{max}) than the hillslope classes. Among the hillslope classes, forests are expected to have the deepest root zone and highest Su_{max}, followed by pine plantations and then agriculture.

$$Su_{max_{Forest}} > Su_{max_{Plantation}} > Su_{max_{Agriculture}} > Su_{max_{Wetland}} \tag{6.27}$$

The splitter parameter (D) is dependent on soil texture. The percolation in forests is expected to be the greatest due to its soil texture, followed by the landscape class pine plantions and least in in agriculture.

$$D_{Forest} > D_{Plantation} > D_{Agriculture} \tag{6.28}$$

The maximum unsaturated root-zone storage capacity ($S_{u_{max}}$ in agriculture should be larger than the maximum infiltration capacity (F_{max}) of agriculture.

$$Su_{max_{Agriculture}} > F_{max} \tag{6.29}$$

For fast flow recession coefficient (k_f), wetlands are assumed to have a higher fast flow recession coefficient than hillslope classes, assuming that the velocities of saturation overland flow in wetlands exceed those of flow velocities in preferential flow networks (Anderson et al., 2009). Also, the flow in preferential flow networks is assumed to be faster than the groundwater flow.

$$k_{f_{Wetland}} > k_f > k_s \tag{6.30}$$

Process constraints incorporate the assumption that forest and plantation classes have higher evaporative fluxes than agricultural land, attributed to their greater vegetation cover and deeper root systems. While it is anticipated that cloud forests would have reduced evaporative fluxes due to low radiation levels and high atmospheric humidity, this study assumes that the evaporative fluxes in forests generally surpass those in agricultural lands (Zadroga, 1981; Jarvis and Mulligan, 2010; Bruijnzeel, 2001). This assumption is based on the fact that not all forests within the forest landscape class are cloud forests.

Process constraints incorporate the assumption that forest and plantation classes exhibit higher evaporative fluxes than agricultural land, attributed to their greater vegetation cover and deeper root systems. While it is anticipated that cloud forests would have reduced evaporative fluxes due to low radiation levels and high atmospheric humidity, this study assumes that the evaporative fluxes in forests generally surpass those in agricultural lands. This assumption is based on the premise that not all forests within the forest landscape class are cloud forests, which may have lower evaporative rates (Zadroga, 1981; Jarvis and Mulligan, 2010; Bruijnzeel, 2001).

$$Ei_{Forest} + Ea_{Forest} > Ei_{Agriculture} + Ea_{Agriculture} \tag{6.31}$$

$$Ei_{Plantation} + Ea_{Plantation} > Ei_{Agriculture} + Ea_{Agriculture} \tag{6.32}$$

Following the study of Gharari et al. (2015), the runoff coefficient serves as another constraint. The annual runoff coefficient of observed streamflow is determined, from this the mean runoff coefficient and the standard deviation of the runoff coefficient are calculated. The annual modelled runoff coefficient should not exceed the mean annual coefficient with a deviation of three times the standard deviation.

$$\frac{\sum Q_m}{\sum P} > 0.37 \tag{6.33}$$

$$\frac{\sum Q_m}{\sum P} < 0.85 \tag{6.34}$$

Parameter selection
Following the calibration process, an envelope of parameter sets is generated, representing a variety of potential solutions that fit the observed data. This range defines an interval of plausible model behavior. From this set of solutions, one ”optimal” parameter set is selected using a trade-off analysis of the Pareto front. The knee-point, where improvements in one objective significantly worsen others, is identified as the optimal set for comparison reasons.

Model Evaluation
To avoid over-parameterization, model performance is evaluated using the 2018-2024 dataset. This evaluation tests whether the selected parameter set generalizes well to unseen data, ensuring it does not overfit the calibration period.

6.2.7. Disinformation precipitation events
After calibrating the model without the disinformative precipitation data, the adjustment of these precipitation values was carried out using a scaling factor optimized through an iterative objective function. The objective functions employed were the Nash-Sutcliffe Efficiency (NSE), mainly focusing on high flows in the optimization process.

Assuming that the discharge measurements and the model simulations are accurate, precipitation values were adjusted using multipliers. For cases where the model underestimates discharge, precipitation was scaled up using a factor greater than one, while for overestimated discharges, precipitation was scaled down using a factor less than one.

Once the optimal adjustment factors were determined, the modelled discharge was recalculated using the corrected precipitation data. These updated simulations were then compared visually and statistically with the observed discharge data to assess the effectiveness of the corrections. The adjusted precipitation values aim to improve the modelled streamflow accuracy and reliability of streamflow predictions.

6.3. Land use scenario analysis
Three distinct land use scenarios are developed to assess the impact of land cover change on hydrological processes in the Mestelá catchment.

- **Scenario Deforestation**: This scenario doubles the historical rate of deforestation in the catchment, representing an accelerated deforestation rate compared to observed trends.
- **Scenario Original Forest**: This scenario simulates a return to historical land cover, with 85% of the catchment restored to forest. Pine plantations are removed entirely, and the wetland areas remain unchanged. The remaining land is allocated to agriculture.
- **Scenario Pine Plantation**: In this scenario, all agricultural land on slopes greater than or equal to 30° is replaced with pine plantations.

Each of these land use scenarios is run using the FIESTA model to generate distributed meteorological inputs for the FLEX-Topo model. The calibrated model for the Upper Cahabon catchment is applied to the Mestelá catchment, using its own unique spatial characteristics. Streamflow simulations are first conducted for the baseline scenario of the Mestelá catchment, and then for all the changed land use scenarios to assess the impact of land cover change on streamflow dynamics.

To analyse the effects of land use change, streamflow quantiles are compared across scenarios, allowing for a detailed examination of different portions of the streamflow. Relative values of low and high flows are determined and compared to the baseline scenario. Low flows are defined as streamflow rates in the lowest quantiles, while high flows correspond to those in the highest quantiles. These relative values, expressed as fraction of the baseline, highlight changes in streamflow behavior.

Additionally, water balance components (e.g., total precipitation, evaporation, runoff) and model storage outputs (e.g., soil moisture, groundwater storage) are evaluated to explore the influence of land use on various hydrological processes. Lastly, monthly fluxes are compared to assess seasonal effects.

7

Results

This chapter presents the results from the hydrological modeling in the Upper Cahabon and Mestelá catchment. Firstly, the results of the FIESTA model are presented, which are used to generate spatially distributed meteorological inputs, focusing on precipitation, fog interception and potential evaporation. Following this, the results from calibration and evaluation of the FLEX-Topo are shown, including an analysis of the adjustments made to disinformative precipitation events to improve model accuracy.

Next, this chapter presents the results of different hydrological processes associated with different landscape classes, exploring how each land use type influences water balance components such as evaporation and runoff. Finally, the results of three land use scenarios are presented, comparing streamflow, water balance, and the influence of land use changes on low and high flow conditions as well as extreme events.

Each section builds on the previous analysis to provide a comprehensive understanding of the impact of meteorological inputs, land cover, and land use changes on hydrological dynamics in the catchment.

7.1. Spatially distributed meteorological data

The FIESTA model produced spatially distributed meteorological inputs of the following variables; precipitation [mm/day], fog interception [mm/day] and potential evaporation [mm/day], to be used as input for the hydrological FLEX-Topo model. Results for the Mestelá catchment and its sub-divided 48 spatial classes are shown.

Precipitation

The FIESTA model has been used to generate wind-adjusted precipitation spatially distributed estimates for the Upper Cahabon and Mestelá catchment, results for the Mestelá catchment are shown here. Results show that northern and eastern aspects receive the highest precipitation, as winds predominantly originate from these directions. While elevation does not significantly affect precipitation values, slope plays a subtle role, with minor variations based on the slope's orientation, see Section 7.1.3 for the spatial variability of precipitation in the Mestelá catchment. Figure 7.1a illustrates the mean monthly precipitation [mm/day] for all spatial classes, including the ranges of minimum and maximum mean values across these classes.

The mean annual precipitation for the Mestelá catchment varies, ranging from 1,606 mm per year during a dry year in 2009 to 3,331 mm per year in 2020, which was an exceptionally wet year. For the period with available streamflow data, the modelled mean annual precipitation is 2,249 mm/year, slightly lower than the measured mean annual precipitation in Cobán, which is 2,288.0 mm/year. The year with the highest number of dry days was 2005, with a total of 176 days without rainfall, followed by 2019 and 2023 with 158 dry days each. There is no spatial variation in dry days across the catchment, as the input precipitation is applied uniformly. The longest period without rainfall, in the recent 10 years, occurred in 2023, lasting 21 consecutive days from February to March.

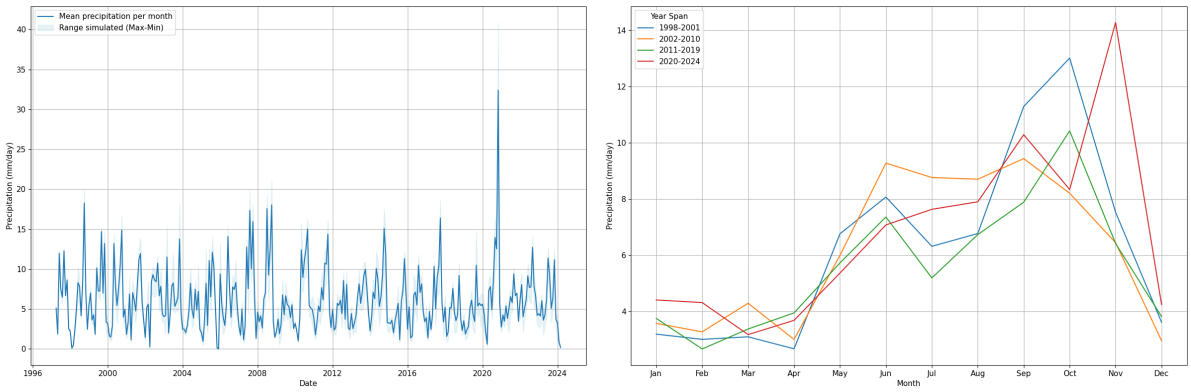

(a) Average precipitation per month in mm per day, with the maximum and minimum range of all the spatial classes

(b) Mean daily of precipitation per month of the year for different year spans

Figure 7.1: Wind-adjusted precipitation for the Mestelá catchment (1997-2024)

Over the entire 1997-2024 period, October experienced the highest daily rainfall at 9.7 mm/day, while February recorded the lowest at 3.3 mm/day. Figure 7.1b shows the monthly distribution of daily precipitation across different time spans. Notably, the periods 1998-2001 and 2020-2024, both associated with La Niña events, experienced more intense rainfall events.

A noticeable shift in in wet and dry season can be observed in Figure 7.1b, with recent years showing a delayed start of the rainy season, longer dry periods, and a peak in precipitation occurring in October to November, averaging 12.8 mm/day. Whereas, before 2011, the dry season typically spanned from December to April and the wet season occurring from May to October.

7.1.1. Fog Interception

The modelled fog interception in the Mestelá catchment from 1997 to 2024 is shown in Figure 7.2. The results indicate a notable decline in fog interception over the years, categorized by spatial classes with the same elevation. Figure 7.2a displays the mean daily fog interception for all years, showing a clear distinction between spatial classes below and above an elevation of 1840 m. Above an elevation 1840 meters the fog interception gives similar values. Prior to 2017, the average annual fog interception across all spatial classes was 122 mm/year. However, post 2017, this value decreased to just 54 mm/year, representing a 56% reduction. The highest recorded mean daily fog interception occurred in 1999 at 0.95 mm/day, whereas in 2019 the lowest estimated mean daily fog interception was modelled at 0.15 mm/day.

Figure 7.2b highlights the seasonal variation in fog interception. At an elevation of 1515 metres, fog interception is relatively low, averaging at 0.08 mm/day. This is because the mean lifting condensation level is at approximately 1740 meters. During the certain months; October, November, December and January, the lifting condensation level drops, allowing vegetation at this elevation to intercept more fog. These months also show the highest fog interception of the year, due to elevated humidity and lower temperature levels. Conversely, in April, when the humidity levels are at its lowest, lifting condensation levels highest, the fog interception is the least of the year.

Figure 7.2c shows the mean fog interception for spatial classes at 2540 meters, highlighting both minimum and maximum monthly values for all the spatial classes at this elevation. This figure reveals a broad range of daily fog interception values across the Mestelá catchment, with an average of 0.313 mm/day at this elevation. Some months record a mean daily interception exceeding 6 mm/day.

Land use also plays a critical role in fog interception. Areas with a high forest fraction (forest fraction between 0.8 to 1) show the highest mean daily fog interception, averaging 0.6 mm/day. In contrast, regions with sparse forest cover (forest fraction between 0 and 0.2) show much lower interception rates, ranging from 0 to 0.1 mm/day. Agricultural areas show the lowest fog interception values.

(a) Mean daily fog interception for each year grouped by elevation of spatial classes

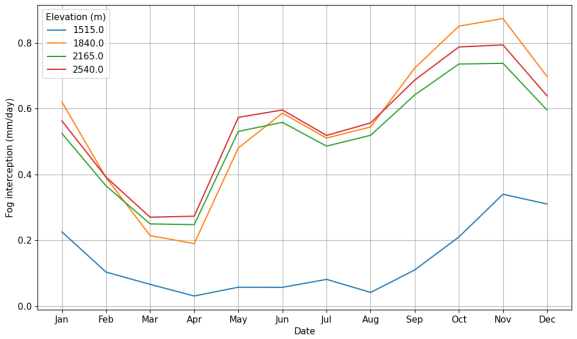

(b) Mean daily fog interception for each month of the year grouped by elevation of spatial classes

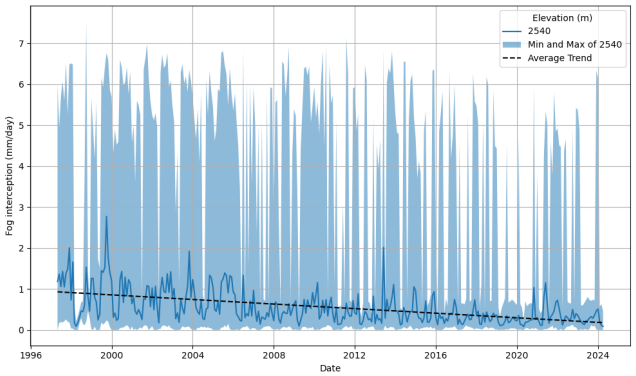

(c) Mean daily fog interception for all months of all spatial classes at elevation 2540m

Figure 7.2: Results fog interception in mm/day of FIESTA model for the Mestelá catchment 1998-2024

Figure 7.3 show the percentages of fog interception relative to all the water inputs. Considering all elevation classes above 1515 meters, the average value of fog interception wind-driven precipitation is 8.3% across the years 1997-2024. After 2012, this value decreases to an average of 5%.

Figure 7.3a shows the highest percentage of fog interception compared to precipitation occur in the months December and January, when fog interception rates are high, but precipitation rates are not. Figure 7.3b further illustrates a declining trend in the percentage of fog interception relative to precipitation over time, due to fog interception values decreasing over time.

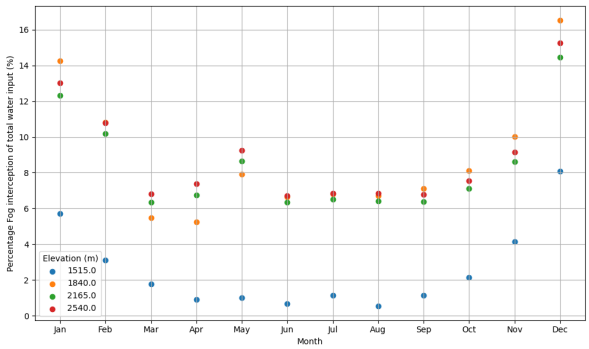

(a) Percentage fog interception of total water input per month of the year

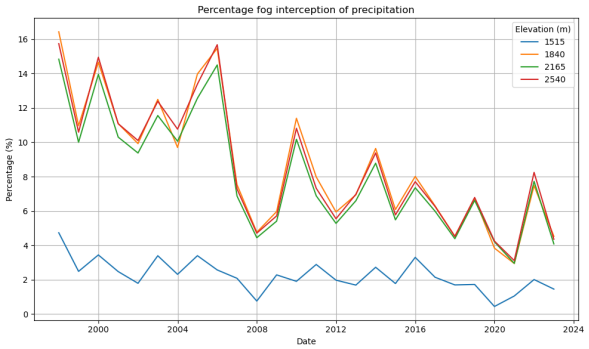

(b) Percentage fog interception of total water input for each year

Figure 7.3: Percentage fog interception of total net precipitation for the Mestelá catchment 1997-2024

7.1.2. Evaporation

The potential evaporation values modeled by the FIESTA, to be used for the FLEX-Topo model are shown in Figure 7.4. There is no trend observed over the years, all mean potential evaporation values of all the spatial values are between 0.36 mm/day and 4.7 mm/day. Seasonality is shown in Figure 7.4b, April being the month with the most potential evaporation and the month October the least. There is only a small difference in potential evaporation values when comparing mean values of elevation classes.

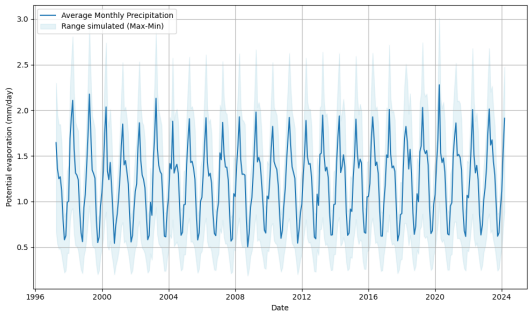

(a) Mean daily potential evaporation for each month, including mean, minimum and maximum value of all spatial classes.

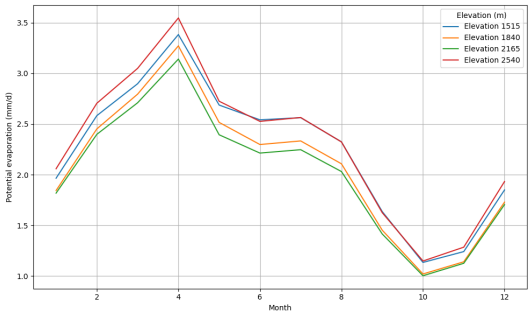

(b) Mean potential evaporation rate for each month of the year characterized by elevation spatial classes

Figure 7.4: Potential evaporation modeled for the Mestelá catchment 1997 - 2024

7.1.3. Analysis of spatial patterns

The spatial variability of the meteorological inputs for the hydrological model for the Mestelá catchment is shown in Figure 7.5.

The mean annual precipitation varies across the catchment, as can be seen in Figure 7.5a, with the lowest values, 1,645 mm/year, observed in areas with the steepest slopes and aspects facing south. In contrast, areas with a northern aspect, which capture the predominant northward wind, receive the highest precipitation, averaging 2,425 mm/year on gentle slopes. Before the wind-driven adjustment has been made, the mean annual precipitation is measured to be 2,273 mm/year everywhere in the catchment. Eastern slopes receive slightly less rainfall than northern slopes, with a mean difference of about 30 mm/year. Overall, the results of the FIESTA model show that northern and eastern aspects capture 21% more wind-driven precipitation than Southern aspects.

Figure 7.5b shows the spatially distributed mean annual potential evaporation values. North facing aspects show least potential evaporation rates, due to the least solar radiation, with an mean annual evaporation rate of 653 mm/year, compared to south facing aspects with the highest mean annual potential evaporation value of 920 mm/year. Additionally, low slopes (925 mm/year) show a trend of having more potential evaporation compared to high slopes (596 mm/year).

Fog interception demonstrates the highest spatial variability among all meteorological inputs, as shown in Figure 7.5c. For spatial classes at an elevation of 1515 meters, the mean annual fog interception is 48.1 mm/day, representing only 24.4% of the mean fog intercepted at an elevation of 2540 meters, with a mean annual interception of 196.5 mm/year. Elevation classes at 1840 meters and 2165 meters record annual mean fog interceptions of 196.9 mm and 182.9 mm, respectively.

Consistent with precipitation patterns, aspects facing north and east receive approximately 11% more annual fog interception compared to those facing south and west. Additionally, higher slopes generally have higher interception capacities, often due to higher slopes being located on higher elevations. The highest fog interception occurs at an elevation of 1840 meters on a North-facing slope of 50 degrees, with mean annual fog interception of 260 mm/year, followed by a similar slope at an elevation of 2165 meters with 200 mm/year.

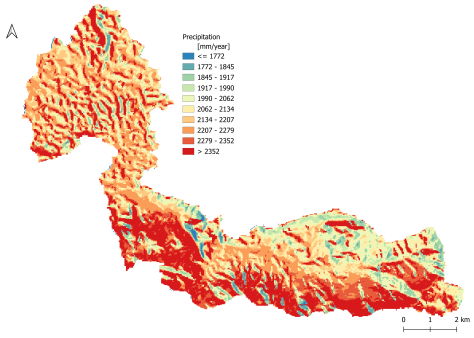

(a) Spatial patterns of mean annual precipitation of the Mestelá catchment.

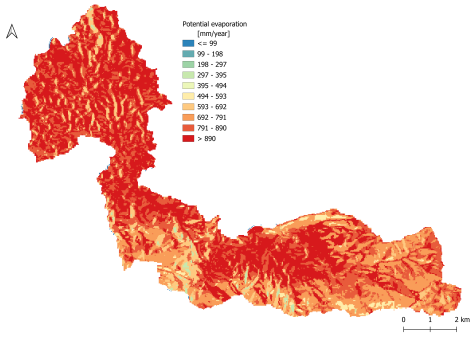

(b) Spatial patterns of mean annual potential evaporation of the Mestelá catchment.

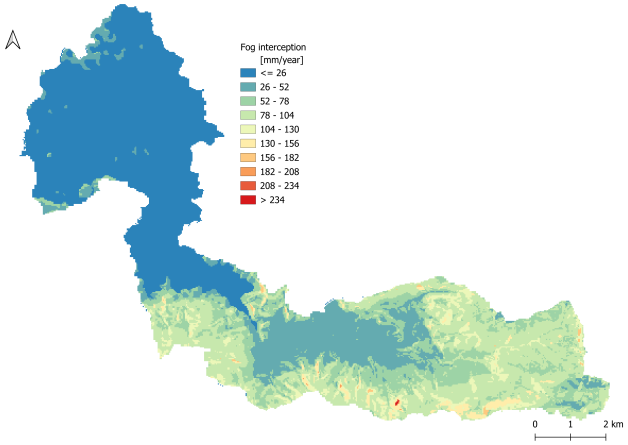

(c) Spatial patterns of mean annual fog interception of the Mestelá catchment.

Figure 7.5: Spatial distribution of meteorological data developed with the FIESTA model mean annual values for 1997-2024

7.2. FLEX-Topo model

The FLEX-Topo model is utilized to simulate streamflow in the Upper Cahabón and Mestelá catchment, considering four key landscape classes: hillslope forest, hillslope pine plantation, hillslope agriculture and wetland. The catchment is divided into 48 spatial classes, each spatial class with individual forcing data. Across spatial classes parameters are shared, but are different for each landscape class. The Upper Cahabon catchment is used for calibration.

The developed FLEX-Topo model structure incorporates spatially distributed input data and a shared groundwater reservoir, which is run to simulate the streamflow in the Upper Cahabon catchment. Once the streamflow for the Mestelá catchment is determined, scenarios are run to assess the impact of land use changes on the streamflow dynamics.

This section will present the results of the calibration and evaluation which is performed to identify optimal parameter sets for the region. Following this, the model will be run with the forcing input for the Mestelá catchment to simulate the streamflow. The influence of each of the different landscape classes; hillslope forest, hillslope pine plantation, hillslope agriculture and wetland are also presented.

7.2.1. Disinformative data

The hydrological data is divided into 577 individual events, among which 186 events of varying lengths have been classified as disinformative data. Figure 7.6a shows the informative marked data, with precipitation data shown in blue and streamflow in black, which is used for calibration. Figure 7.6b shows the hydrological events which are marked as disinformative, with each color representing a different event.

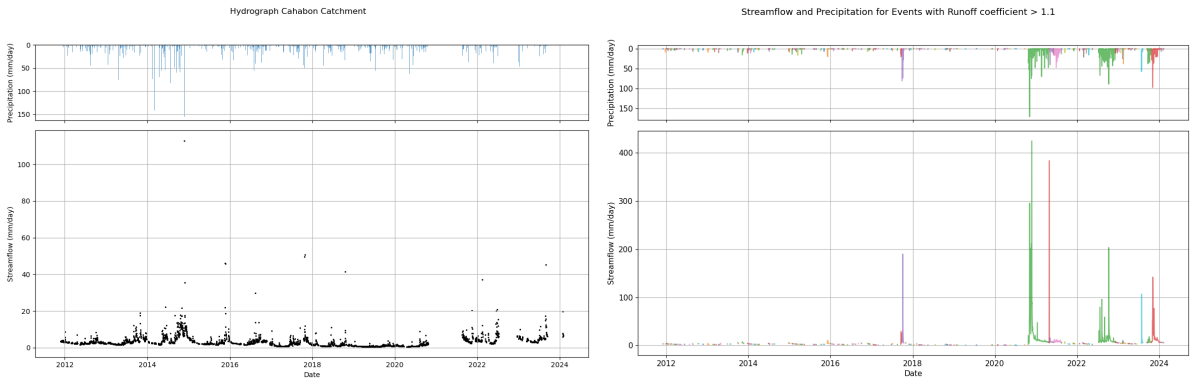

(a) Informative precipitation (blue) and streamflow (black) data used for calibration

(b) Disinformative hydrological data, sorted in different events represented with different colors

Figure 7.6: Division of informative and disinformative data

7.2.2. Calibration and model evaluation

The calibration of the model was conducted over the period from 2014 to 2017, with the subsequent evaluation period from 2018 to beginning of 2024. The choice of theses periods is based on the availability and quality of data, with 2014-2018 providing more informative and reliable data compared to 2018-2024.

To assess the model's performance, a multi-objective calibration was carried out using the Nash-Sutcliffe Efficiency (NSE) for streamflow, its logarithmic variant (logNSE). The results are illustrated by the Pareto front in Figure 7.7, showing the trade-off between these two objective functions.

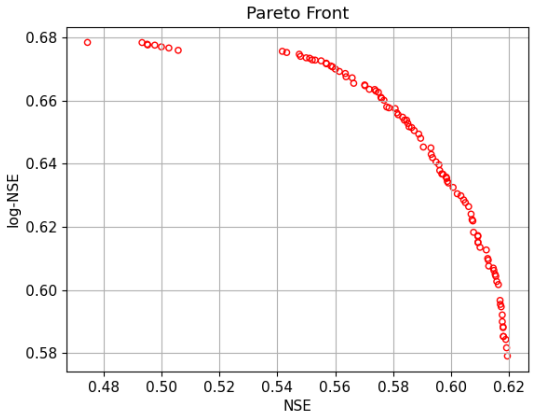

Figure 7.7: Pareto front of multi-objective calibration using Nash-Sutcliffe Efficiency for streamflow and log-transformed streamflow.

A selection of parameter sets from the Pareto front is considered, with a focus on baseflows, resulting in a total of 53 parameter sets. This selection allows for the calculation of prediction intervals for streamflow, as all these parameters represent potential outcomes. The variability of the different parameter results of this envelope of parameters is shown in Figure 7.8 and 7.9, including the variability among different landscape classes. These swarm plots show the number of times a certain value of a parameter set occurs, by representing it with a data point.

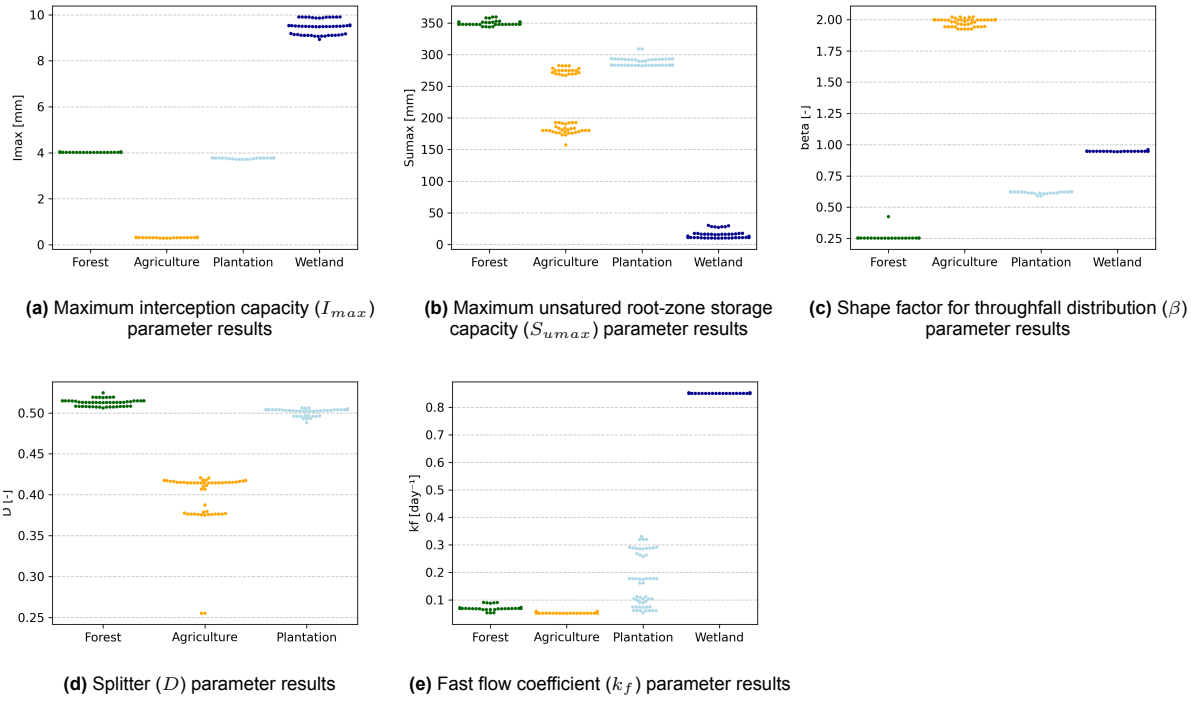

(a) Maximum interception capacity (I_{max}) parameter results

(b) Maximum unsatured root-zone storage capacity (S_{umax}) parameter results

(c) Shape factor for throughfall distribution (β) parameter results

(d) Splitter (D) parameter results

(e) Fast flow coefficient (k_f) parameter results

Figure 7.8: Swarm plot illustrating the distribution of parameter values for each landscape class. Each data point represents an individual parameter value, highlighting the frequency and variability of parameter occurrences across the different landscape classes.

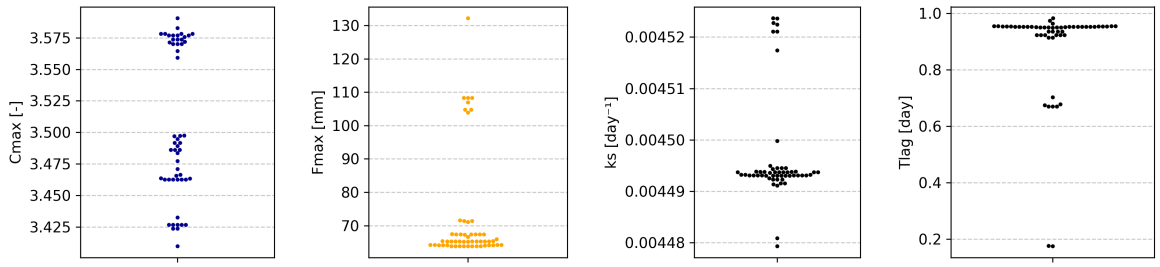

(a) Recharge coefficient ($Cmax$) parameter results

(b) Maximum infiltration capacity (F_{max}) parameter results

(c) Slow recession coefficient (k_f) parameter results

(d) Travel lagged time (T_{lag}) parameter results

Figure 7.9: Swarm plot illustrating the distribution of parameter values. Each data point represents an individual parameter value, highlighting the frequency and variability of parameter occurrences.

An ”optimal” parameter set was chosen from the non-dominated knee point of the Pareto-front, for assessment of model performance and comparison of precipitation adjustment performance. This parameter set is shown in Table 7.1.

Table 7.1: Optimal Parameters from Calibration of FLEX-Topo Model

Parameter	Unit	Wetland	Agriculture	Forest	Plantation	Catchment
I_{max}	[mm]	9.87	0.32	4.04	3.76	–
$S_{u,max}$	[mm]	27.02	182.95	359.45	289.45	–
β	[-]	0.95	2.00	0.25	0.62	–
C_{max}	[-]	3.49	–	–	–	–
D	[-]	-	0.39	0.51	0.50	–
F_{max}	[mm]	–	65.25	–	–	–
k_f	[1/d]	0.85	0.054	0.068	0.33	-
k_s	[1/d]	–	–	–	–	0.0045
T_{lag}	[d]	–	–	–	–	0.95

The objective function scores for the calibration period and evaluation period, excluding disinformative precipitation events, is shown in Table 7.2. The calibration period shows higher performance in the objective function scores compared to the evaluation period. It is important to note that the evaluation results are influenced by the considerable number of disinformative dates, which were not considered in the calculation of these objective functions.

Table 7.2: Objective function scores comparing model performance of calibration and evaluation period with only selected informative data of selected ”optimal” parameter set.

	Calibration period	Evaluation period
NSE	0.589	0.167
NSE_{log}	0.649	0.235
NSE_{FDC}	0.548	0.233
$\text{NSE}_{\text{logFDC}}$	0.955	0.759

The simulated streamflow values are compared to the observed data for both the calibration and evaluation periods. The results, shown in Figure 7.10, include precipitation, with ranges from all spatial classes, and the average dynamic land-use fraction of the catchment.

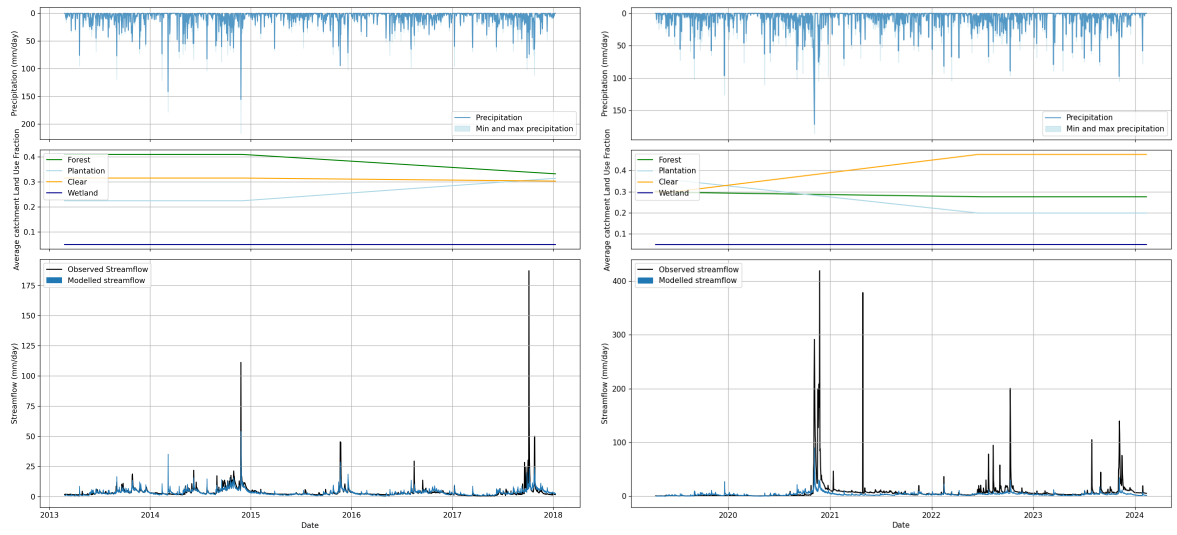

(a) Streamflow simulation during the calibration period

(b) Streamflow simulation during the evaluation period

Figure 7.10: Comparison of observed and modeled streamflow during calibration and evaluation, using the parameter set envelope from the Pareto front. Precipitation and average land use fractions of the catchment are also presented.

Additionally, flow duration curves (FDC's) are generated to assess the model's ability to capture streamflow behavior across the full range of flow conditions. Figure 7.11 shows the FDC's for both the calibration and evaluation period, further highlighting model performance. For the evaluation period the flow duration curve shows underestimation of streamflow during high flow events and overestimation of streamflow during low streamflow values. The modelled streamflow in the model is developed with the determined optimal parameter set, while for the prediction interval all the parameter sets are considered.

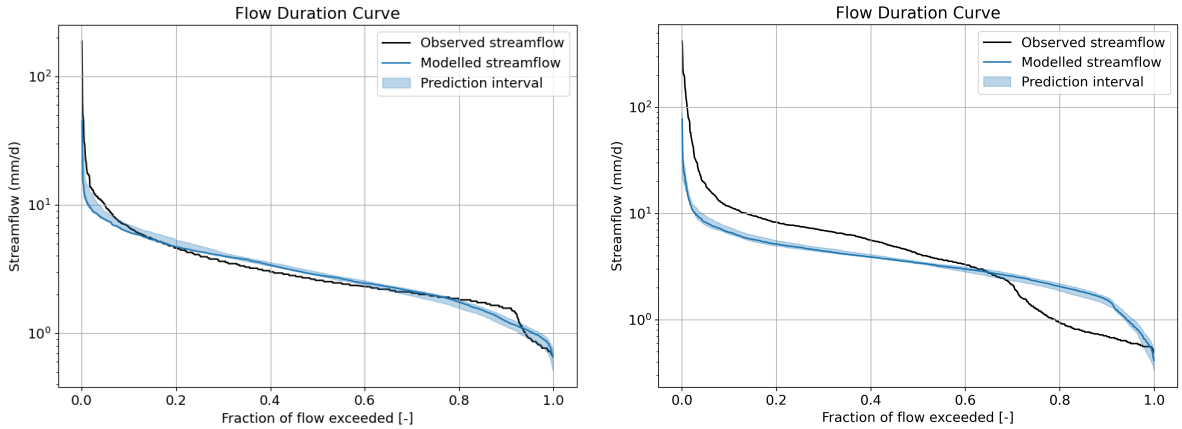

(a) Flow duration curve for the calibration period

(b) Flow duration curve for the evaluation period

Figure 7.11: Comparison of observed streamflow and modelled streamflow Flow Duration Curve

7.2.3. Precipitation adjustment

The optimal scaling factors used to correct the precipitation data are presented in Figure 7.12. A total of 229 precipitation dates were adjusted according to the scaling rates shown.

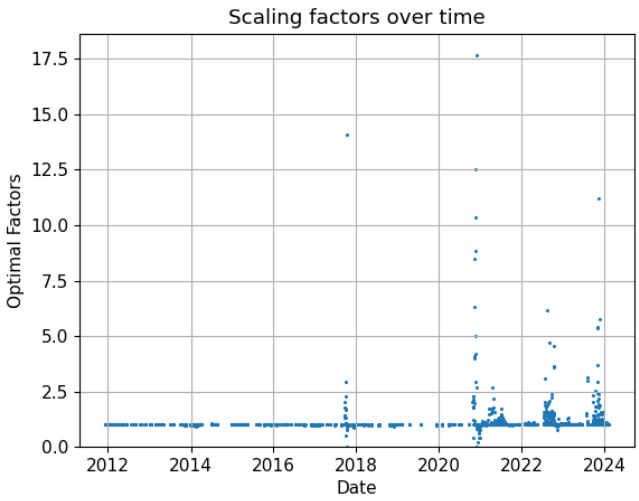

Figure 7.12: Optimal scaling factors for precipitation correction

Figure 7.13 demonstrates the model performance before and after precipitation adjustment. Before correction, the model shows a consistent underestimation of streamflow, with a noticeable upward trend indicating a growing error between modelled and observed values. After applying the adjusted precipitation, there is a significant improvement in the fit between the observed and the modelled streamflow, though some bias remains. Overall, the adjusted precipitation enhances model accuracy.

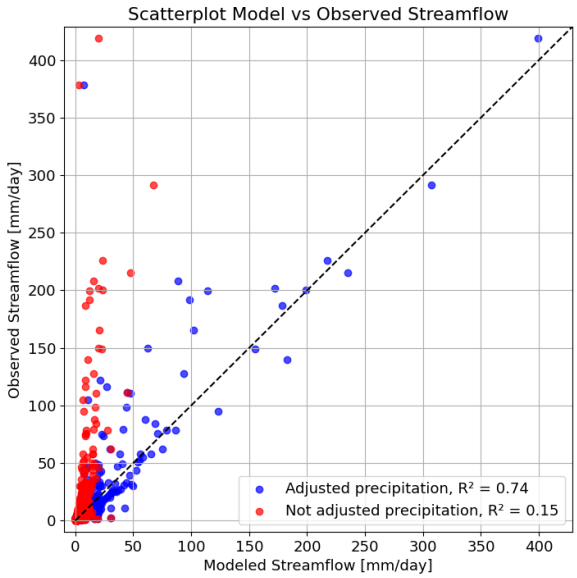

Figure 7.13: Scatterplot showing modelled vs. observed streamflow using original precipitation and adjusted precipitation

The improvement in model performance is further reflected in the objective function values, as shown in Table 7.3. These values, calculated using the optimal parameter set, highlight the positive impact of precipitation correction, even when considering disinformative data points.

Table 7.3: Objective function scores comparing model performance with and without precipitation correction

	Calibration (Non-Corr.)	Calibration (Corr.)	Evaluation (Non-Corr.)	Evaluation (Corr.)
NSE	0.302	0.755	0.133	0.737
NSE_{log}	0.639	0.627	0.484	0.715
NSE_{FDC}	0.505	0.873	0.204	0.941
NSE_{logFDC}	0.943	0.966	0.741	0.845

7.2.4. Simulated streamflow

Upper Cahabón catchment

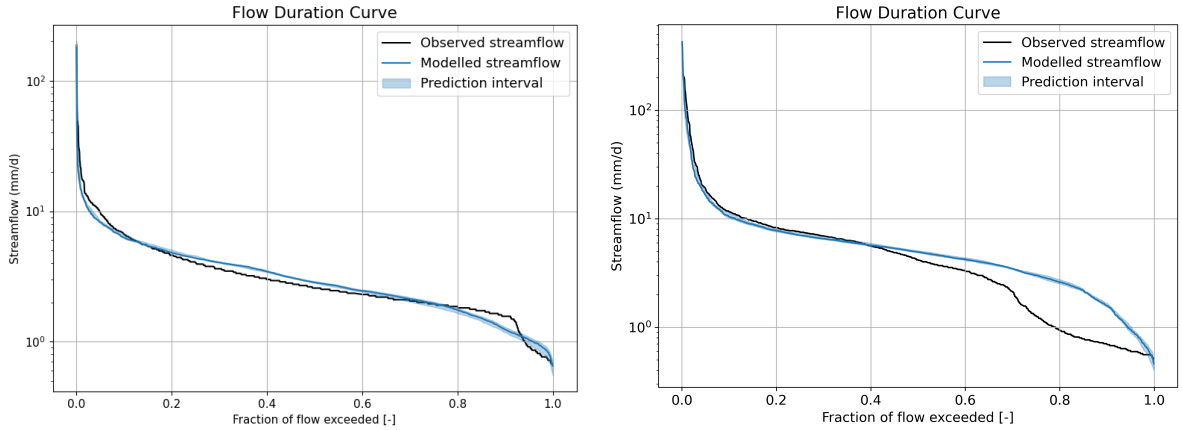

(a) Flow duration curve for the calibration period

(b) Flow duration curve for the evaluation period

Figure 7.14: Comparison of observed streamflow and modelled streamflow Flow Duration Curve

Figure 7.14 presents the flow duration curves for the modelled flow using the adjusted precipitation values. The adjusted values show an improved fit across the various flow components of the observed streamflow data. However, an overestimation of low flows persists during the evaluation period.

The corrected precipitation scaling factors are applied, and the resulting hydrograph for both the calibration and evaluation period is shown in Figure 7.15. This figure displays the model inputs, precipitation and fog interception, with the corresponding minimum and maximum ranges across all spatial cells. It also illustrates changes in mean landscape fractions over times, which are used as inputs in the model. A notable peak flow in 2020 is not captured by the modelled streamflow despite the adjusted precipitation values. This discrepancy occurs because the measured precipitation during that period was very low, requiring an unusually high scaling factor to align it with observed data.

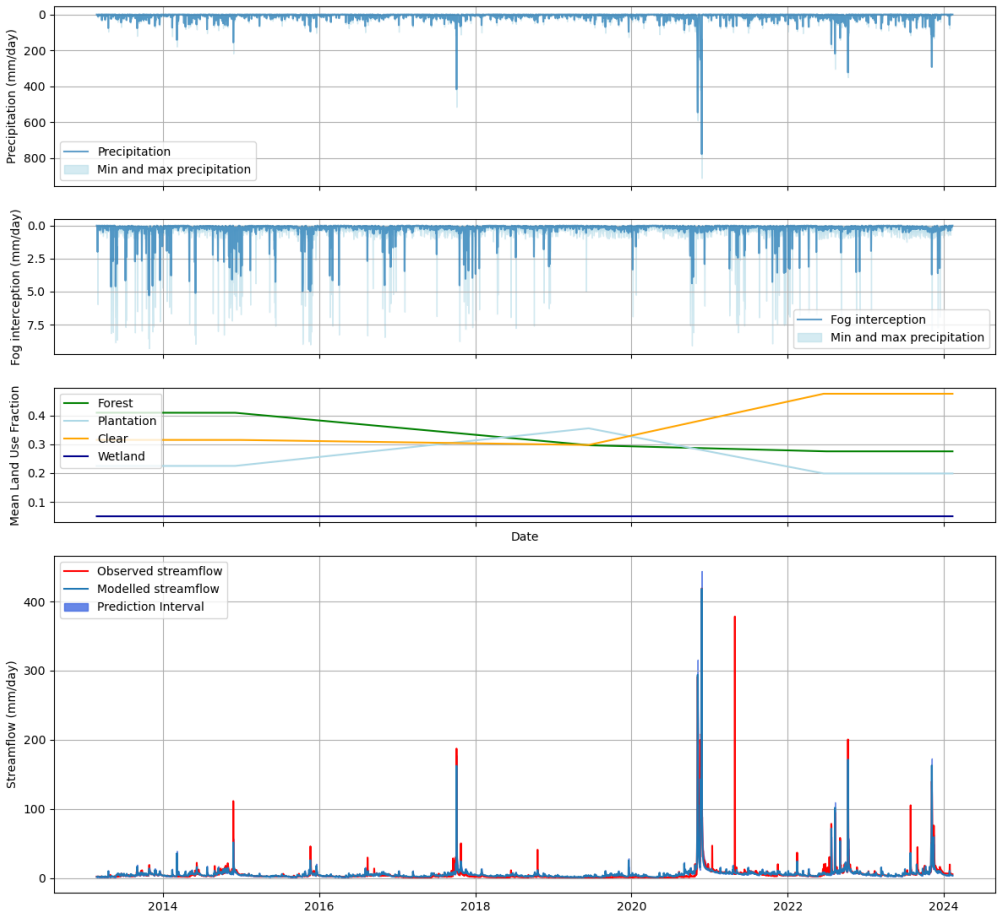

Figure 7.15: Observed and modeled streamflow hydrographs for the calibration and validation period, including the envelope of Pareto-optimal parameter sets. The mean precipitation, mean fog interception, and mean landscape fractions used as inputs to the FLEX-Topo model are also displayed.

An overview of all the mean annual water balance components of the modelled streamflow is shown in Table 7.4. This table includes the possible ranges of mean annual fluxes and the percentage of its contribution to the total water balance.

Table 7.4: Summary of average annual fluxes, ranges, and percentage contributions for different hydrological components in the Upper Cahabon catchment.

Flux Type	Mean (mm/year)	Range (mm/year)	Percentage Range (%)
Streamflow (Q)	2007.4	(1994.0, 2037.5)	—
Transpiration (Ea)	701.1	(694.64, 703.51)	(24.33, 24.89)
Interception Evaporation (Ei)	113.9	(113.15, 114.52)	(3.96, 4.04)
Shallow Subsurface Flow (Qf)	1094.3	(1094.26, 1200.24)	(38.37, 41.97)
Groundwater Flow (Qs)	657.1	(576.79, 690.11)	(20.18, 24.33)
Overland Flow (Qff)	256.8	(160.29, 260.69)	(5.67, 9.16)
Recharge (Qr)	13.2	(12.85, 14.71)	(0.45, 0.52)

The average annual modelled streamflow is 2007.4 mm/year, slightly lower than the observed streamflow of 2042.2 mm/year, primarily due to underestimation of peakflow. The largest outgoing flux is shallow subsurface flow (Qf), averaging 1094.3 mm/year and accounting for 38.6% of the total outgoing fluxes. The second largest flux is transpiration (Ea), contributing to 24.7% with an annual mean of 701.1 mm/year. Groundwater flow (Qs) represents 23.2% of the outgoing fluxes, with 657.1 mm/year, while overland flow (Qff) has an annual average of 256.8 mm/year, contributing 9.0% to the fluxes. Interception evaporation (Ei) accounts for 4.0%, at 113.9 mm/year. Recharge contributes only around 0.5%, indicating that it rarely adds to streamflow, this is a negative flux, meaning that water is recharged towards the groundwater. These ranges indicate the sensitivity of each hydrological component to the parameter sets. The interception evaporation (Ei) and recharge (Qr) have the smallest variation in both absolute values and percentages, whereas fast flow (Qf) and slow flow (Qs) show higher variability.

The contribution of water balance components for each landscape class individually is shown in Table 7.5, highlighting the hydrological processes of each landscape class. These fluxes are determined using the optimal parameter set. These fluxes provide insight into how different landscape classes contribute to the overall modeled streamflow, with taken into consideration the fraction of land cover present in the catchment, shown in Figure 7.15. Figure 7.16 illustrated the individual contributions of each landscape class, assuming the entire catchment was represented by that specific class. This analysis excludes land-use distribution and focuses solely on flux contributions per landscape type.

Table 7.5: Contribution of landscape classes to the modelled streamflow by showing the modelled fluxes.

	Hillslope Forest	Hillslope Pine plantation	Hillslope Agriculture	Wetland
P [mm/year]	929.6	788.5	1136.6	152.8
Ph [mm/year]	32.5	-	-	-
Ea [mm/year]	232.6	181.9	251.4	34.7
Ei [mm/year]	54.8	40.4	6.2	12.5
Qf [mm/year]	327.4	282.7	363.9	119.8
Rs [mm/year]	347.6	287.2	257.7	-
Qff [mm/year]	-	-	257.7	-
Qr [mm/year]	-	-	-	14.2

For land-use comparison, the forest landscape its largest flux is groundwater recharge (Rs) (36.4%), followed by shallow subsurface flow (Qf) with 35.1%. For evaporative fluxes, interception evaporation (Ei) (5.4%) together with transpiration (Ea) (23.2%) contribute to almost 30% of all the fluxes, showing the dominant evaporation function of forests. Pine plantations show a similar trend, where groundwater recharge (Rs) is a key flux (35.9%), followed by shallow subsurface flow (Qf) (35.6%). Compared to forests there is a slight larger contribution to shallow subsurface flow than to groundwater. High evaporation rates are also observed, with 23.5% of fluxes being transpiration and 5.0% interception evaporation. Agriculture, on the other hand, demonstrated overland flow (13.5%) and high fast flow rates (36.6%), showing the large contribution of agriculture to rapid runoff, with smaller evaporating fluxes with a total of 23.7%. Wetlands, while having the smallest overall contribution have a large proportion of fast flow (72.4%) with small recharge fluxes (1.8%).

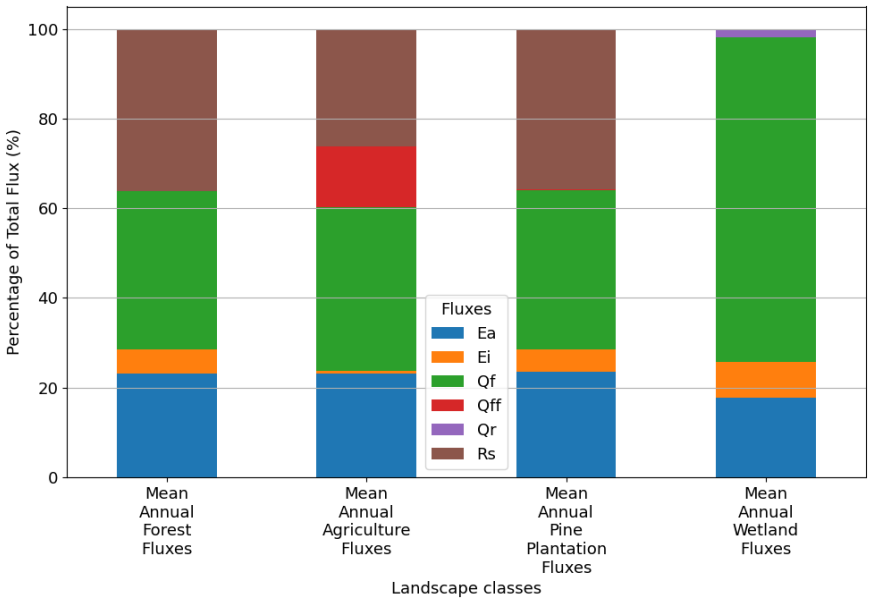

Figure 7.16: Outgoing fluxes percentages of the different landscape classes

These results show how different landscape types influence water movement within the catchment. Forest and pine plantations contribute less to fast streamflow with more evaporation and large contributions to the groundwater flow. Showing the importance of these forests for maintaining baseflow during dry periods. Agriculture, however, is associated with higher runoff, contributing more to peak flow. These contributions to the streamflow parts are shown in Figure 7.17 for different time periods.

The figures below illustrates the contribution of different landscape classes to flow generation. Figures 7.17a and 7.17b show that storm response is primarily dominated by hillslope agriculture, due to overland flow (Qff), while the other landscape classes contribute to peakflow trough subsurface flow. There is an increase in baseflow after the peak streamflow event. Figure 7.17c and 7.17d shows that hillslope forest plays a key role in sustaining flow, with contribution to fast flow components and groundwater flow, the same is true for the landscape class pine plantation, though in a lesser extent. Hillslope agriculture has a constant contribution to streamflow through shallow subsurface flow, resulting in smaller peaks and fast response to precipitation.

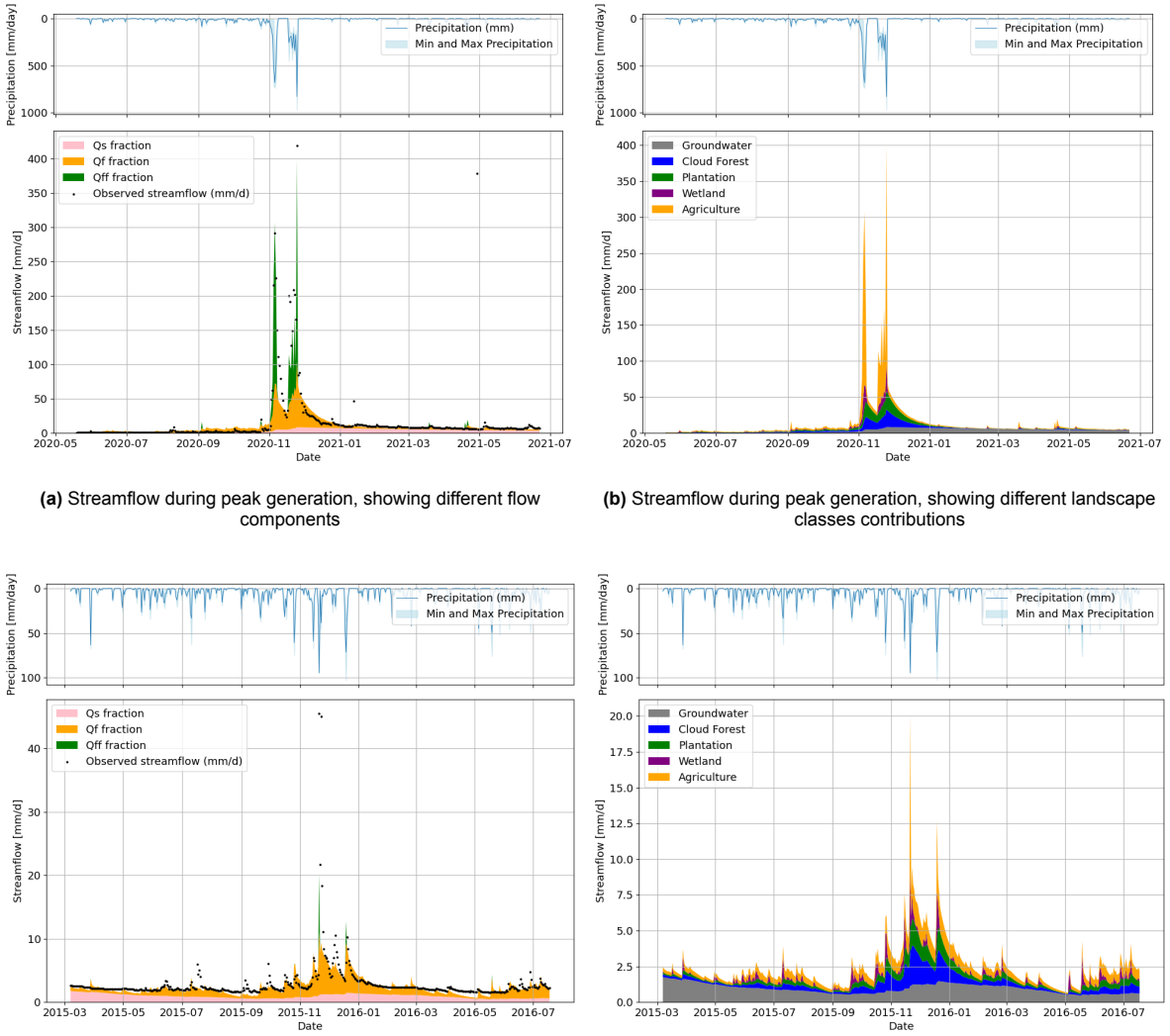

(a) Streamflow during peak generation, showing different flow components

(b) Streamflow during peak generation, showing different landscape classes contributions

(c) Streamflow during mean flow conditions, showing different flow components

(d) Streamflow during mean flow conditions, showing different landscape classes contributions

Figure 7.17: Hydrographs with precipitation showing different components contributing to streamflow, flow components and land use classes, during times of peak flow and mean flow conditions

Mestelá catchment

Using the optimal parameter sets and the meteorological inputs developed by the FIESTA model, the streamflow for the Mestelá catchment is simulated. The results are shown in Figure 7.18. The mean annual modelled streamflow is 2135.9 mm/year. Considering the larger fraction of forest and smaller fraction of pine plantation hillslope, there are more fluxes from the forest landscape class compared to the Upper Cahabon catchment. The Mestelá catchment is used to make land use scenarios, and therefore the land use contributions are further analysed in the following section.

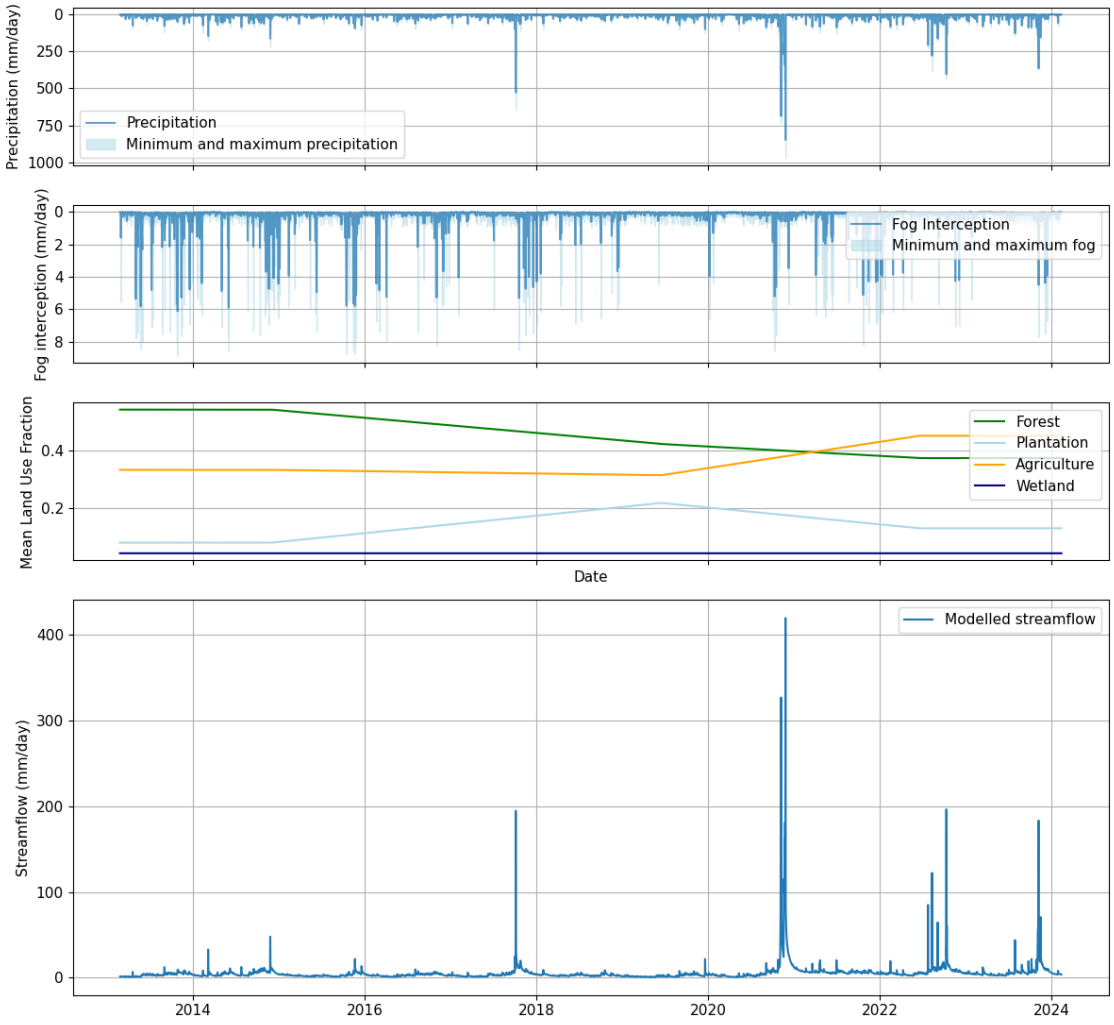

Figure 7.18: Hydrograph Mestelá catchment including precipitation, fog interception and the land use fractions.Envelope of optimal parameter sets shown.

7.3. Land use change

The following scenarios are run to analyse the impact of land use changes on the streamflow dynamics in the Mestelá catchment:

- **Scenario Deforestation**: This scenario doubles the historical rate of deforestation in the catchment, representing an accelerated deforestation rate compared to observed trends.
- **Scenario Original Forest**: This scenario simulates a return to historical land cover, with 85% of the catchment restored to forest. Pine plantations are removed entirely, and the wetland areas remain unchanged. The remaining land is allocated to agriculture.
- **Scenario Pine plantation**: In this scenario, all agricultural land on slopes greater than or equal to 30° is replaced with pine plantations.

7.3.1. Results of land use change of FIESTA model

Figure 7.19 compares the FIESTA model results for each land use scenario, representing the mean values across all spatial classes without accounting for their specific areas. The areas of each spatial class are incorporated in the FLEX-Topo model simulations. Figure 7.19a shows the mean annual fog

interception rates for the different land use scenarios. The Original Forest scenario consistently shows higher fog interception rates compared to the other scenarios. From 2014 onward, the Deforestation scenario shows lower fog interception rates, with the difference increasing with time. Figure 7.19b demonstrates that scenarios with a higher fraction of trees have slightly higher potential evaporation rates. Precipitation remains unchanged across land use scenarios. Additional results comparing the FIESTA model outputs for each land use scenario can be found in Appendix B.3.

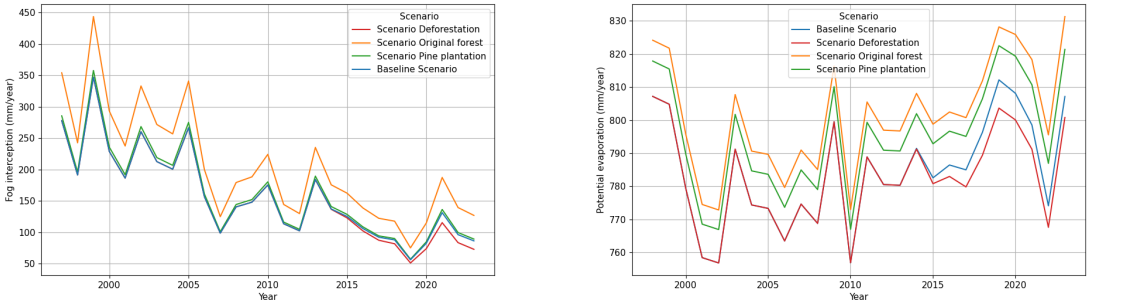

(a) Mean annual fog interception across land use scenarios

(b) Mean annual potential evaporation across land use scenarios

Figure 7.19: Comparison of mean FIESTA model outputs across all spatial classes for the different land use scenarios

7.3.2. Effect of land use change on streamflow

Figure 7.20 shows the flow duration curves for all land use scenarios in a single plot. Upon closer examination, it is evident that the Deforestation scenario (red) shows higher streamflow during low flow conditions and the highest peak flow. In contrast, the Original Forest scenario exhibits the lowest low flows and the highest high flows compared to the other scenarios and the baseline, but it has the lowest peak flow. The Pine Plantation scenario behaves similarly to the Original Forest scenario, but to a slightly lesser extent. These different flow components are further analysed in Section 7.3.2.

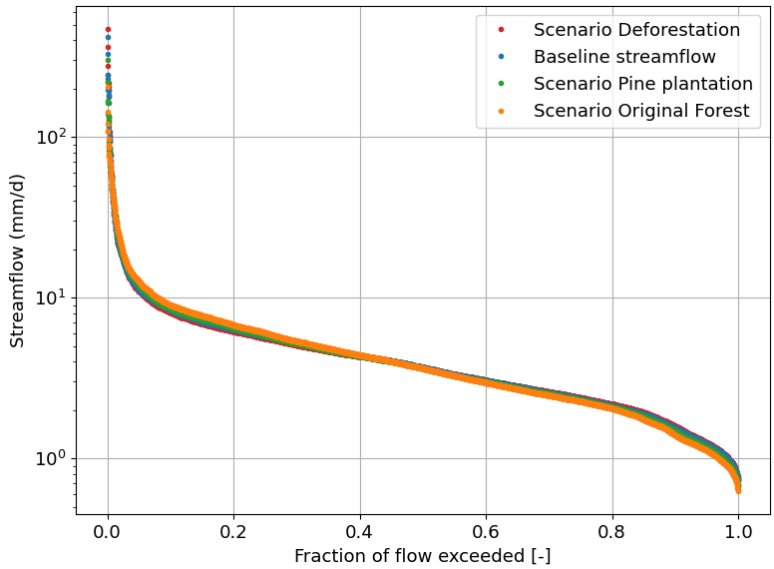

Figure 7.20: Flow duration curve comparison of all the scenarios

Figure 7.21 shows the modelled hydrograph of all the streamflow scenarios compared to the baseline scenarios, together with the mean land use fractions of the land use scenario. The graph mainly visualises the increase in peak streamflow of scenario Deforestation and the decrease in peakflow of scenarios Original Forest and Pine Plantation.

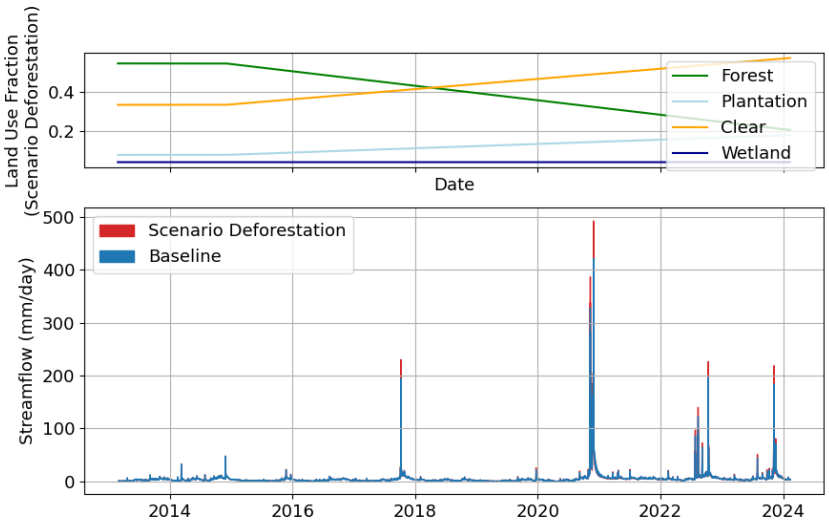

(a) Hydrograph Scenario Deforestation

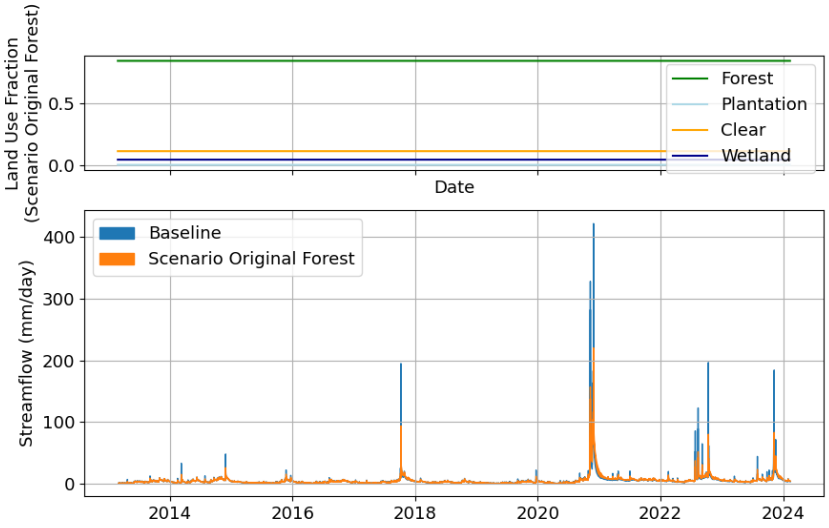

(b) Hydrograph Scenario Original Forest

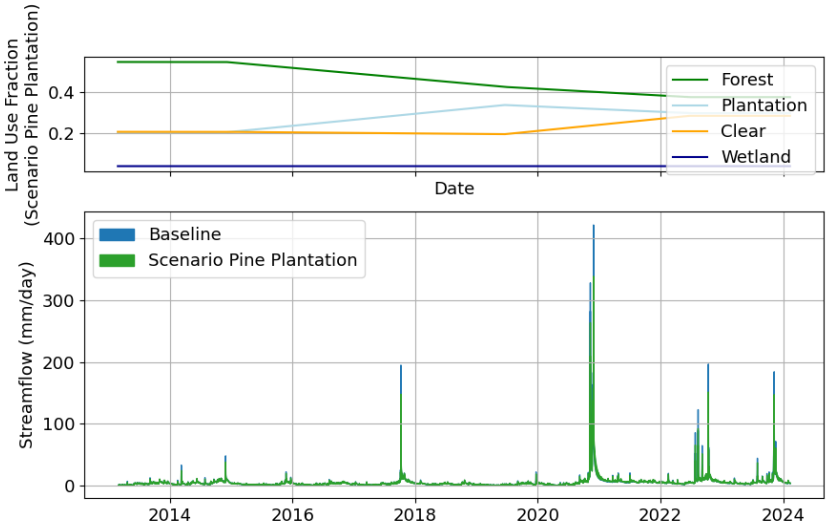

(c) Hydrograph Scenario Pine Plantation

Figure 7.21: Hydrograph of all three land use change scenarios compared to baseline scenario with mean land use fractions

Quantiles

Quantiles are calculated to provide a comparison of streamflow across the baseline and the three different land-use scenarios: Deforestation, Original Forest and Pine Plantation. The quantiles represent different thresholds of streamflow, with Q99.9 representing extreme high flows and Q1 representing low flows. The quantiles in Table 7.6 are determined using the ”knee-point” optimal parameter set. Figures 7.22, 7.23, 7.24 illustrate the variability of quantiles across the different land use scenarios and for all optimal parameter sets through boxplots for some of the quantiles. These boxplots display the range of quantiles of all streamflow possibilities, showing the sensitivity of each land use scenario and a representation of how streamflow distribution changes under different land use conditions. Each boxplot corresponds to a specific quantile, additional boxplots can be found in Appendix C.

Table 7.6: Streamflow quantiles comparison of land use scenarios using the knee-point optimal parameter set

Q [mm/d]	Q99.9	Q99	Q95	Q90	Q70	Q50	Q30	Q10	Q5	Q1
Baseline	**196.50**	**35.88**	**11.24**	**8.43**	**5.21**	**3.68**	**2.55**	**1.55**	**1.23**	**0.93**
Scenario Deforestation	221.59	34.42	10.98	8.09	5.08	3.68	2.59	1.59	1.25	0.95
Scenario Original Forest	107.38	39.04	12.60	8.98	5.37	3.63	2.47	1.39	1.12	0.83
Scenario Pine Plantation	139.76	39.79	11.89	8.59	5.19	3.65	2.52	1.48	1.17	0.88

For extreme high flow quantiles (Q99.9), Scenario Deforestation shows the highest value at 221.59 mm/d, which is significantly higher than the Baseline’s 196.50 mm/d and notably higher than Scenario Original Forest’s 107.38 mm/d and Scenario Pine Plantation’s 139.76 mm/d . This suggests that scenario Deforestation is associated with more extreme high flow events compared to the other scenarios, while scenarios Deforestation and Pine Plantation lead to less extreme high flow events. Figure 7.22a shows the small sensitivity towards the extreme high streamflow of scenario Deforestation, by showing a small variability. The distribution of Q99.9 values indicates that the Scenario Deforestation consistently yields higher extreme flow values compared to the scenarios with more forest.

In terms of the 99th percentile (Q99), Scenario Pine Plantation has the highest streamflow value of 39.79 mm/d, surpassing the Baseline (35.88 mm/d) and Scenario Deforestation (34.42 mm/d). Scenario Original Forest follows with a value of 39.04 mm/d. When looking at the boxplot, it indicates that Scenario Pine plantation and Scenario Deforestation are associated with the most intense high flow events at this percentile. Figure 7.22b, shows a large range for the streamflow values of the Baseline, suggesting a large variability. Although scenario Deforestation occasionally has a lower 99th percentile value than the baseline, it predominantly results in higher values in most cases.

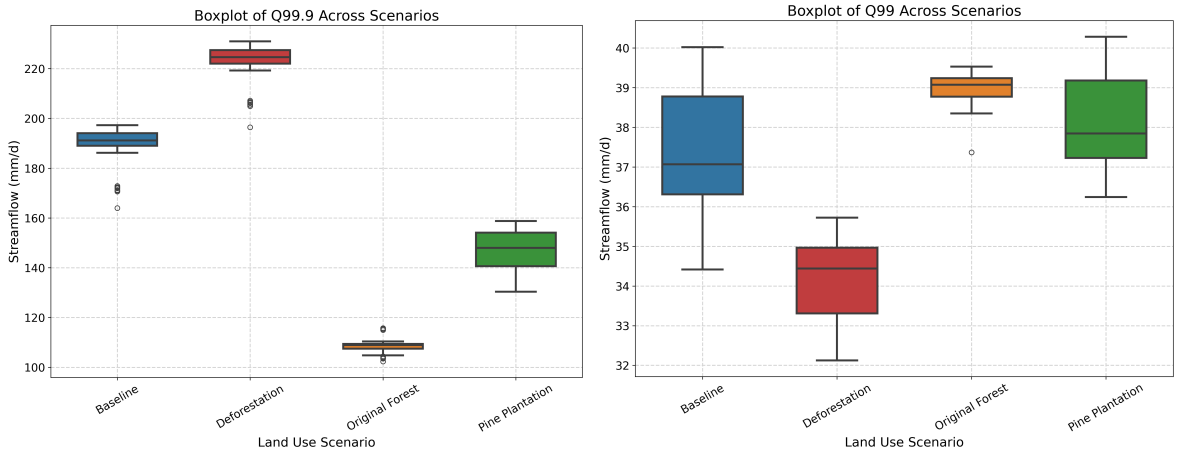

(a) Boxplot 99.9th percentile of flows

(b) Boxplot 99th percentile of flows

Figure 7.22: Boxplots of the Q99.9 and Q99 quantiles for different land use scenarios, representing high flows and extreme high flows. Boxplots are developed with all parameter sets results.

The 95th percentile (Q95) also reflects high flow conditions, with scenario Deforestation showing the highest value of 12.60 mm/d, followed by scenario Pine Plantation (11.89 mm/d), this is higher than the Baseline (11.24 mm/d) and scenario Deforestation (10.98 mm/d). The same proportions hold true accross the scenarios at the 90th percentile (Q90).

For moderate flow conditions at the 70th percentile (Q70), median flow (Q50) and the 30th percentile (Q30), the streamflow values are all close across scenarios. The median streamflow conditions in Figure 7.23b, show the shift of the flows of the scenarios with more trees being higher in the 70th percentile and the scenarios with less trees being higher than the scenarios with more forest in the 50th percentile.

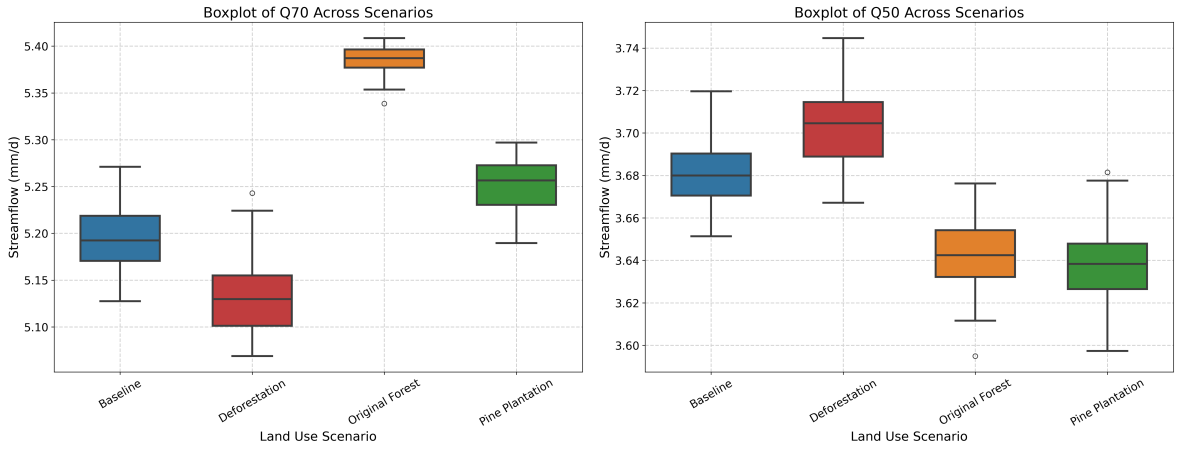

(a) Boxplot 70th percentile of flows

(b) Boxplot 50th percentile of flows

Figure 7.23: Boxplots of the Q70 and Q50 quantiles for different land use scenarios, representing median flows. Boxplots are developed with all parameter sets results.

For lower flow conditions at the 10th percentile (Q10), Scenario deforestation has the highest streamflow value of 1.59 mm/d, followed by the Baseline at 1.55 mm/d, Scenario P ne Plantation at 1.48 mm/d, and Scenario Original Forest at 1.39 mm/d. At the 5th percentile (Q5), the Baseline and Scenario Deforestation have streamflow values of 1.23 mm/d and 1.25, respectively, while Scenario Deforestation has a lower value of 1.12 mm/d. Finally, at the 1st percentile (Q1), which captures the lowest streamflow conditions, the Baseline and scenario Deforestation, have similar values. While scenario Deforestation shows the lowest value of 0.83 mm/day.

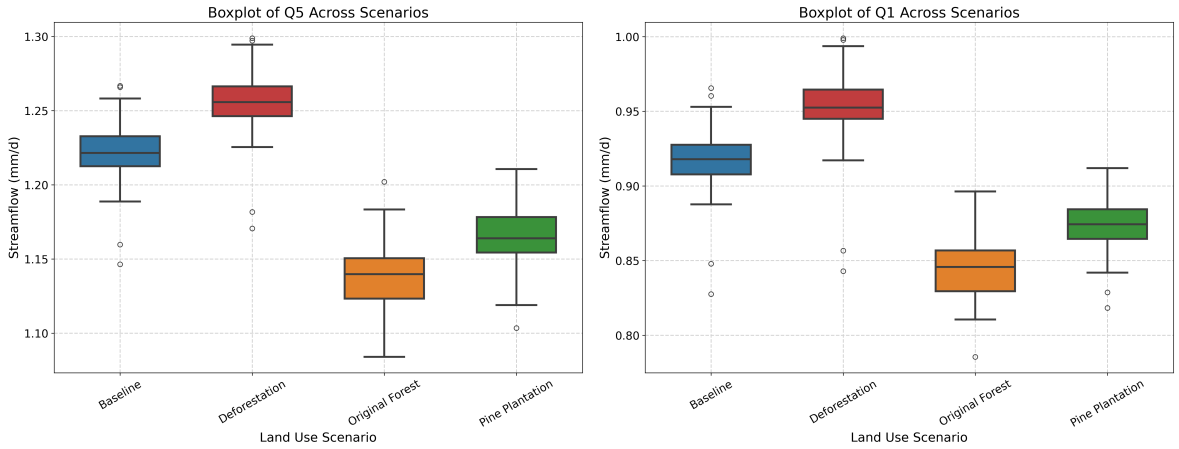

(a) Boxplot 5th percentile of flows

(b) Boxplot of the 1st percentile of flows

Figure 7.24: Boxplots of the Q5 and Q1 quantiles for different land use scenarios, representing low flows. Boxplots are developed with all parameter sets results.

Overall, this comparison highlights how each land use scenario affects the distribution of streamflow quantiles. Scenario Original Forest, which involves increased forest cover, results in reduced extreme high streamflow. It generally shows higher values for high quantiles and lower values for low quantiles compared to the other scenarios. This leads to a reduction in flood events, but potentially drier conditions during low-flow periods. In contrast, Scenario Deforestation, results in more extreme high flows. Scenario Pine Plantation, which incorporates slope-based land use adjustments, demonstrates an increase in high flows, a decrease in extreme high flows and shows no significant difference in low flows compared to the baseline.

Relative flows

Figure 7.25 illustrates boxplots of the relative values of each scenario in comparison to the baseline scenario, by showing deviations from a relative value of 1 for both low and high flows at each time step. Scenario Deforestation shows similar values compared to the baseline scenarios, with the streamflow values in some cases being higher and in other cases lower. Scenario Original Forest shows the highest relative values for low flows and the lowest relative values for high flows. Scenario Pine Plantation shows a similar trend as scenario Original Forest, with a smaller relative difference with the baseline than the scenario Original Forest.

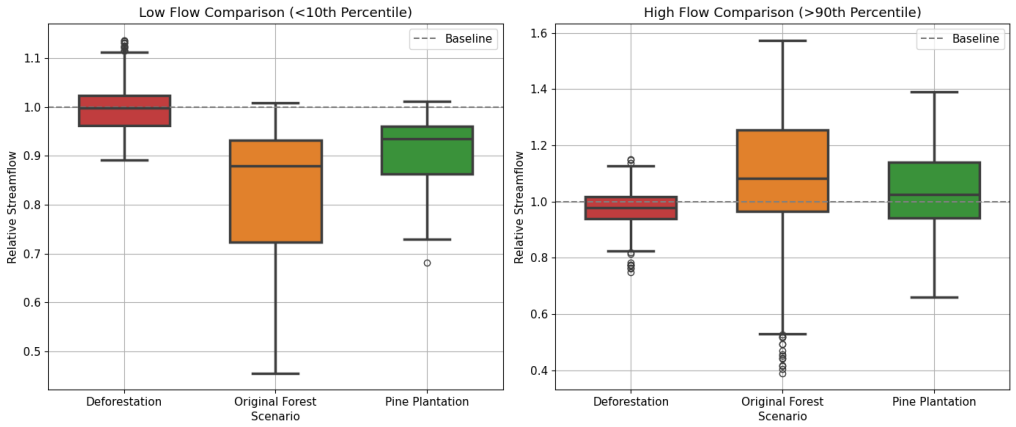

Figure 7.25: Boxplots of relative flow differences compared to the baseline scenario, boxplots represents variability of relative streamflow values of low flows and high flows for all land use scenarios

Flow contribution events

Figure 7.26 presents an overview of how different land use scenarios affect streamflow and its components. The analysis focuses on the hydrological responses during the first months of 2023, showing the response of the different land use scenarios on periods of an period with several consecutive days without rainfall.

During the analysed period, precipitation and fog interception remains constant across all scenarios. This consistency is due to negligible fog input during this time, resulting in uniform precipitation inputs for each scenario. Therefore, the variations observed in streamflow and flow contributions are solely attributed to differences in land use characteristics.

The second subplot in the figure, illustrates the modelled streamflow for each scenario. During the periods of no precipitation, scenario Original Forest shows the smallest response, indicating that it retains the highest groundwater storage. This enhanced storage allows scenario Original Forest to maintain relatively stable streamflow even during periods of low rainfall. In contrast, scenario Deforestation shows the lowest streamflow during the same period, reflecting reduced groundwater storage and less capacity to buffer dry conditions, even it is only a very small amount.

When rainfall resumes, the differences in streamflow responses between scenarios become more pronounced. Scenario Original Forest shows the least increase in streamflow following the onset of rain. This reduced response is attributed to the high transpiration rates and the significant contribution to groundwater storage in Scenario Original Forest, which moderates the immediate impact of rainfall on

streamflow. Due to the little fraction of agricultural land in Scenario Original Forest, there is almost no overland flow resulting in less peak flow. Conversely, Scenario Deforestation exhibits the highest streamflow during rainfall events. This is because Scenario Deforestation directs a larger fraction of runoff to shallow subsurface storage and high rainfall rates result in overland flow, resulting in a quicker runoff response.

The flow contributions from different sources are also depicted in the figure. During the shown period of time, Scenario Original Forest's streamflow comprises approximately of 73% groundwater flow and 27% shallow subsurface flow. This reflects its substantial groundwater storage and slower response to precipitation. In comparison, Scenario Deforestation's flow contributions are more balanced, with about 63% from groundwater flow, 35% from shallow subsurface flow and 2% from overland flow. This indicates a more rapid response to rainfall, with less groundwater storage acting as a buffer.

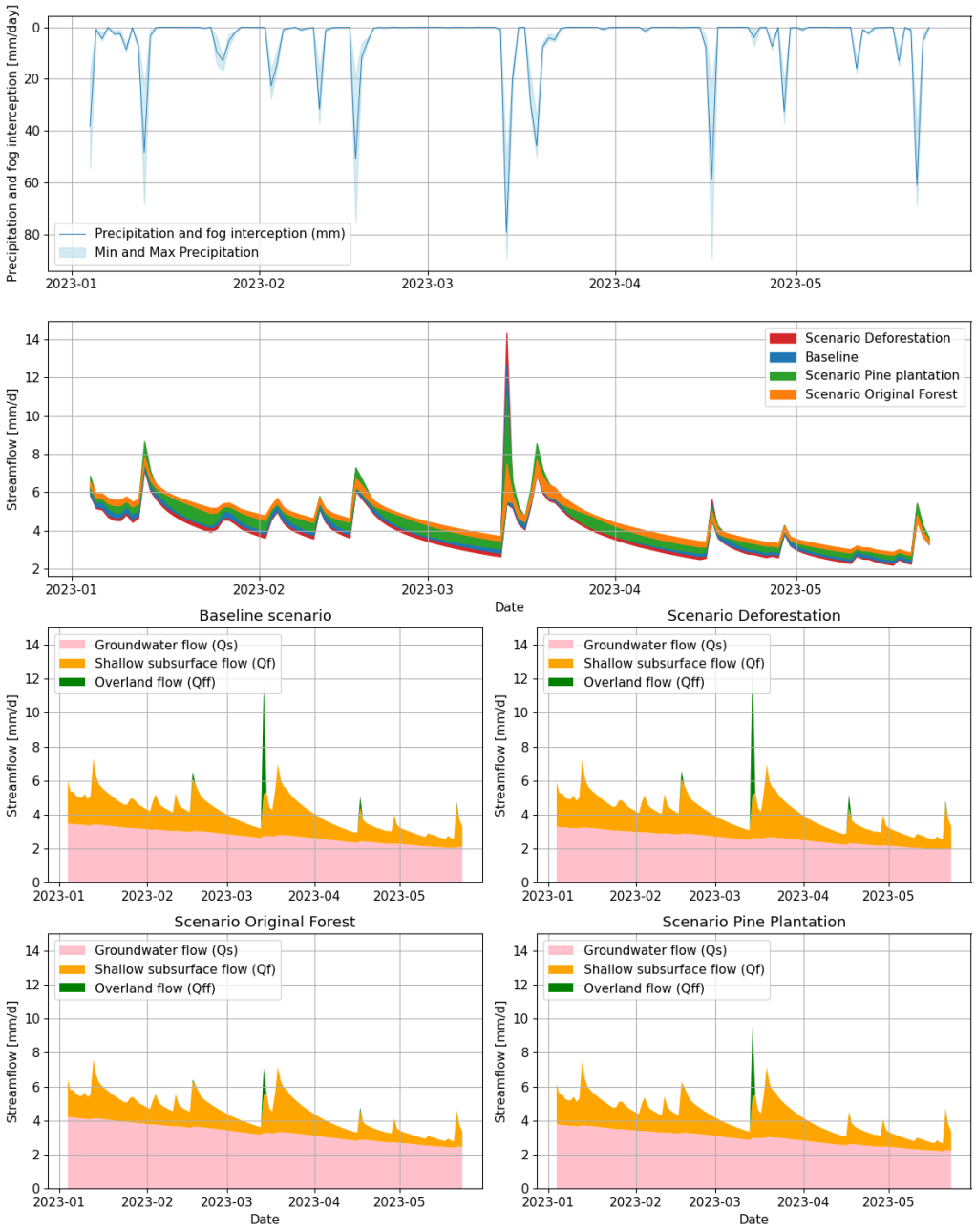

Figure 7.26: streamflow and its different contributions to streamflow shown for the different scenarios. Including an overview of the fog and precipitation inputs (top) and overall streamflow compared for each scenario (middle).

Figure 7.27 shows total precipitation inputs, comparison of streamflow values and total evaporative fluxes for all land use scenarios during very low flow conditions, additionally the bottom plots show the storage components of the four different land use scenarios.This figure illustrates that, during very low flow conditions, the Original Forest scenario exhibits the lowest streamflow values of all scenarios, while simultaneously showing the highest evaporative fluxes. When analyzing the various storage components, it is evident that groundwater storage shows minimal differences among the scenarios. In contrast, shallow subsurface storage is greatest in the Baseline and Deforestation scenarios, followed by the Pine Plantation scenario, with the Original Forest scenario exhibiting the smallest shallow subsurface storage. These two storage components are the primary direct contributors to streamflow in the catchment.

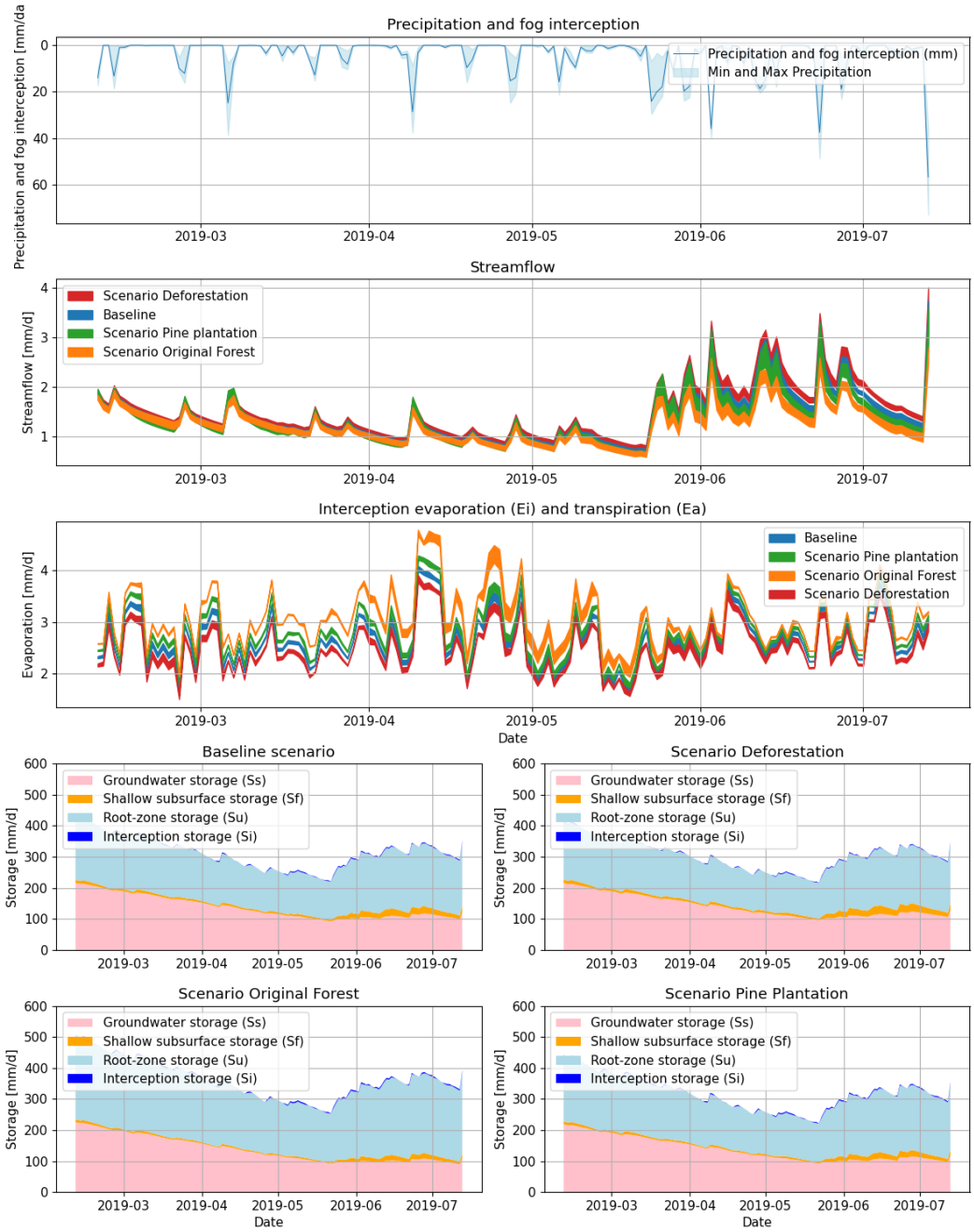

Figure 7.27: streamflow and its different storage components shown for the different scenarios during very low flow conditions. Including an overview of the fog and precipitation inputs (first plot), overall streamflow compared for each scenario (second plot), total evaporative fluxes for each scenario (third plot) and the four lower plots show the different storage components of each scenario.

7.3.3. Effect of land use change on mean annual water balance

Table 7.7 presents a comparison of key water balance components for the baseline scenario and the three land use scenarios. The table includes minimum and maximum values modelled using the envelope of Pareto optimal parameter solutions.

Table 7.7: Scenario comparison of water balance components

	Baseline		Scenario Deforestation		Scenario Original Forest		Scenario Pine Plantation	
	Min	Max	Min	Max	Min	Max	Min	Max
P [mm/year]	**2292.8**		2292.8		2292.8		2292.8	
Ph [mm/year]	**68.9**		63.0		99.3		72.1	
Q [mm/year]	**1912.4**	**2222.8**	1917.1	2256.8	1917.1	2144.6	1867.9	2215.7
Ei [mm/year]	**112.5**	**114.1**	100.2	101.9	155.4	156.7	131.4	133.0
Ea [mm/year]	**693.5**	**714.8**	682.6	707.2	733.5	743.9	710.3	726.2
Qff [mm/year]	**158.8**	**257.7**	200.7	322.7	45.4	72.7	98.9	160.4
Qf [mm/year]	**1023.1**	**1249.7**	1019.1	1257.3	1028.9	1239.7	986.8	1278.3
Qs [mm/year]	**639.7**	**765.4**	589.9	741.1	803.1	857.1	723.3	802.9
Si [mm/day]	**1.9**	**2.0**	1.7	1.8	2.7	2.7	2.2	2.3
Su [mm/day]	**195.8**	**222.4**	180.6	210.4	260.4	284.8	214.2	235.8
Sf [mm/day]	**33.2**	**46.5**	34.6	47.9	30.6	51.5	27.2	44.6
Ss [mm/day]	**388.7**	**464.3**	358.4	449.6	488.0	521.1	439.4	487.1

Precipitation remains constant across all scenarios at 2292 mm/year, since land use has been modelled to not influence precipitation. There is a noticeable variation in fog interception across scenarios. Scenario Original Forest shows a significant increase in fog interception (99.3 mm/year) compared to the baseline (69.0 mm/year). This is expected given the increase in forest cover, which enhances fog interception. Conversely, Scenario Deforestation shows a decrease (63.0 mm/year) due to the reduction in forested areas. Scenario Pine Plantation, which has more pine trees, has an interception value of 72.0 mm/year, which is closer to the baseline.

The total streamflow varies across scenarios, reflecting the impacts of runoff. The baseline scenario has a range of 1971.5 to 2307.9 mm/year. Scenario Deforestation shows an increase in mean annual streamflow by 0.88% ($\pm 0.64\%$) compared to the baseline, likely due to reduced evaporation, interception and increased runoff from deforested areas due to less root-zone storage. Scenario Original Forest shows slightly larger variations in mean annual streamflow compared to the baseline, ranging from -3.52% to 0.24%. This difference is likely due to increased interception, evaporation and therefore decreased runoff. Scenario Pine plantation shows a small reduction in mean annual streamflow compared to the Baseline with -1.33% ($\pm 0.64\%$).

Evaporation from interception (Ei) decreases in scenario Deforestation compared to the baseline, as visually presented in Figure 7.28. It shows an increase in scenario Original Forest and Pine Plantation due to larger forest leading to more interception capacities. Transpiration (Ea) also varies significantly, with scenario Original Forests shows the highest values (733.5 to 743.9 mm/year) due to the extensive forest cover. These evaporative fluxes for scenario Original Forest are significantly higher than the baseline and other scenarios.

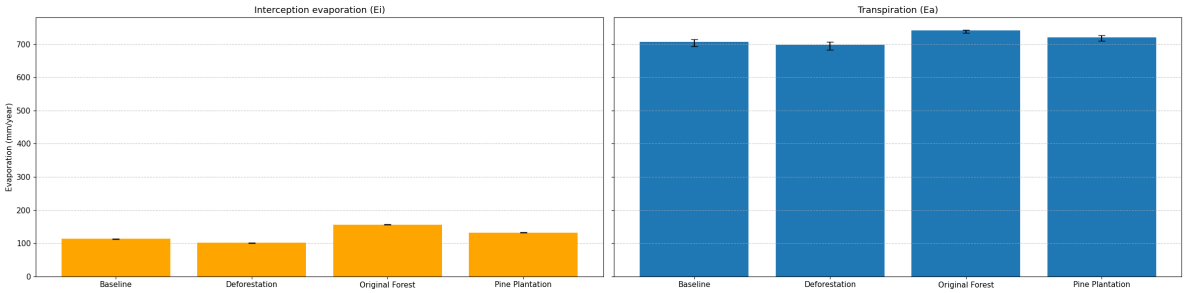

Figure 7.28: Barplot of evaporative fluxes compared along scenarios and showing possible variability due to multiple parameter sets represented by error bar.

All results from the annual flow components are visually presented in Figure 7.29. Scenario Deforestation shows the highest values for overland flow (Qff), ranging from 200.7 to 322.7 mm/year, consistent with increased runoff from increased agricultural lands. Scenario Original Forest shows a substantial decrease in overland flow (45.4 - 72.7 mm/year), as more forested areas lead to less agricultural overland flow. Scenario Pine Plantation has moderate Overland flow values, ranging from 98.9 to 160.4 mm/year, showing a high variability. These ranges reflect the effects of pine plantations replaced with agricultural lands. Shallow subsurface flow (Qf) shows similar values along all scenarios, with a slight variation in ranges. The groundwater flow decreases in scenario Deforestation, due to less percolation to the soil and increased fast runoff. Scenario Original Forest shows an significant increase in groundwater flow, likely due to more infiltration and storage of water in forested areas. Due to these reasons, also scenario Pine Plantation shows an increase in groundwater flow compared to the baseline scenario.

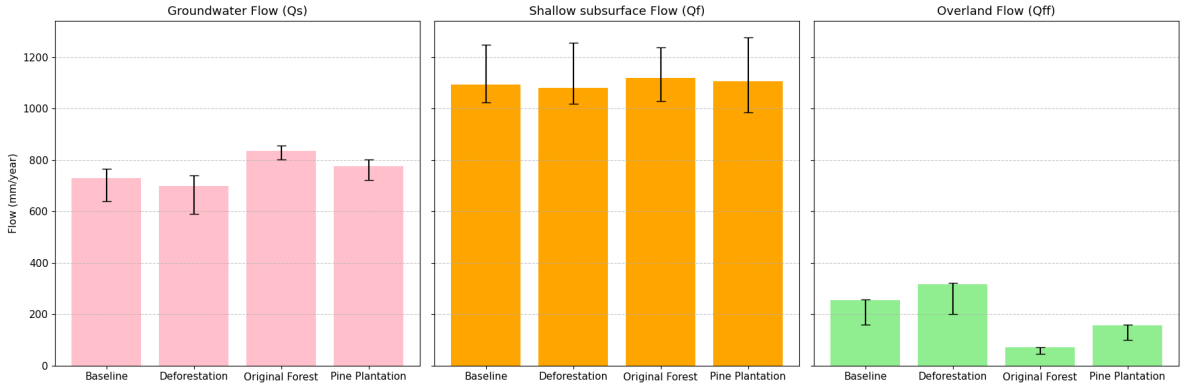

Figure 7.29: Barplot of flow components compared along scenarios and showing possible variability due to multiple parameter sets represented by error bar.

Overall, an increase in water storage is observed in scenario Original Forest and Pine Plantation, showing an increase in unsaturated root-zone storage due to a larger root-zone and more groundwater storage due to more infiltration into the soil. There is also an increase in interception storage for scenarios Original Forest and Pine Plantation with more forest cover. Scenario Deforestation shows less storage in all storage components. In total, scenario Deforestation leads to a decrease in daily storage of approximately 5.31 ($\pm 1.8\%$) %, while scenarios with more forest lead to more water collection. Scenario Original Forest has a mean daily increase of storage of 21.6 ($\pm 4.6\%$) and scenario Pine Plantation 7.5 ($\pm 2.8\%$).

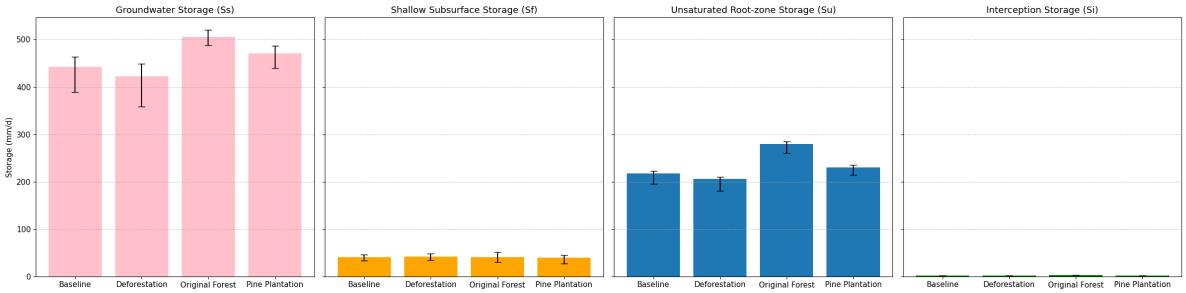

Figure 7.30: Barplot of storage components compared along scenarios and showing possible variability due to multiple parameter sets represented by error bar.

7.3.4. Monthly fluxes

The monthly streamflow values for each modelled land use change scenario are illustrated in 7.31a, showing the largest differences in the months January, February and December. In these months, the scenarios Original Forest and Pine Plantation streamflow are on average higher compared to the other scenario and the baseline. Conversely, in November, Scenario Deforestation shows the highest streamflow, surpassing the baseline, while the Original Forest and Pine Plantation scenarios present lower streamflow values than the baseline during this month. The ranges of possible streamflow values are not displayed in this figure to enhance visibility.

Figure 7.31b shows the percentage of differences of streamflow per each month of the year compared to the baseline scenario. During the months with overall lower streamflow (December to April), the Deforestation and Pine Plantation scenarios yield higher values than the baseline. In contrast, for the wetter months from June to November, the streamflow values are lower than those of the baseline scenario.

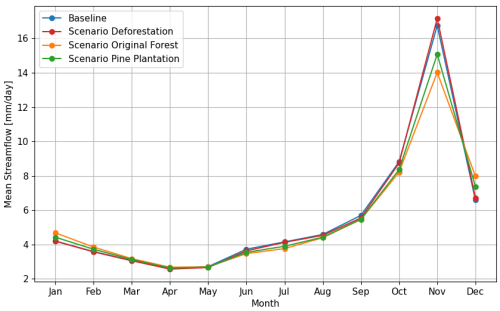

(a) Mean streamflow values per month of the year for all land use scenarios

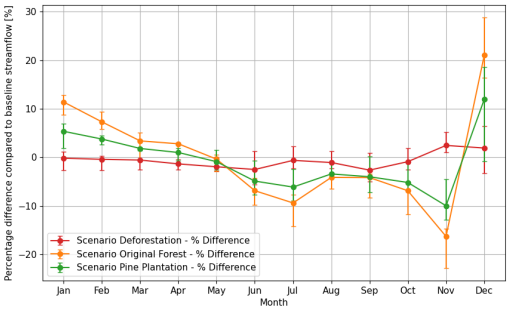

(b) Percentage difference compared to the baseline scenario for each land-use scenario, including error bars showing the variability of possible solutions

Figure 7.31: Comparison of streamflow values for each scenario for each month of the year

8

Discussion and Recommendations

8.1. Discussion of meteorological inputs using the FIESTA model

8.1.1. Spatially variable precipitation

The FIESTA model is utilized to generate spatially distributed meteorological inputs for simulating streamflow in the Mestelá catchment. When evaluating spatial distribution of precipitation data, deviations from the measured mean annual precipitation of 2273 mm/year were observed, ranging from +152 mm/year to -628 mm/year within different regions of the catchment. These variations indicate that the model captures spatial heterogeneity to some extent.

Despite applying wind-driven precipitation adjustments to the precipitation data measured in Cobán, the impact on the modelled precipitation was minimal when considering the catchment's total mean annual precipitation. The adjustment resulted in only a slight increase of approximately 5 mm/year. This minor adjustment suggests that, for the Mestelá catchment, the influence of wind-driven precipitation on the overall water input is limited. This result contrasts with the expectations from other studies (e.g. Mulligan and Burke (2005); Frumau et al. (2011)), which suggest that wind-driven precipitation is often underestimated in steep montane topographies with northern slopes. The absence of meteorological stations within the catchment contributes to this difficulty of capturing this variability, particularly in regions characterized by highly variable spatial patterns, such as tropical montane areas.

This variability of precipitation data within the catchment suggests that while the FIESTA model captures the spatial distribution conceptually, which could improve hydrological modelling, it struggles with underestimation of actual precipitation values. Correcting values that were initially underestimated proves challenging, especially in a region with high spatial variability. This result highlights a limitation of the FIESTA model in accurately representing small-scale wind-driven precipitation patterns with limited data, as the model is designed for larger-scale applications with multiple measurement stations. As such, the adjustments to precipitation inputs may be less relevant in this specific small catchment context.

8.1.2. Fog interception and Evaporation

Fog interception accounts for only around 5% of the total water input in the Mestelá catchment, mainly due to the high precipitation levels in the catchment. However, fog interception plays a role in refining the water balance by simulating a key hydrological process characteristic of cloud forests. Fog interception becomes particularly interesting during months with little rainfall, such as January and December, where it contributes a notable 13% and 15% to the total water input, respectively.

Potential evaporation, which is estimated using available energy and atmospheric demand, showed minimal variability between land-use types. This is because net radiation and temperature, key factors in determining potential evaporation, do not differ significantly between land use classifications. However, incorporating spatial variability of potential evaporation using slope and aspect in the model provided a more detailed representation of these variables across the catchment.

In terms of actual evaporation processes, the FIESTA model did not fully capture the unique behavior of cloud forests, where higher humidity and lower solar radiation typically results in lower evaporation rates compared to other land cover types. The model relied on a single humidity value from outside the catchment, and no adjustments were made to account for local conditions, such as influence of the presence of epiphytes in cloud forests or cloud cover. These factors, which are interconnected and drive complex hydro-meteorological processes, were oversimplified in the model, limiting its accuracy in capturing cloud forest specific evaporation dynamics.

8.1.3. Limitations and model evaluation

A challenge in employing the FIESTA model for the Mestelá catchment is the lack of available in-situ datasets within the Mestelá catchment to accurately capture local meteorological processes. This limitation is especially pronounced in mountainous regions like the Mestelá catchment, where steep slopes and complex topography can greatly influence wind patterns, rainfall distribution, and fog formation.

The absence of inter-grid cell fluxes in the FIESTA model further restricts its ability to account for interactions between neighboring cells, such as wind deflection or orographic effects. This shortcoming reduces the model's capacity to fully reflect the coupled hydro-meteorological dynamics of the catchment.

Additionally, evaluation of the FIESTA model performance proves difficult due to the scarcity of localized data, particularly data concerning the topographical influence on meteorological variables. In the absence of more detailed, localized measurements, it is difficult to fully assess the model's accuracy in representing the unique conditions of the catchment.

8.1.4. Implications for hydrological modelling

Despite its limitations, the FIESTA model has the potential to improve the representation of spatial variability in meteorological inputs. However, it remains uncertain whether this spatial variability genuinely improved due to the lack of data to evaluate the model's outputs.

Regarding fog interception, the model provides valuable information on water inputs that are often overlooked in hydrological modelling, contributing to a reduction of the often underestimated total water input in modelling cloud forests. However, the relatively small overall contribution of fog to the water balance indicates that other meteorological factors, such as rain and evaporation, continue to play a more dominant role in determining hydrological responses in the catchment.

8.2. Precipitation adjustment

The need for adjusting precipitation values arises from observed inconsistencies between the measured precipitation and the measured streamflow in the Mestelá catchment, arising from inconsistencies in the water balance. Precipitation, particularly during storm events, appear to be underestimated, introducing errors into the hydrological model. Storms can result in highly variable rainfall over small areas and short time spans, making accurate measurement difficult. These localized variations in storm intensity are not fully captured by the measurement station in Cobán, resulting in an underestimation of rainfall in the catchment.

Notably, there is no consistent correction factor, which is applied to adjust precipitation, across the entire dataset, which suggests that the issue is not simply a problem with the measurement equipment. Additionally indicating that certain storm events are missed by the Cobán station, likely due to the spatial limitations of a single measurement point.

One of the major influences on precipitation in the region is wind and the mountainous terrain, which has already been considered in the wind-driven precipitation corrections of the FIESTA model. However, these adjustments may not fully account for the difference in precipitation between the Mestelá catchment and Cobán. Several factors can contribute to higher rainfall in the Mestelá and Upper Cahabón catchments compared to Cobán:

- The Sierra Yalijux mountain range plays a crucial role in enhancing precipitation. As moist air from the north encounters the mountains, the air is forced to rise, leading to cooling, condensation and ultimately precipitation, a process known as orographic lift (Ray et al., 2006). The higher

elevations in the Mestelá and Upper Cahabón catchment can reach up to 1300 meters higher than the elevation of Cobán, resulting in more precipitation in these catchments compared to Cóban.

- The Sierra Yalijux mountain range also acts as a natural barrier, capturing moisture originating from the North and enhancing precipitation in the catchment, while Cobán, at a lower elevation does not benefit from this effect.
- The cloud forests in these mountainous regions, characterized by their dense canopy and frequent cloud cover, also play a critical role in increasing precipitation. The presence of moist clouds near the forest canopy leads to elevated humidity and frequent light rain, while fog interception further boosts the water input. These forests create micro-climates that trap moisture, and epiphytes contribute to additional evaporation and moisture recycling, further increasing local humidity and potentially affecting precipitation patterns, something that is not captured in the measurements from Cobán.
- While temperature does not directly affect precipitation, the cooler temperatures at higher altitudes favor moisture condensation. In cloud forests, the higher humidity combined with cooler temperatures leads to more precipitation. In contrast, the lower elevations, such as Cobán, experience higher temperatures, lower humidity, and, consequently, less precipitation. The FIESTA model may not fully capture these temperature-related effects on humidity and rainfall.

While the adjusted precipitation values lead to better model performance in terms of streamflow simulation, it is important to recognize that the discharge data itself may also contain errors. Various factors, such as faulty measurement equipment, an inaccurate rating curve, or difficulties in measuring very high discharge levels, could introduce errors into the streamflow data, particularly during extreme flood events.

The calibration of scaling factors used for precipitation adjustments is based on optimizing the performance of the hydrological model. This assumption implies that the model accurately simulates streamflow. While this assumption holds for improving the match between observed and modelled discharge, it introduces a degree of uncertainty, as both the precipitation and discharge data may contain errors. This suggests that improving model performance through precipitation adjustments should be viewed with caution, and a more comprehensive understanding of local hydro-meteorological conditions may be needed for future refinements.

8.3. FLEX-Topo model

8.3.1. Calibration and evaluation of the FLEX-Topo model

To guide the calibration process, a priori constraints are applied to parameter distributions, along with additional process-based checks, such as evaporative fluxes specific to each landscape class and the runoff coefficient. These measures aim to help the model realistically represents the hydrological dynamics of the catchment and simulate the processes within each landscape class, based on a process-based understanding of the system.

The calibration of the FLEX-Topo model uses both the Nash-Sutcliffe Efficiency (NSE) and the logarithmic Nash-Sutcliffe Efficiency (log-NSE) as objective functions. This approach balances calibration for low-flow and high-flow periods, both critical for assessing the impact of land-use change on streamflow dynamics. The calibration process is performed only on data marked as 'informative', which improves model performance compared to using all available data. This selection process is intended to ensure that the model is better tuned to capture relevant streamflow patterns, while minimizing the influence of noisy or unrepresentative data, thereby leading to more accurate simulations.

During the initial calibration and evaluation, the model demonstrated good calibration results, but the evaluation performance was poor. This suggested that the meteorological data, particularly rainfall, was not correctly capturing the variability of the system. After adjusting the precipitation data, both calibration and evaluation results showed improvement, achieving good to very good performance in both phases. This highlights the importance of accurate meteorological inputs and the model's sensitivity to rainfall data in streamflow prediction.

The dynamic inclusion of landscape classes and land-use changes over time is aimed to improve the

reliability of parameter calibration. The model simulates how different land covers potentially impact streamflow, with forests and pine plantations likely contributing significantly to groundwater recharge, and having high evaporative fluxes. Model results indicate that hillslope agriculture contributes heavily to fast flow, both through shallow subsurface flow and overland flow, leading to greater peak streamflow contributions. Although wetlands may contribute significantly to shallow subsurface streamflow, its overall impact is smaller due to limited coverage in the catchment.

The analysis of land use change in relation to streamflow dynamics in the Mestelá catchment reveals an absence of clear trends over time, despite the expectation that such changes would influence hydrological responses. This lack of trend may originate from several interrelated factors, including the variations in climatic data.

The model simulates streamflow in the Mestelá catchment similarly to the Upper Cahabon catchment, reflecting their shared topographical and hydrological characteristics.

8.3.2. Role of spatially distributed meteorological inputs

The use of spatially distributed meteorological inputs generated by the FIESTA model has not specifically shown to improve the reliability of streamflow predictions. However, since threshold processes are controlled by extremes, reducing the averaging of meteorological data suggests less misinterpretation of the results. Additionally, the inclusion of the spatially distributed fog interception flux has lead to a more representative model structure. Water budgets in cloud forests remain challenging to assess due to the complex interactions between forest cover and atmospheric conditions, which influence hydrological fluxes. Though difficult to quantify precisely, the fog interception process plays an essential role in the hydrological cycle of montane cloud forests.

8.3.3. Parameterization and model limitations

The model does not focus on subsurface flow processes, which are particularly hard to estimate in karst environments like the Upper Cahabon and Mestelá catchments. Features such as sinkholes, caves, and underground channels affect water storage and flow, and these complexities are not well-represented in the current model structure. This introduces uncertainties in predicting subsurface water movement.

Additionally, the model uses averaged parameter values for each land-use class, overlooking important factors such as specific tree characteristics, soil degradation, and the seasonality of hydrological processes. Over long periods, the evolution of the landscape, vegetation regeneration, and changes in soil conditions are not fully incorporated, which may reduce the accuracy of long-term simulations and the model's ability to capture individual landscape characteristics. While the model relies on static parameters, the introduction of dynamic land-use fractions might help mitigate some of these uncertainties.

In conclusion, while the FLEX-Topo model provides a useful framework for simulating streamflow in the Mestelá catchment, challenges and uncertainties remain. Improvements in data collection, especially for precipitation and discharge, as well as more refined parameterization methods, could enhance the model's accuracy and reliability for long-term predictions.

8.4. Land use scenarios

To quantitatively assess the impacts of varying land use change scenarios, such as deforestation and reforestation, on streamflow dynamics within the FIESTA and FLEX-Topo model framework, the FLEX-Topo model is used to simulate different land use scenarios by adjusting land use fractions. The FIESTA model complements this by adjusting precipitation inputs due to altered fog interception, particularly significant in cloud forest regions where fog interception plays a role in water input.

8.4.1. Interpretation of results

The analysis of the land use scenarios on streamflow dynamics reveals insignificant impacts on total streamflow dynamics in the Mestelá catchment. For the Deforestation scenario, where deforestation rates were doubled compared to the past ten year, the model simulates an increase of 0.88% (± 0.64%) in mean total streamflow. This increase is likely attributed to reduced vegetation cover leading to lower

evaporation and increased surface runoff. For the scenario Original Forest, where forest cover is restored to approximately 80% in the catchment, the simulated change in streamflow shows only slight variations compared to the baseline, ranging from -3.52% to 0.24%. Similarly, in the scenario Pine Plantation, where agriculture on slopes greater than 30° is replaced with pine trees, the model suggests a -1.33% (± 1.01%) reduction in mean total streamflow. This decrease might be linked to the higher water uptake and evaporation rate of trees compared to agricultural lands.

Although the impact on total streamflow appears minor, the simulations indicate a more pronounced effect on low flows and high flows. For high flows, scenario Deforestation shows that deforestation may increase the magnitude of extreme runoff events with approximately 18.5% (± 1.4%) compared to the baseline scenario. Overland flow increases by approximately 25.8% (± 0.6%), which is consistent with expectations of reduced soil infiltration, reduced storage capacity of the soil and therefore increased surface runoff following deforestation. These potential changes suggest that deforestation might lead to higher peak flows during heavy rainfall events.

In contrast, scenario Original Forest and Pine Plantation show a significant decrease in magnitude of extreme high streamflow events, with a decrease of 39.5% (± 1.9%) and 20% (± 0.5%) respectively. The simulated increase in forest cover leads to greater interception and deeper rooting systems, both of which enhance soil infiltration and water storage. Consequently, more water is stored in the root zone, and less contributes to overland flow and shallow subsurface flow. During storm events, these scenarios result in less intense peak flows, with more water being directed to the groundwater storage reservoirs. The increased storage capacity in forested areas potentially mitigates the magnitude of extreme events and reduces flood risks. The delayed response in streamflow and high transpiration rates may additionally contribute to a dampened high flow response.

Interestingly, the model does not suggest a strong link between cloud forests and increased streamflow via fog interception, despite this being expected.The minimal contribution of fog interception to total precipitation limits its impact. While there is more water retained within the system, much of it is diverted to other fluxes, such as evaporation, rather than streamflow. While results indicate that forested areas store more water in the soil, this storage does not appear to contribute significantly to streamflow during droughts. Instead, the higher water demand by vegetation, coupled with increased root-zone storage, larger contribution to groundwater storage, shows a reduction of the baseflow.

Although Scenario Original Forest shows an overall decrease in streamflow due to higher forest cover, the scenario provides some resilience during droughts. Forested landscapes exhibit less severe declines in streamflow during periods of no rainfall because of the greater storage in groundwater and root zones. However, this groundwater contribution to baseflow is insufficient to prevent overall streamflow reductions during dry periods, due to high evaporation rates.

It should also be noted that the simulations assume that forests generally display higher evaporation rates than agricultural land despite the expectation of reduced evaporative losses in cloud forests due to lower solar radiation and high atmospheric humidity. These assumptions, based on available literature (e.g. Zadroga (1981); Jarvis and Mulligan (2010); Bruijnzeel (2001)), should be revisited in future studies, as the specific evaporative conditions of cloud forests might not be fully captured by the model. However, it needs to be considered that not all the forest present in the catchment is cloud forest and have these micro-climatic conditions of cloud forests.

8.4.2. Monthly and seasonal fluxes

The analysis of monthly fluxes reveals distinct patterns across the different land use scenarios. The scenarios Original Forest and Pine Plantation exhibit higher streamflow from December to May, the dry season, while Scenario Deforestation overall shows decreased streamflow values for the dry season. During the wet season, June to November, the scenarios Original Forest and Pine Plantation indicate reduced streamflow values. This seasonal variation highlights the different impacts of land use changes on streamflow during varying climatic conditions.

Fog interception, while contribution relatively little to total streamflow, appears more significant during the dry months. For the forested scenarios, in January and December, the model suggests that fog interception provides a relatively larger share of water input compared to precipitation, helping to sustain streamflow during the driest part of the year.

These findings suggest that while increased forest cover could help maintain streamflow during the dry season by improving groundwater storage and fog interception, it may also reduce streamflow during extreme droughts due to higher water demand from vegetation.

8.5. Recommendations for Future research

While this study provides valuable insights into hydrological processes through synthetic land use simulations, future research should focus on refining the representation of cloud forest micro-climatic conditions. For the FLEX-Topo model, incorporating additional evaporation dynamics specific to cloud forests, such as those driven by high humidity and shading effects, could improve model accuracy. This might be achieved by introducing a separate cloud forest landscape class, better reflecting the unique processes in these regions. Similarly, the FIESTA model could be enhanced to better capture spatial variability by integrating localized temperature variations in agricultural and forested areas, humidity changes that influence cloud formation and precipitation, and processes like moisture recycling. Additionally, investigating how downhill airflow influences upstream cloud formation could offer new insights into precipitation and fog interception dynamics.

The FIESTA model could also be adapted to capture more effectively capture wind-driven rainfall variability by including modelling interactions between spatial cells to simulate complex processes such as wind deflection and orographic lifting. Incorporating downhill airflow effects on upstream cloud formation could also improve the simulation of precipitation and evaporation in this mountainous environment.

Further research should also explore the contribution of fog interception to streamflow, as this might offer valuable insights into cloud forest hydrology during drier periods. Investigating the relationship between groundwater storage and streamflow—both in wet and dry conditions—is crucial for understanding how land use changes affect the hydrological balance of the catchment. Additionally, there remains uncertainty around subsurface flow processes, where closer examination is suggested.

Improved data collection within the catchment will be essential for supporting these refinements, providing more accurate inputs and increasing evaluation possibilities for both the FIESTA and FLEX-Topo models. Especially, since in this study evaluation of the FIESTA model has not been integrated.

While the models used in this study simulate the impacts of land use changes on streamflow, addressing uncertainties around evaporation and fog interception will further enhance their reliability. Improving model accuracy will strengthen the models' utility as decision-making tools for policymakers, enabling more precise predictions to guide sustainable land management strategies and water resource policies.

9

Conclusion

This study demonstrates that the combined application of the FLEX-Topo and FIESTA models offers valuable insights into hydrological responses to land use changes, particularly in cloud forest regions. These results highlight their potential for informing policy decisions related to land conservation and water management in tropical montane cloud forests, a critical consideration in the face of climate change and increasing flood and drought risks.

While the FIESTA model contributes to an enhanced conceptual understanding of spatial variability in the Mestelá catchment, the absence of localized data for evaluation and the model's design limitations mean that improvements in the representation of meteorological inputs cannot be conclusively demonstrated. The underestimation of total precipitation, particularly in cloud forest regions, remains a challenge. Wind-driven precipitation adjustments made only minor improvements, highlighting the need for more comprehensive data collection, especially in complex mountainous terrains. Despite these challenges, the inclusion of fog interception contributed to a more realistic representation of the water balance, showing the importance of spatial characteristics in developing meteorological inputs.

The FLEX-Topo model, tailored to the unique characteristics of the study area, performed well in simulating streamflow when compared to observed data. Calibration optimized for distinct land use classes enhanced the model's ability to capture the hydrological dynamics of the Mestelá catchment across various land use scenarios.

The findings from both the FIESTA model and the FLEX-Topo model indicate that deforestation scenarios tends to increase the intensity of flood events, while enhancing forest cover can mitigate the severity of extreme streamflow events. This is particularly relevant in the context of climate change, which has been associated with rising high streamflow values and increasing flood risks. Moreover, introducing pine trees on steep slopes not only potentially reduces extreme flow but also helps address other issues, such as landslides, that are commonly associated with deforestation on steep terrains. The scenario analysis revealed that deforestation potentially increased peak flows by 25% (±5%), most likely due to less soil infiltration, while restoring forest cover by 85% reduced extreme flows by 38% (±5%) and replacing agriculture with pine trees on steep slopes reduced extreme flows by 15% (±5%). While, scenarios with increased forest cover indicated higher streamflow values during the dry season, likely due to more storage capacity of water. However, this increase in forest cover may also contribute to more extreme droughts due to the high water usage of vegetation. Overall, these results suggest that reforestation and conservation efforts can play a significant role in moderating extreme streamflow events and enhancing the resilience of the catchment to climatic variations.

In summary, this study highlights the potential of the FLEX-Topo and FIESTA models in simulating the impacts of land use changes on streamflow dynamics. However, further improvements, particularly in representing fog interception and evaporation processes, could enhance model accuracy and reliability. Strengthening these aspects would increase the utility of these models as decision-making tools for policymakers, providing more precise predictions to support sustainable land management and water resource conservation strategies in the Mestelá catchment.

Bibliography

National Aeronautics and Space Administration (NASA). Overview of land cover remote sensing. Technical report, NASA, 2022. URL https://appliedsciences.nasa.gov/sites/default/files/2022-11/LandCoverRS_Edited_SC.pdf.

D. Arias Agudelo, F. Bulsing, J. Schrijver, M. Luger, and L. Cahill. Cloud forest hydrology in a changing context: An approach to understand the impact of climate change and deforestation on the water balance of the sierra yalijux, alta verapaz, guatemala. Master's thesis, Technical University of Delft, 2023.

Claudine Ah-Peng, Anabelle Williamson Cardoso, Olivier Flores, Adam West, Nicholas Wilding, Dominique Strasberg, and Terry Hedderson. The role of epiphytic bryophytes in interception, storage, and the regulated release of atmospheric moisture in tropical montaine cloud forest. *Journal of Hydrology*, 548:665–673, 2017. doi: doi.org/10.1016/j.jhydrol.2017.03.043Getrightsandcontent.

L.A. Alvarenga, C.R. de Mello, A. Colombo, L.A. Cuartas, and L.C. Bowling. Assessment of land cover change on the hydrology of a brazilian headwater watershed using the distributed hydrology-soil-vegetation model. *CATENA*, 143:7–17, 2016. doi: https://doi.org/10.1016/j.catena.2016.04.001.

A.E. Anderson, M. Weiler, Y. Alila, and R.O. Hudson. Subsurface flow velocities in a hillslope with lateral preferential flow. *Water Resources Research*, 45, 2009. doi: https://doi.org/10.1029/2008WR007121.

Diana Arroyo. Guatemala humanitarian response plan. Technical report, United Nations Office for the Coordination of Humanitarian Affairs, 2023. URL https://humanitarianaction.info/plan/1173/article/guatemala-1.

Keith Beven. A brief history of information and disinformation in hydrological data and the impact on the evaluation of hydrological models. *Hydrological Sciences Journal*, 69:519–527, 2024. doi: doi.org/10.1080/02626667.2024.2332616.

Keith Beven and Paul James Smith. Concepts of information content and likelihood in parameter calibration hydrological simulation models. *Journal of Hydrologic Engineering*, 2013. doi: doi.org/10.1061/(ASCE)HE.1943-5584.0000991.

Keith Beven and Ida Westerberg. On red herrings and real herrings: disinformation and information in hydrological inference. *Hydrological Processes*, 25:1676–1680, 2011. doi: doi.org/10.1002/hyp.7963.

C. Birkel, C. Soulsby, and D. Tetzlaff. Modelling the impacts of land-cover change on streamflow dynamics of a tropical rainforest headwater catchment. *Hydrological Sciences Journal*, 2012. doi: doi.org/10.1080/02626667.2012.728707.

L. A. Bruijnzeel. Hydrological functions of tropical forests: not seeing the soil for trees? *Agriculture, Ecosystems and Environment*, 104:185–228, 2004.

L.A. Bruijnzeel. Hydrology of tropical montane cloud forests: A reassessment. 2001. doi: doi.org/10.22004/ag.econ.47849.

L.Adrian Bruijnzeel and Mark Mulligan. Hydrometeorology of tropical montane cloud forests: Emerging patterns. *Hydrological Processes*, 25:465–498, 2011. doi: doi.org/10.1002/hyp.7974.

B. Cilia, F. Hilmer, A. Jongkind, P. van Leeuwen, and R. Rosman. A study into cloud forests: The installation of a long-term setup to investigate the impact of a cloud forest canopy on the mestelá river catchment and its effect on various stakeholders. Master's thesis, Technical University of Delft, 2023.

(CCFC) Community Cloud Forest Conservation. Q'eqchi agriculture. Technical report, Community Cloud Forest Conservation, 2020a. URL https://cloudforestconservation.org/knowledge/community/qeqchi-agriculture/.

(CCFC) Community Cloud Forest Conservation. Conservation. Technical report, Community Cloud Forest Conservation, 2020b. URL https://cloudforestconservation.org/knowledge/conservation/.

(CCFC) Community Cloud Forest Conservation. Our work. Technical report, Community Cloud Forest Conservation, 2020c. URL https://cloudforestconservation.org/our-work/.

L.A. Cuartas, J. Tomasella, A.D. Nobre, C.A. Nobre, M.G. Hodnett, M.J. Waterloo, S.M. de Oliveira, R. de Cássia von Randow, R. Trancoso, and M. Ferreira. Distributed hydrological modelling of a micro-scale rainforest watershed in amazonia: Model evaluation and advances in calibration using the new hand terrain model. *Journal of Hydrology*, 462-463:15–27, 2012. doi: https://doi.org/10.1016/j.jhydrol.2011.12.047.

K. Deb, A. Pratap, S. Agarwal, and T. Meyarivan. A fast and elitist multiobjective genetic algorithm nsga-ii. *IEEE Transactions on Evolutionary Computation*, 2002.

Leonard F. DeBano. The effect of fire on soil properties. *Proceedings, Management and Productivity of Western-Montane Forest Soils*, 1990.

Sean Dixon-Sullivan. Agroforestry regeneration communities. Technical report, Contour Lines, 2024. URL https://agroforestryrc.org/projects/guatemala/.

Steve Earle. *Environmental Geology*. Pressbooks, 2024.

F. Fenicia, H. Savenije, P. Matgen, and L. Pfister. Understanding catchment behavior through stepwise model concept improvement. *Water Resources Research*, 44, 2008.

Fabrizio Fenicia, Dmitri Kavetski, and Hubert Savenije. Elements of a flexible approach for conceptual hydrological modeling: 1. motivation and theoretical development. *Water Resources Research*, 47, 2011. doi: doi.org/10.1029/2011WR010748.

(OCHA) United Nations Office for the Coordination of Humanitarian Affairs. Guateala - floods ocha situation report no. 1. Technical report, OCHA, 2000. URL https://www.unocha.org/publications/report/guatemala/guatemala-floods-ocha-situation-report-no-1.

Arnoud Frumau, L. Adrian Bruijnzeel, and Conrado Tobon. Precipitation measurement and derivation of precipitation inclination in a windy mountainous area in northern costa rica. *Hydrological Processes*, 25:499 – 509, 2011.

H. Gao, M. Hrachowits, F. Fencia, S. Gharari, and H. Savenije. Testing the realism of a topography-driven model (flex-topo) in the nested catchments of the upper heihe, china. *Hydrology and Earth System Sciences*, 2014.

S. Gharari, M. Hrachowitz, F. Fenicia, H.Gao, and H.H.G. Savenije. Using expert knowledge to increase realism in environmental system models can dramatically reduce the need for calibration. *Hydrology and Earth System Sciences*, 18:4839–4859, 2015. doi: 10.5194/hess-18-4839-2015.

P. Grubb. Control of forest growth and distribution on wet tropical mountains: with special reference to mineral nutrition. *Annual Review of Ecology and Systematics*, 1977.

Hoshin Gupta, Soroosh Sorooshian, and Patrice Ogou Yapo. Toward improved calibration of hydrological models: Multiple and noncommensurable measures of information. *Water Resources Research*, 34, 1998. doi: 10.1029/97WR03495.

Juventino Gálvez, Cecilia Cleaves, and Idalia Monrroy. Cambio climático y biodiversidad, elementos para analizar sus interacciones en guatemala con un enfoque ecosistémico. Technical report, (iarna) Instituto de Agricultur, Recursos Naturales y Ambiente, 2011. URL http://www.infoiarna.org.gt/wp-content/uploads/2017/11/Documento37.Cambioclimticoybiodiversidad.ElementosparaanalizarsusinteraccionesenGuatemalaconunenfoqueecosistmico.pdf.

W. A. Haber, N. Nadkarni, and N. Wheelwright. in monteverde: Ecology and conservation of a tropical cloud forest. *Eds. Oxford Univ. Press*, page 39–70, 2000.

L.S. Hamilton. Montane cloud forest conservation and research: a synopsis. *Mountain Research and Development*, 15:259–266, 1995.

Hijmans. Mapa de zonas de vida de guatemala basado en el sistema de clasificatión de holdrige. Technical report, Inforiarna, 2005. URL `http://www.infoiarna.org.gt/recursos-informativos/mapas/`.

L. R. Holdridge. Ecología basada en zonas de vida. *IICA*, 1978.

F. Holwerda and A.G.C.A. Meesters. Soil evaporation in a shaded coffee plantation derived from eddy covariance measurements. *Journal of Geophysical Research: Biogeosciences*, 124:1472–1490, 2019. doi: https://doi.org/10.1029/2018JG004911.

M. Hosseini, H. McNairn, A. Merzouki, and A. Pacheco. Estimation of leaf area index (lai) in corn and soybeans using multi-polarization c- and l-band radar data. *Remote sensing of Environment*, 2015.

Instituto Nacional de Estadistica Guatemala (INE). Estimaciones y proyecciones de la población. Technical report, INE, 2019.

Instituto Nacional de Sismología, Vulcanología, Meteorología e Hidrologia (INSIVUMEH). Meteorological public information. 2024.

International Organization for Migration (IOM). Guatemala crisis response plan 2024. Technical report, 2024.

Andy Jarvis and Mark Mulligan. The climate of cloud forests. *Hydrological processes*, 2010. doi: doi.org/10.1002/hyp.7847.

B. Johansson and D. Chen. The influence of wind and topography on precipitation distribution in sweden, statistical analysis and modelling. *International journal of climatology*, 2003.

V. Kapos, J. Rhind, M. Edwards, and M.F. Price. Developing a map of the world's mountain forests. *Sustainable Mountain Development: A State-of-knowledge Report for 2000*, 2000.

Kim Keating and Peter Gogan. A simple solar radiation index for wildlife habitat studies. *Journal of Wildlife Management*, 2010. doi: doi.org/10.2193/2006-359.

Philip J. Klotzbach. Caribbean/central american hurricane landfall probabilities. *3A.4*, 2008.

M. Knorr-Evans, W. Anderson, R. Nogueron, T. Schneider, and R. Zamora-Cristales. 3 ways well-interntioned forest laws and their enforcement can block restoration. Technical report, World Resource Institute, 2019.

Pavel Krasilnikov. Monatane cloud forests. *Encyclopedia of the World's Biomes*, 3:138–145, 2020.

E. L. Kuniansky, C. J. Taylor, J.H. Williams, and F. Paillet. Introduction to karst aquifers. *The Groundwater Project*, 2022. doi: doi.org/10.21083/978-1-77470-040-2.

K.A. Longman and J. Jenik. Tropical forests and its environment. *John Wiley and Sons*, 23:374, 1987.

S.M. López-Ramírez, L. Sáenz, A. Mayer, L.E. Muñoz-Villers, H. Asbjornsen, Z.C. Berry, N. Looker, R. Manson, and L.R. Gómez-Aguilar. Land use change effects on catchment streamflow response in humid tropical montane cloud forest region, central veracruz, mexico. *Hydrological processes*, 34: 3555–3570, 2020.

F. López-Serrano, T. Landete-Castellejos, J. Martínez-Millán, and A. del Cerro-Barja. Lai estimation of natural pine forest using a non-standard sampling technique. *Agricultural and Forest Meteorology*, 2000.

(MAGA) Ministerio de Agricultura Ganadería y Alimentación de la República de Guatemala. Data de los departamentos de alta verapaz y baja verapaz. 2024.

G. Magrin, J. Marengo, J. Boulanger, M. Buckeridge, E. Castellanos, G. Poveda, F. Scarano, and S. Vicuña. Central and south america, in: Climate change 2014: Impacts, adaptation, and vulnerability, part b: Regional aspects, contribution of working group ii to the fifth assessment report of the intergovernmental panel on climate change. *Cambridge University Press*, 2014.

A. Malmer, D. Murdiyarso, L.A. Bruijnzeel, and U. Ilstedt. Carbon sequestration in tropical forest and water: a critical look at the basis for commonly used generalizations. *Global Change Biology*, 16: 599–604, 2010. doi: https://doi.org/10.1111/j.1365-2486.2009.01984.x.

A. Merkel. Climate: Guatemala. Technical report, Climate Data, 2021a. URL `https://en.climate-data.org/north-america/guatemala-229/`.

A. Merkel. Climate: Alta verapaz. Technical report, Climate Data, 2021b. URL `https://en.climate-data.org/north-america/guatemala/alta-verapaz/san-juan-chamelco-46096/`.

M. Mulligan and S. Burke. Fiesta fog interception for the enhancement of streamflow in tropical areas final technincal report for ambiotek contribution to dfid frp r7991. 2005. URL `http://www.ambiotek.com/fiesta/FIESTA_ftr_ambiotek_final.pdf`.

J.E. Nash and J.V. Sutcliffe. River flow forecasting through conceptual models part i - a discussion of principles. *Journal of Hydrology*, 10:282–290, 1970. doi: https://doi.org/10.1016/0022-1694(70)90255-6.

The Editors of Encyclopaedia Britannica. Cloud forest ecology. Technical report, Britannica, 2022.

Robert J. Oglesby, Thomas L. Sever, William Saturno, David J. Erickson III, and Jayanthi Srikishen. Collapse of the maya: Could deforestation have contributed? *Papers in the Earth and Atmpspheric Sciences*, 469, 2010.

Organización Meterológica Mundial (OMM). El estado del clima en américa latina y el caribe 2021. Technical report, 2022. URL `https://library.wmo.int/idurl/4/28347`.

A. Peduzzi, H. Allen, and R. Wynne. Leaf area of overstory and understory in pine plantations in flatwoods. *Southern Journal of Applied Forestry*, 2010.

I. Pope, D. Bowen, J. Harbor, G. Shao, L. Zanotti, and G. Burniske. Deforestation of montane cloud forest in the central highlands of guatemala: contributing factors and implications for sustainability in q'eqchi'communities. *Internation Journal of Sustainable Development and World Ecology*, 2015.

I. Pope, J. Harbor, L. Zanotti, G. Shao, D. Bowen, and G. Burniske. Cloud forest conservation in the central highlands of guatemala hinges on soil conservation and intensifying food production. *The Professional Geographer*, 68, 2016.

D. K. Ray. Vulnerability of water resources to climate. *Climate Vulnerability*, 2013.

Deepak K. Ray, Udaysankar S. Nair, Robert O. Lawton, and Roger A. Pielke Sr. Impact of land use on costa rican tropical montane cloud forests: Sensitivity of orographic cloud formation to deforestation in plains. *Journal of Geophysical Research*, 111, 2006. doi: 10.1029/2005JD006096.

Camilo Rennó, Antonio Nobre, Luz Cuartes, JoÃo Soares, Martin Hodnett, Javier Tomasella, and Maarten Waterloo. Hand, a new terrain descriptor using srtm-dem: Mapping terra-firme rainforest environments in amazonia. *Remote sensing of Environment*, 112:3469–3481, 2008. doi: doi.org/10.1016/j.rse.2008.03.018.

H. Savenije. Topography driven conceptual modelling (flex-topo). *Hydrology and Earth System Sciences*, 2010.

Hubert H.G. Savenije. Determination of evaporation from a catchment water balance at a monthly time scale. *Hydrology and Earth System Sciences*, 1, 1997.

T. Schneider, T. Bischoff, and G. Haug. Migrations and dynamics of the intertropical convergence zone. *Nature*, 2014.

Kevin Scott. The reduction of a local barometric pressure to a mean sea level value. *Practical Techniques and Know-How for making and measuring in the laboratory*, 2011.

M. Serio, F. Carollo, and V. Ferro. Raindrop size distribution and terminal velocity for rainfall erosivity studies. a review. *Journal of Hydrology*, 2019.

Justine M. Shaw. Climate change and deforestation: Implications for the maya collapse. *Ancient Mesoamerica*, 14, 2003. doi: https://doi.org/10.1017/S0956536103132063.

R. Smith. The influence of mountains on the atmosphere. *Advances in Geophysics*, 1979.

Solargis, 2024. obtained from the “Global Solar Atlas 2.0, a free, web-based application is developed and operated by the company Solargis s.r.o. on behalf of the World Bank Group, utilizing Solargis data, with funding provided by the Energy Sector Management Assistance Program (ESMAP). For additional information: https://globalsolaratlas.info.

Reihaneh Taslimi. Land use maps in the mestela catchment. Personal communication, 2024. Unpublished raw data.

P. Thanapakpawin, J. Richey, D. Thomas, S. Rodda, B. Campbell, and M. Logsdon. Effects of landuse change on the hydrologic regime of the mae chaem river basin, nw thailand. *Journal of Hydrology*, 334:215–230, 2007. doi: https://doi.org/10.1016/j.jhydrol.2006.10.012.

C. Uhl, R. Buschbacher, and J. Serrao. Abandoned pastures in eastern amazonia i. patterns of plant succession. *Journal of Ecology*, 76:663–681, 1988.

United Nations Office for the Coordination of Humanitarian Affairs (OCHA). Humanitarian needs overview guatemala 2023. Technical report, 2022.

United Nations Office for the Coordination of Humanitarian Affairs (OCHA). Humanitarian response plan guatemala 2024. Technical report, 2023. URL `https://humanitarianaction.info/plan/1173/article/guatemala-1`.

J.M Vargas, F. Pérex-Arce, and S. Valdés-Prieto. Spatial analysis of poverty in guatemala: The case of alta verapaz department. *Economía, Sociedad y Territorio*, 16:291–322, 2016.

E.J. Veneklaas, R. Zagt, A. van Leerdam, R. van Ek, A. Broekhoven, and M. van Genderen. Hydrological properties of the epiphyte mass of a montane tropical rain forest, colombia. *Vegetatio*, 89: 183–192, 1990.

J. Walper. Geology of cobán-purulhá area, alta verapaz, guatemala. *Bulletin of the American Association of Petroleum Geologists*, 1960.

Jan H.D. Wolf. *Ecology of epiphytes and epiphyte communities in montane rain forests, Colombia*. PhD thesis, Universiteit van Amsterdam, 1993.

World Meteorological Organisation (WMO). Reduction of atmospheric pressure (preliminary report on problems involved). *Technical note No. 7 (WMO-No. 36)*, 1954.

Yanfeng Wu, Jingxuan Sun, Boting Hu, Guangxin Zhang, and Alain N. Rousseau. Wetland-based solutions against extreme flood and severe drought: Efficiency evaluation of risk mitigation. *Climate Risk Management*, 2023.

F. Yang, J. Sun, H. Fang, Z. Yao, J. Zhang, Y. zhu, K. Song, Z. Wang, and M. Hu. Comparison of different methods for corn lai estimation over northeastern china. *Internation Journal of Applied Earth Observation and Geoinformation*, 18:462–471, 2012. doi: https://doi.org/10.1016/j.jag.2011.09.004.

F. Zadroga. The hydrological importance of a montane cloud forest area of costa rica. *Tropical Agricultural Hydrology*, pages 59–73, 1981.

Ren-Jun Zhao. The xinanjiang model applied in china. *Journal of Hydrology*, 135:371–381, 1992.

E. Zitzler and L.Thiele. Multiobjective evolutionary algorithms: a comparative case study and the strength pareto approach. *IEEE Transactions on Evolutionary Computation*, 1999.

A

FIESTA model Description

This Appendix shows the equations used in the FIESTA model to develop spatially distributed wind-adjusted precipitation, fog interception and evaporation. The equations shown in this Appendix are taken from the FIESTA Technical report by Mulligan and Burke (2005).

A.1. Precipitation

Wind-adjusted precipitation

Equation A.1 shows Equation 15 from the FIESTA model to determine the wind-adjusted precipitation.

$$\text{Wind correction factor} = 1 + (\text{Slope}) * \frac{W_s}{v_{term}} * cos(\text{Aspect} - W_d) \tag{A.1}$$

Where, W_s represents the wind speed in m/s, W_d is the wind direction in radians, v_{term} [m/s] is the constant terminal velocity of a raindrop and the slope and aspect are given in radians.

A.2. Fog Interception

Temperature

The temperature modified according to the diurnal temperature range, see Equation A.2, using Equation 6 from the FIESTA model are shown below, for four times of the day. For all the equations T represents the temperature in $[\circ C]$. The temperature represents the already adjusted temperature for elevation and land cover.

$$\text{Diurnal Temperature Range} = T_{max} - T_{min} \tag{A.2}$$

If the hour of the day is 24:00:

$$T_{adj} = T - 0.25 * \text{Diurnal Temperature Range} \tag{A.3}$$

If the hour of the day is 06:00:

$$T_{adj} = T \tag{A.4}$$

If the hour of the day is 12:00:

$$T_{adj} = T + 0.25 * \text{Diurnal Temperature Range} \tag{A.5}$$

If the hour of the day is 18:00:

$$T_{adj} = T \tag{A.6}$$

Lifting condensation level

The Lifting condensation level (LCL) is calculated using the ground temperature based on elevation (Temp) [°C], the dewpoint temperature (Td) [°C], elevation [m] and the mean sea level pressure (MSLP) [mb].

Dewpoint temperature (Td) [°C] is calculated using vapour pressure (E) and relative humidity (RH). First, the saturated vapour pressure (Es) is calculated using its relationship with temperature (Equation A.7, followed by vapour pressure (E) using its relation to relative humidity A.8 (Equation 7 FIESTA model).

$$Es = \exp\left(26.66082 - 0.0091379024 * (T + 273.25) - \frac{6106.396}{T + 273.15}\right) \tag{A.7}$$

$$E = \frac{RH}{100} * Es \tag{A.8}$$

The dewpoint temperature (Td) is then calculated using the vapour pressure and the relationship shown in equation A.9 (Equation 9 FIESTA model).

$$Td = \frac{(26.66082 - \log(E)) - \sqrt{(26.66082 - \log(E))^2}}{0.0182758048} - 273.15 \tag{A.9}$$

The lifting condensation is first calculated in mb and then converted to masl (meters above sea level), shown in Equation A.10 (Equation 10 FIESTA model).

$$LCL = \frac{1}{(\frac{Temp - Td}{223.15}) + 1}^{3.5} * MSLP \tag{A.10}$$

Fog Impaction flux

The amount of water passing by the representative vegetation types is calculated with Equation 16 of the FIESTA model. This impaction flux is determined for two vegetation types: trees, including land cover class forest and pine plantation, and for grass including land cover class agriculture. Equation A.11 calculates the kg/cell of water passing through the agricultural fields. In the case of trees the impaction flux is calculated for both the forest edges and emergent trees, shown in Equation A.12 and Equation A.13.

$$\text{Agriculture Impaction Flux} = LWC * W_s * 0.605 * \text{Fraction Clear} * \text{Cell area} * H_{agr} \tag{A.11}$$

$$\text{Forest Edge Impaction Flux} = LWC * W_s * 0.6053 * 3600 * L_{f_{edge}} * H_{f_{edge}} \tag{A.12}$$

$$\text{Forest Emergent Impaction Flux} = LWC * W_s * 3600 * H_{f_{emergent}} \tag{A.13}$$

These equations are a combination of the wind flux and the amount of water present. The amount of water present in the clouds: The Liquid Water Content (LWC) $[kg/m^3]$ is determined using Equation A.15, Equation 8 of the FIESTA model paper. The LWC of clouds is as a simplification assumed to be proportional to the absolute atmospheric humidity. The absolute humidity (AH) $[kg/m^3]$ is calculated using the vapour pressure (E) [mb] and the Temperature (Temp) [°C], see Equation A.14. The vapour pressure is determined using the temperature and the relative humidity.

$$AH = \frac{E + 100}{(Temp + 273.15) * 461.5} \tag{A.14}$$

$$LWC = \frac{AH}{max(AH)} * max(LWC) \tag{A.15}$$

In order to determine the impaction flux at forest edges and emergent trees, first the sizes of these areas need to be determined. The forest edge length is determined using an empirical equation developed by Mulligan and Burke (Equation 3 FIESTA model) and calculated based on tree cover fraction and cell area, shown in the equations A.16, A.17 and A.18.

$$\text{Forest edge fraction} = -0.0001 * \text{Tree Fraction}^2 + 0.0144 * \text{Tree Fraction} \tag{A.16}$$

$$\text{Forest edge length} = \frac{\text{Forest edge Fraction} * \sqrt{\text{cell area}} * 4}{4} \tag{A.17}$$

$$\text{Emergent edge length} = \frac{0.05 * \text{Tree Fraction} * \sqrt{\text{cell area}} * 4}{4} \tag{A.18}$$

The fraction of exposed emergent trees is calculated as 5% fractional of the area covered by tree. Emergent trees are occasional individual trees that rise beyond the canopy. The division by 4 accounts for the fact that only one edge of a grid cell will face a wind from a particular direction. The forest edge length is calculated in meters. The direction of the forest edges are assumed to be randomly distributed among the eight compass directions.

Once the LWC of clouds $[kg/m^3]$, the forest edge length [m], the emergent edge length [m] are determined, the impaction flux for forest edges, emergent trees and agricultural fields can be calculated in combination with the wind flux determined in Section 6.1.2. The value of 0.6053 in the equations A.11, A.12 and A.13 is the reduction factor which reduces wind speeds as a result of frictional losses with the vegetation. This values is calculated in the FIESTA model using comparisons of forest and pasture site vertical wind profiles. The tree fraction is the fraction of the cell size which consists of trees, the constants used in the equations are defined in Table 6.3.

Fog Deposition flux

The fog deposition flux, or in other words the settling flux, is calculated using Equation 17 from the FIESTA model. The settling flux is calculated with the LWC and the gravity flux which is determined with the fog settling velocity, shown in Equation A.19. Where $v_{fogsettling}$ is the fog settling velocity in m/s.

The fog settling velocity is calculated according to Equation 2 of the FIESTA model. This constant is calculated according to the Stokes Law based on the mean particle size for fog, defined as 7.5 μm as seen in Table 6.3.

$$\text{Fog settling flux} = LWC * v_{fogsettling} * 3600 * \text{Cell area} \tag{A.19}$$

Proportion of impaction and deposition

The total fog interception is a sum of the deposition interception and the impaction interception. This depends on the proportion of fog inputs which is deposited rather than impacted. The previously determined fluxes are multiplied by the proportion of which the flux is occurring and the area over which this process takes place.

The proportion of deposition and impaction is dependent on the cosine of the fog inclination angle over the vegetation fractions. The fog inclination angle is different for trees and for agricultural fields, due to a different frictional loss of wind with the vegetation. For trees the frictional loss factor is set as 0.6053 and for agricultural fields as 0.5030. The fog inclination angle equation is calculated the previously calculated adjusted wind speed and fog settling velocity, shown in Equation A.20.

$$\text{Fog Inclination Angle} = \frac{tan(W_s * \text{frictional factor})}{v_{fogsettling}} \tag{A.20}$$

The proportion of deposition is then determined multiplying the cosines of the fog inclination angle of trees with the fraction of trees in the grid cell with the cosines of the fog inclination angle of agricultural fields with the fraction of agricultural fields present in the grid cell. The proportion of impaction is then logically 1 - the proportion of deposition.

Total fog interception

The total fog interception depends on the proportion which is deposited and which in impacted determined by the fog inclination angle. Then this is taken over the fraction area and only true when fog is present.

$$\text{Fog Interception} = fog*(\text{Settling flux}*\text{Proportion deposition}*\text{Deposition fraction}+\text{Impaction flux}*\text{Proportion Impaction}* \tag{A.21}$$

Equation A.21 is given in $kg/m^2/hr$, in order to convert to mm the fog interception is divided by the true area of the grid cell and multiplied by the factor of cloud frequency. Taken into account the amount of fog present during the day, which is proportional to the amount of clouds present. Since, the fog interception is calculated for four times per day, each time step is multiplied by six to give daily fog interception.

For impaction the trapping surface area of both trees and agricultural fields is determined, using the Equation 18 of the FIESTA model. The fog trapping surface area depends on the leaf area density of the vegetation and the angle of the incoming fog relative to the leaves. The assumption is made that impaction only occurs when air is rising, because the model assumes that air flows close to the ground when moving uphill but above ground in leeward direction. The model assumes that air rising only occurs during the day, therefore air rising is only true during time step 2 and 3. In this adaptation this is assumed because mountain breeze dominates over the prevailing wind. Import to note is that the parameter air rising is only true for the situation where upwind elevations are greater than the downwind cell. The influence of downhill conditions on the uphill fog trapping capacity is not incorporated in this model.

A.3. Evaporation

Net radiation

The effective solar radiation is determined by accounting for transmission losses due to fog and clouds. Using Equation 12 of the FIESTA model and established empirical parameters derived from field measurements, extraterrestrial radiation is converted to ground level radiation. This conversion involves corrections for fog presence (Equation A.22) and absence (Equation A.23). The solar radiation is converted to ground level by multiplying it by 1 - the transmission loss.

$$\text{Transmission loss} = \text{Cloud Frequency Fraction}*0.678-(1-\text{Cloud Frequency Fraction})*0.143 \tag{A.22}$$

$$\text{Transmission loss} = \text{Cloud Frequency Fraction}*0.525-(1-\text{Cloud Frequency Fraction})*0.143 \tag{A.23}$$

Net radiation depends on land cover and effective ground-level solar radiation on the ground. The conversion from ground-level solar radiation to net radiation is based on empirical constants defined by the FIESTA model and outlined in Equation 13 of the FIESTA model report. The linear relationship between net and solar radiation is established using sensors above forest and pasture covers.

$$\text{Net radiation} = 0.9 - 27.9 * \text{Solar ground radiation} \tag{A.24}$$

$$\text{Net radiation} = 0.8 - 27.5 * \text{Solar ground radiation} \tag{A.25}$$

Potential evaporation

Both potential evaporation (Ep) and actual evaporation (Ea) are calculated. The slope of the saturation vapor pressure curve, as shown in Equation A.26, is determined based on the current temperature.

$$\text{Slope} = \frac{4098 * \frac{611*\log 17.27*Temp}{273.15+Temp}}{1000} \over (273.15 + Temp)^2 \tag{A.26}$$

Equation (A.27) calculates potential evaporation (Ep) [mm] using the previously determined slope of the saturation vapour pressure curve. Where 0.0036 is used to convert the evaporation to mm per hour and 2.45 MJ/kg is the latent heat of vaporization.

$$Ep = \frac{(\frac{Slope}{Slope+0.066} * \text{Net Radiation}) * 0.0036}{2.45} \tag{A.27}$$

B

FIESTA model results

This Appendix shows graphical results of the temporal and spatial results of the FIESTA model of the different meteorological data.

B.1. Spatial results

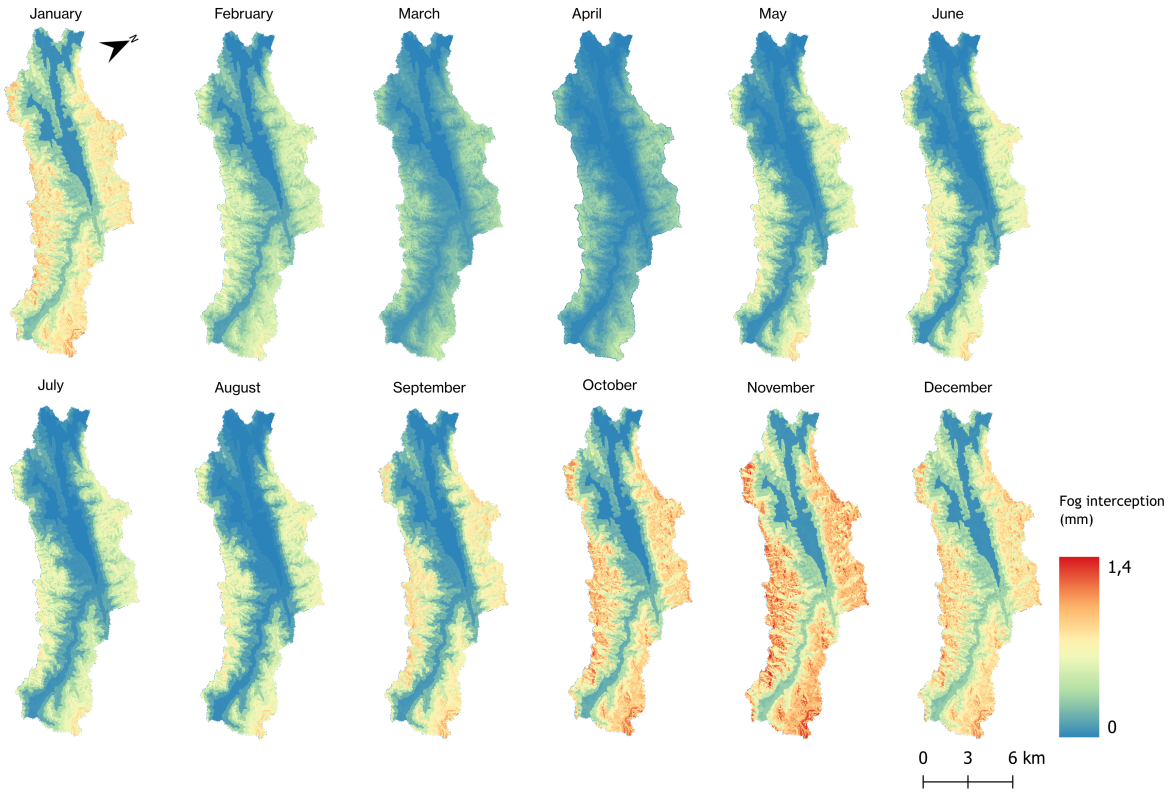

Figure B.1: Monthly variation of fog interception in the Upper Cahabon catchment (1998-2024)

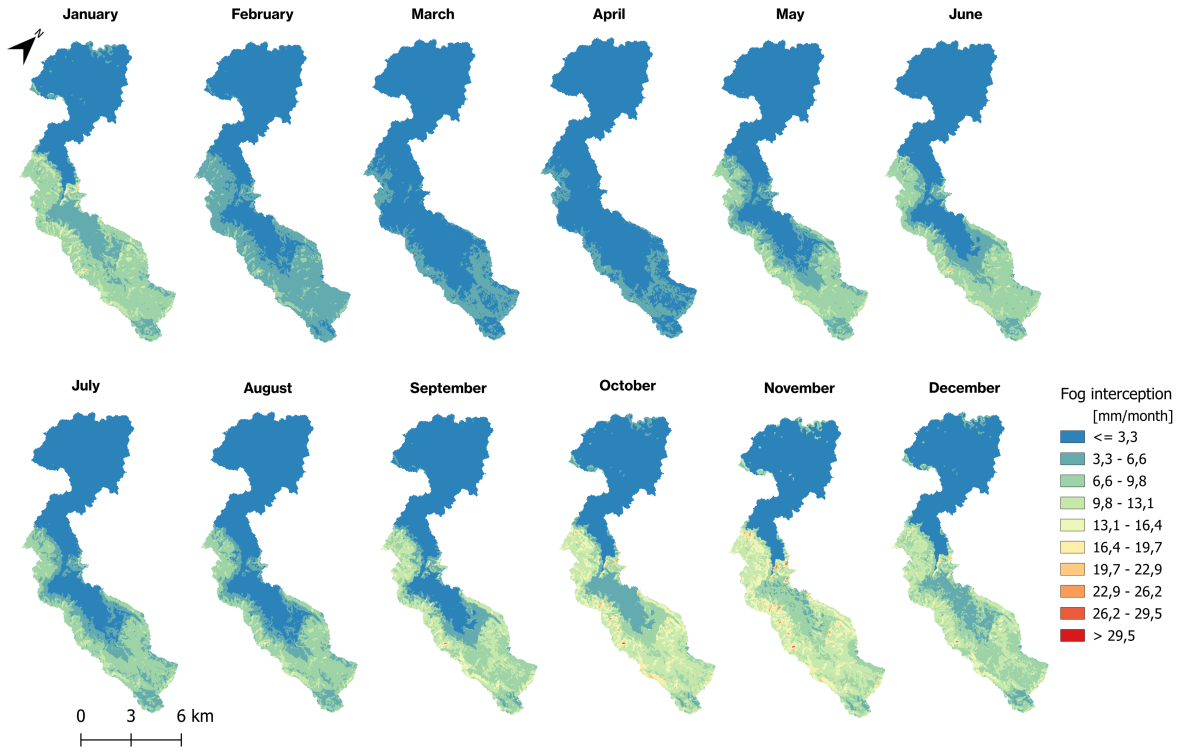

Figure B.2: Monthly variation of fog interception in the Mestelá catchment (1998-2024)

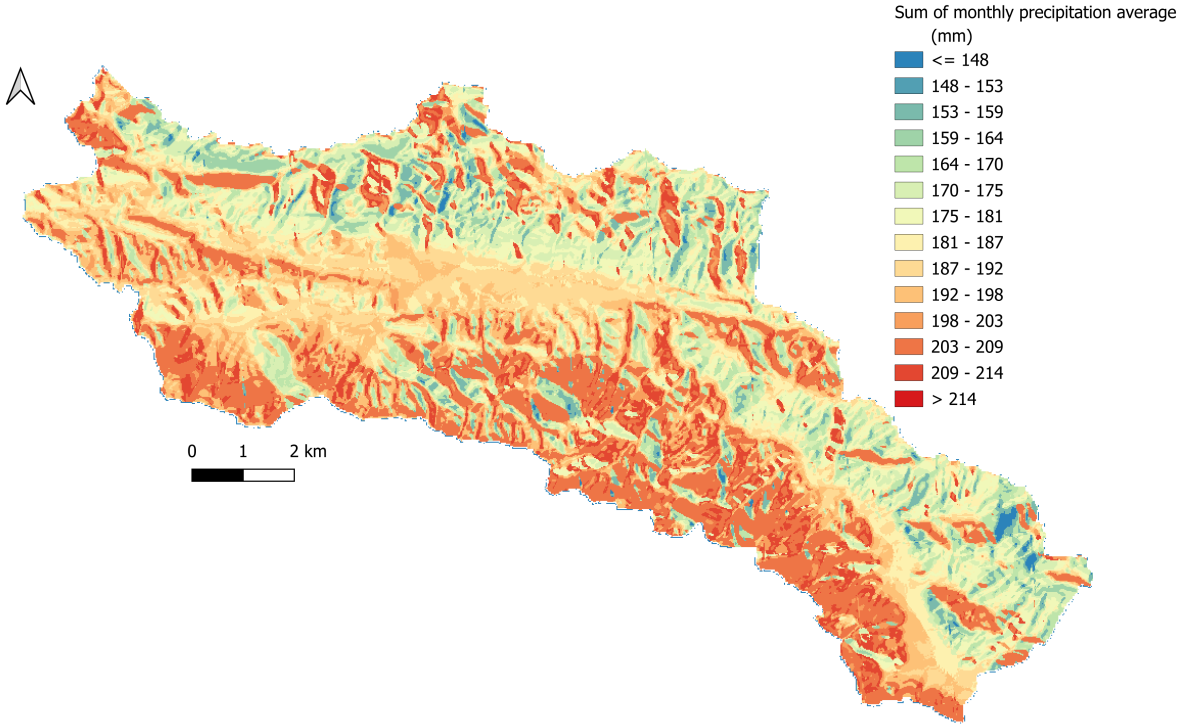

Figure B.3: Mean annual precipitation in the Upper Cahabon catchment (1998-2024)

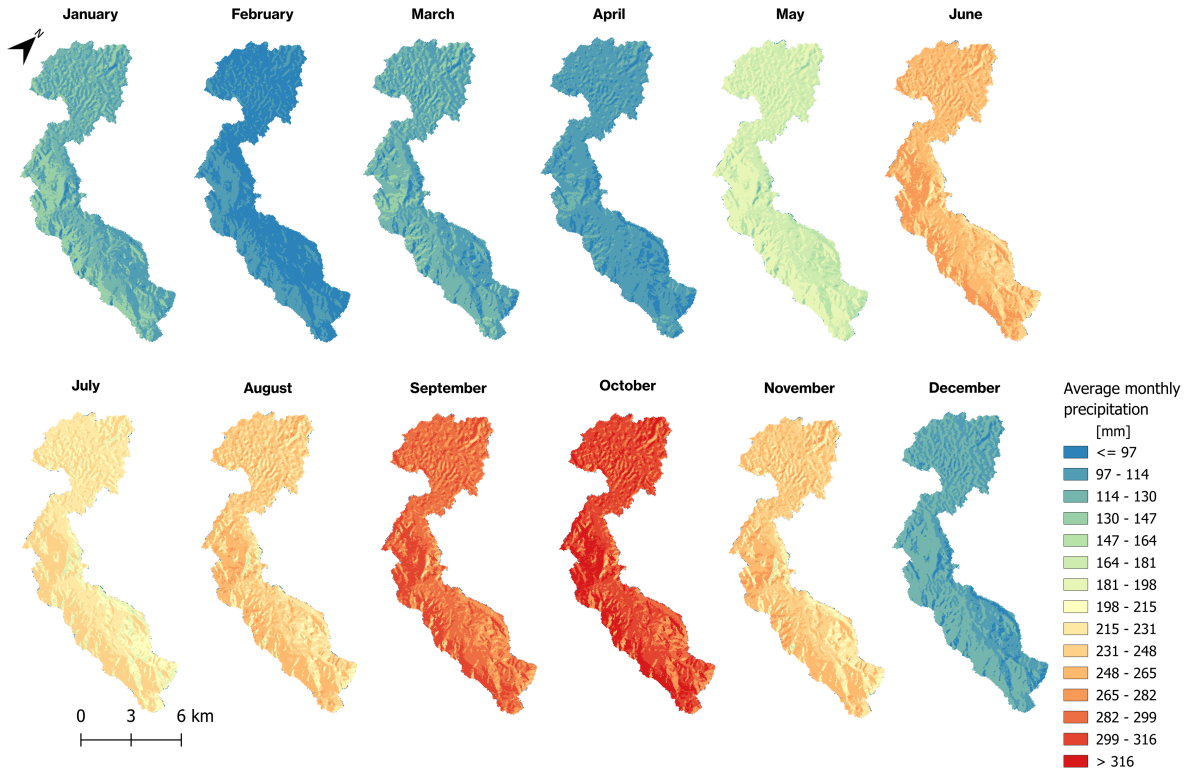

Figure B.4: Mean precipitation per month of the year for the Mestelá catchment (1998-2024)

B.2. Temporal results

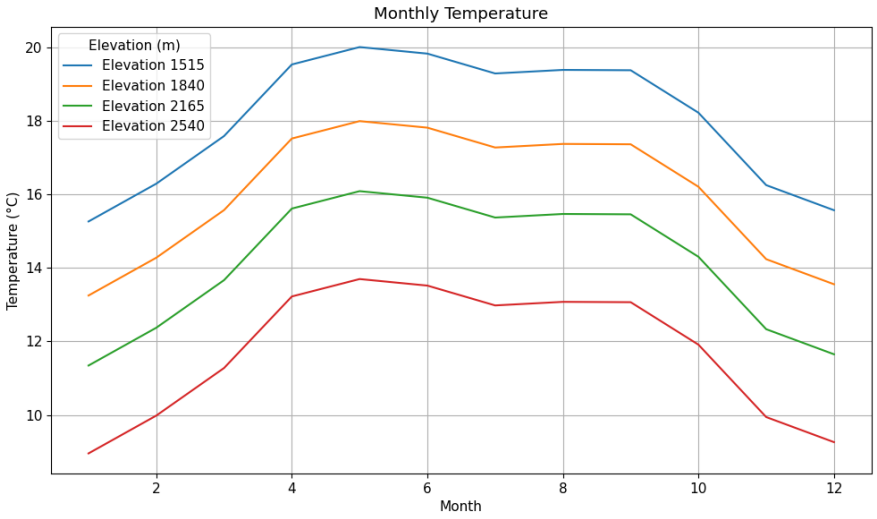

Figure B.5: Mestelá catchment mean temperature per elevation class for each month of the year

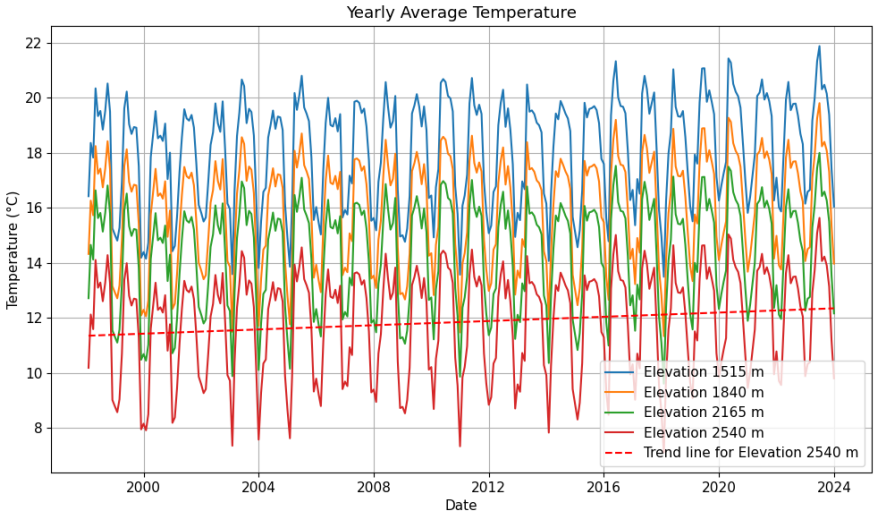

Figure B.6: Mean monthly temperature for the Mestelá catchment per elevation class. Trend line is shown for elevation 2540 m, slope of the trend line is the same for every elevation class.

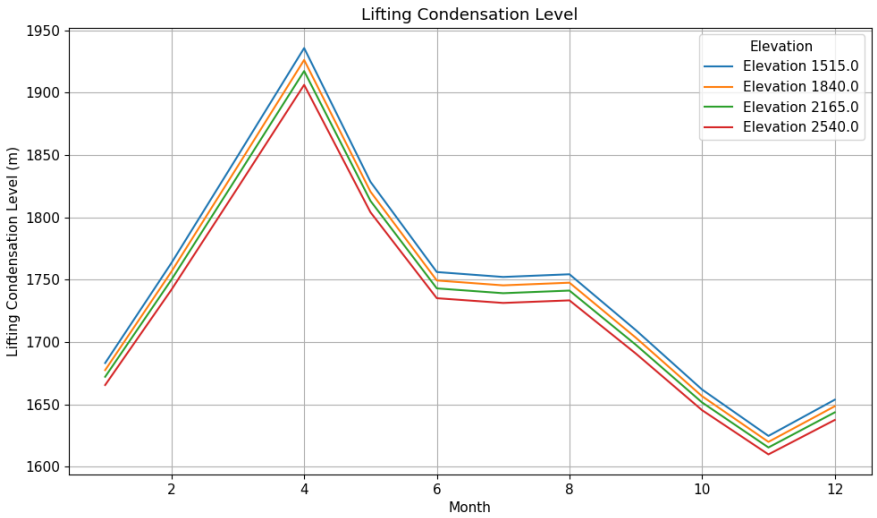

Figure B.7: Mean Lifting Condensation Level (LCL) per month of the year for Mestelá catchment (1998-2024)

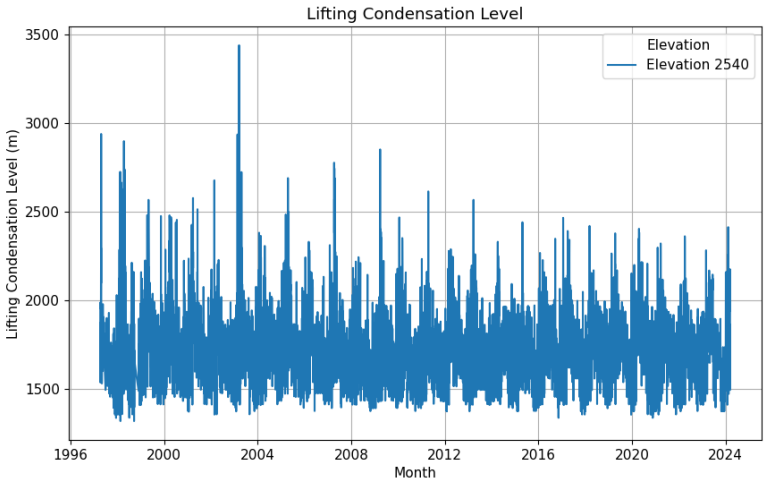

Figure B.8: Lifting Condensation level timeseries in the Mestelá catchment, mean value for all spatial classes with elevation of 2540 meters

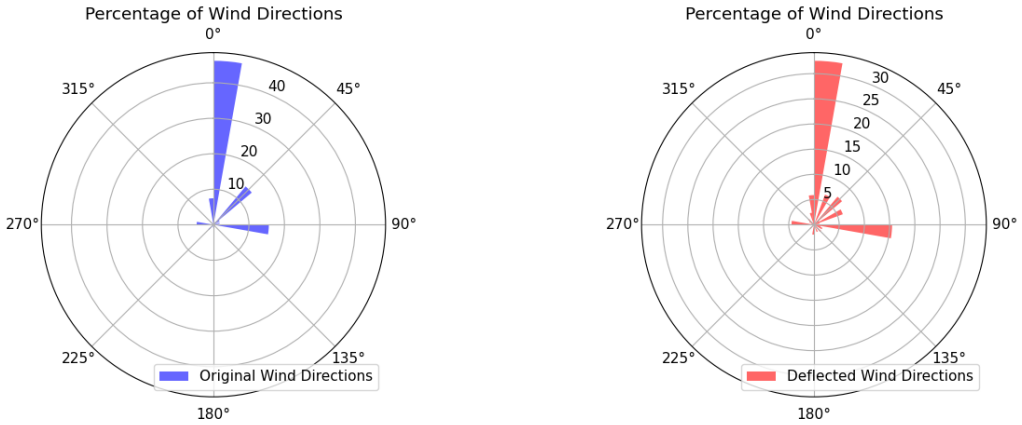

(a) Wind direction percentages of measurement station in Coban

(b) Deflected wind directions based on topography

Figure B.9: Percentages of wind direction of the FIESTA model for the Mestelá catchment

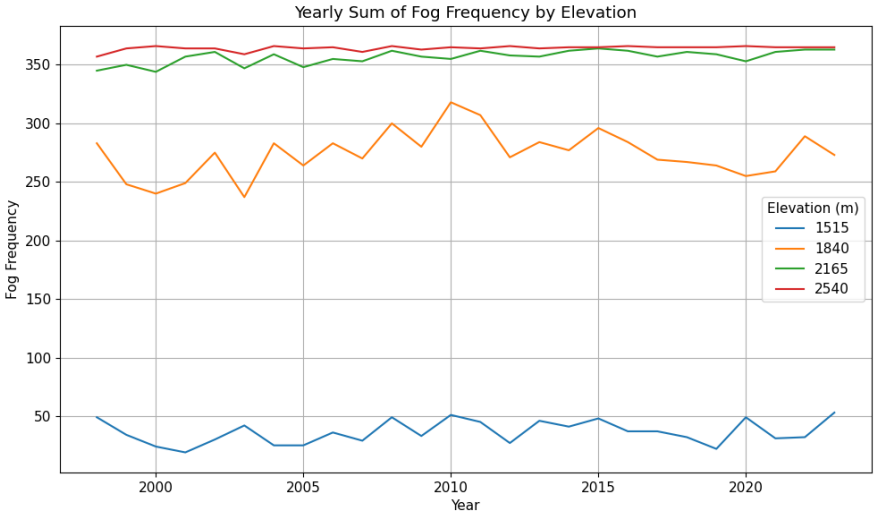

Figure B.10: Annual fog frequency per year for different elevation classes in the Mestelá catchment

B.3. Scenarios

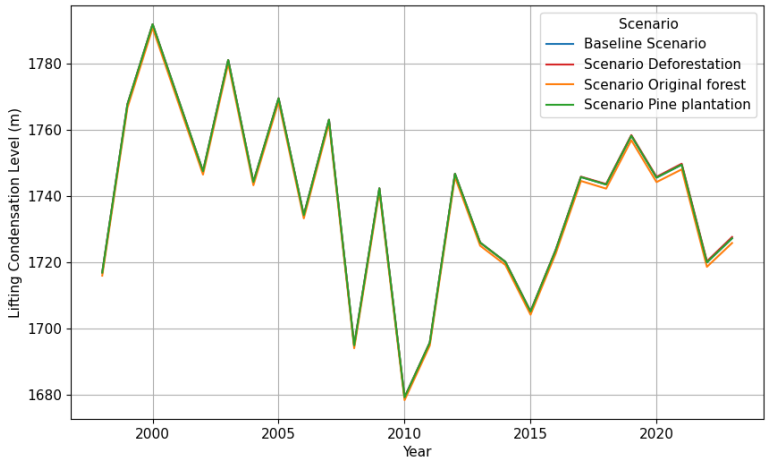

(a) mean lifting Condensation Level of all land use scenarios

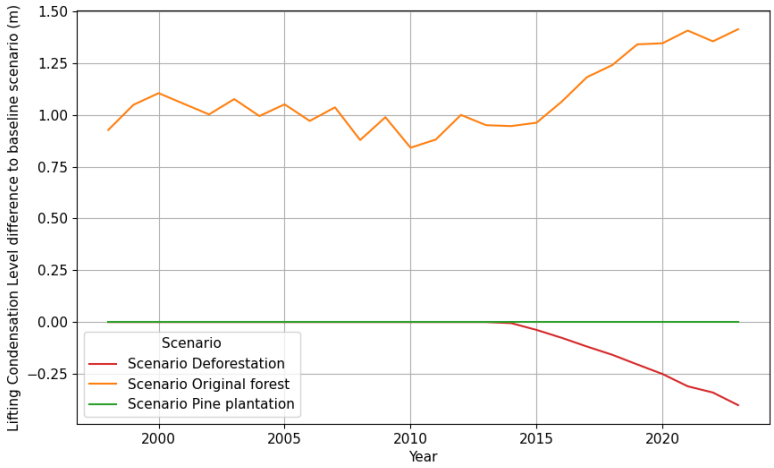

(b) Lifting Condensation Level difference compared to the baseline scenario

Figure B.11: Lifting Condensation level comparison of all land use scenarios compared to the baseline scenario

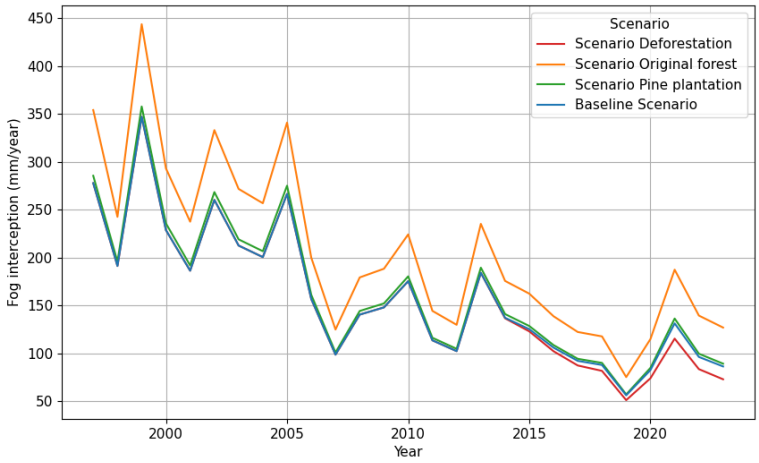

Figure B.13: Mean annual fog interception of all land use scenarios

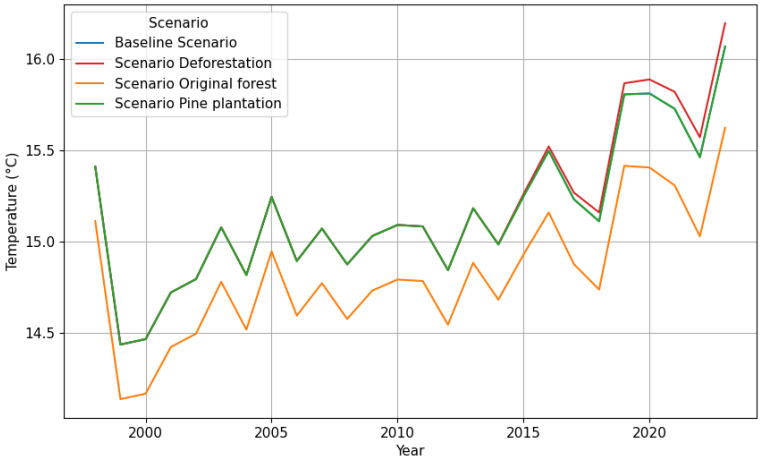

Figure B.12: Yearly mean temperatures of each land use scenario

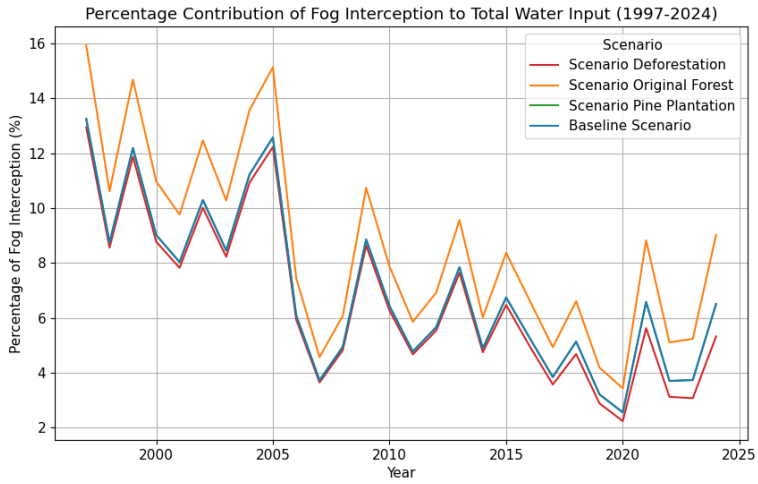

Figure B.14: Percentage of mean fog interception to the total water input compared for all land use scenarios

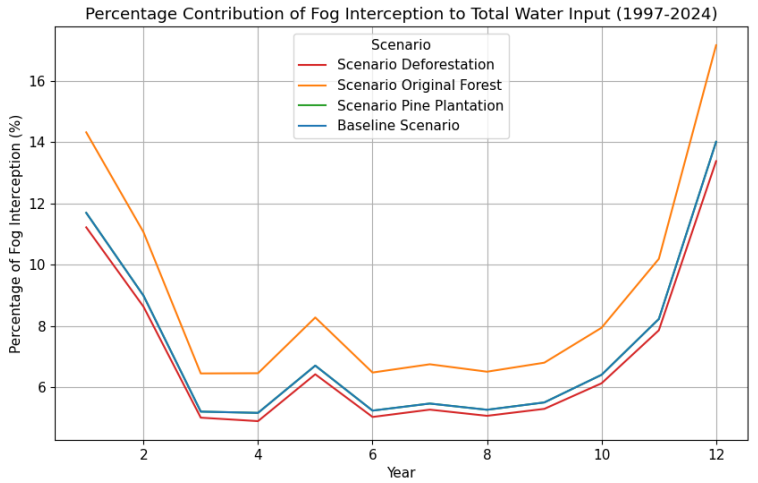

Figure B.15: Percentage of mean fog interception to the total water input compared for all land use scenarios

C

Land Use Scenario comparison plots

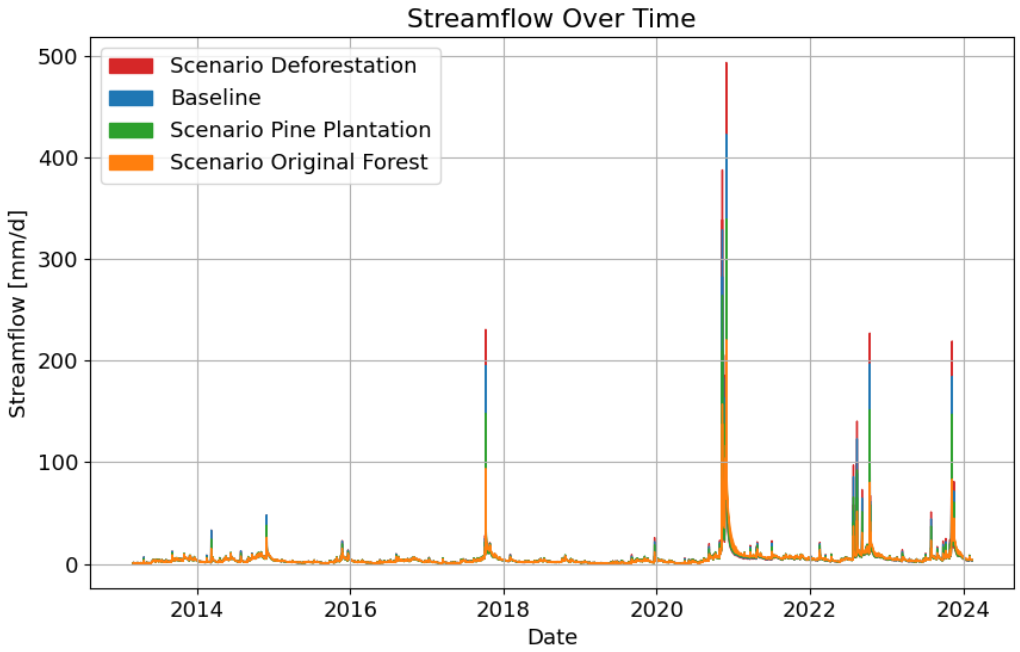

Figure C.1: Hydrograph of all the scenarios compared to the baseline streamflow

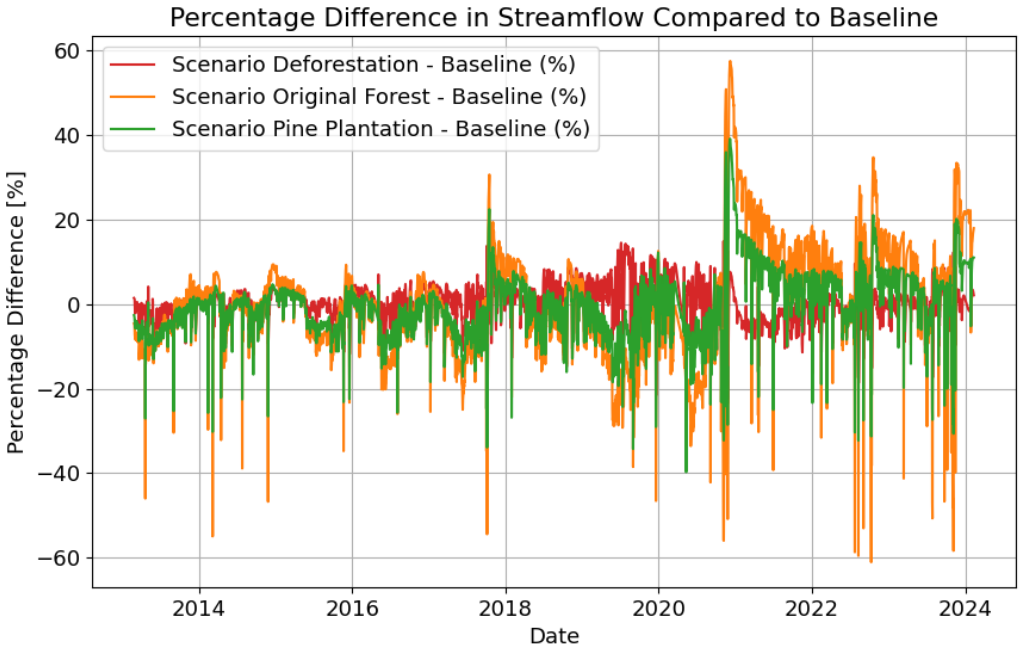

Figure C.2: Percentage difference of scenarios compared to the baseline streamflow shown in the timeseries

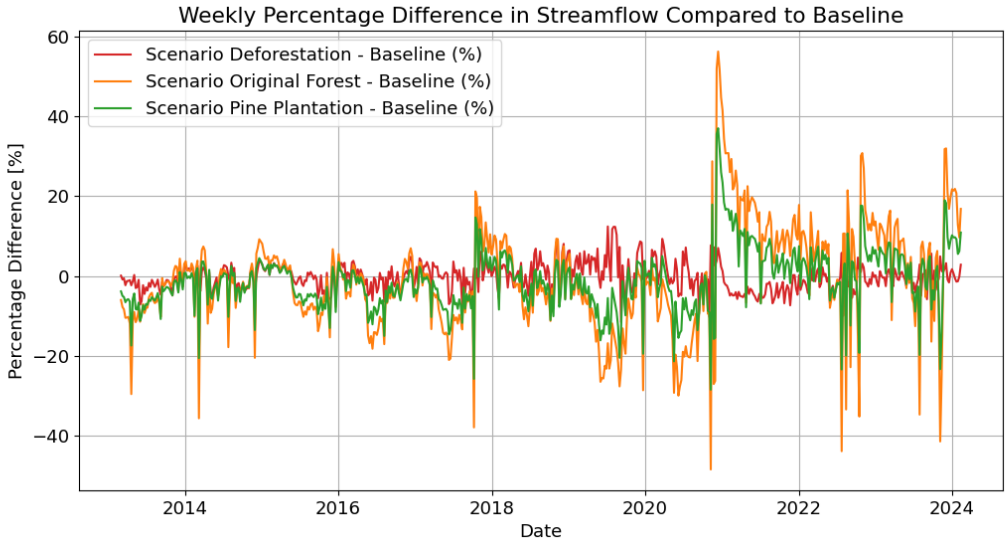

Figure C.3: Average weekly percentage difference of scenarios compared to the baseline streamflow shown in the timeseries

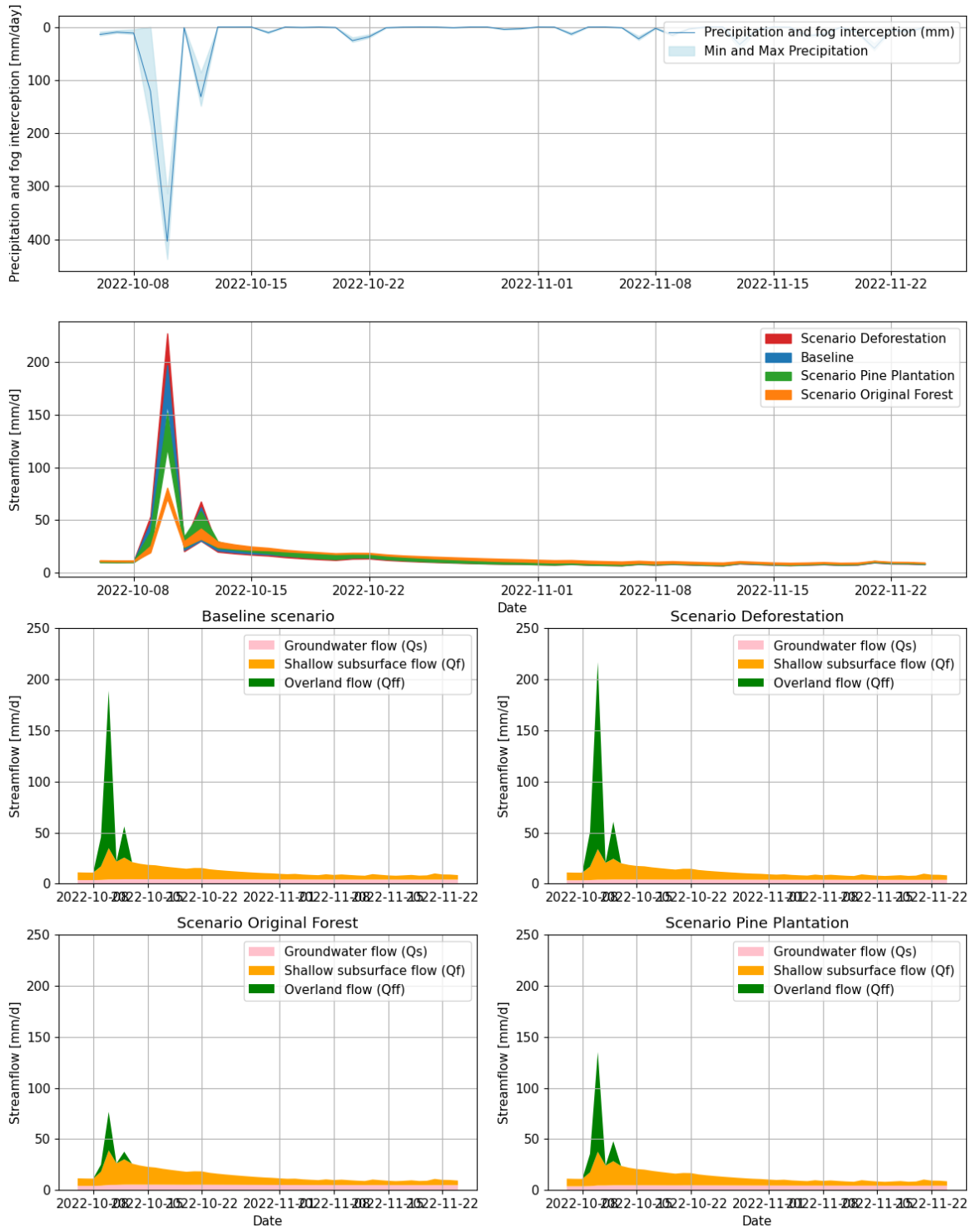

Figure C.4: Streamflow and it different flow contributions to streamflow shown for the different scenarios for high flow conditions. Including an overview of the fog and precipitation inputs (top) and overall streamflow compared for each scenario (middle).

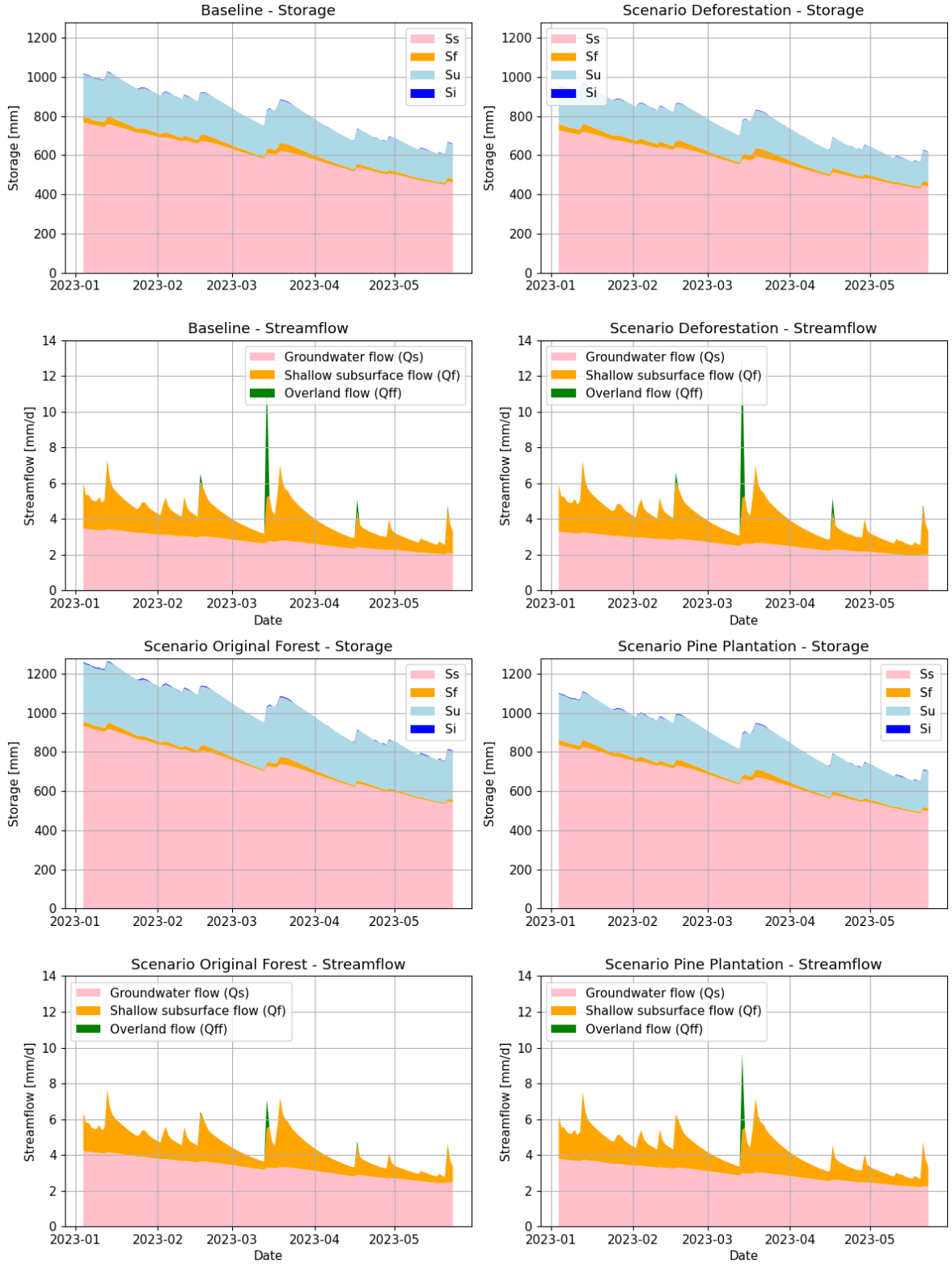

Figure C.5: Streamflow and it different flow contributions and storage components to streamflow shown for the different scenarios during median flow conditions.

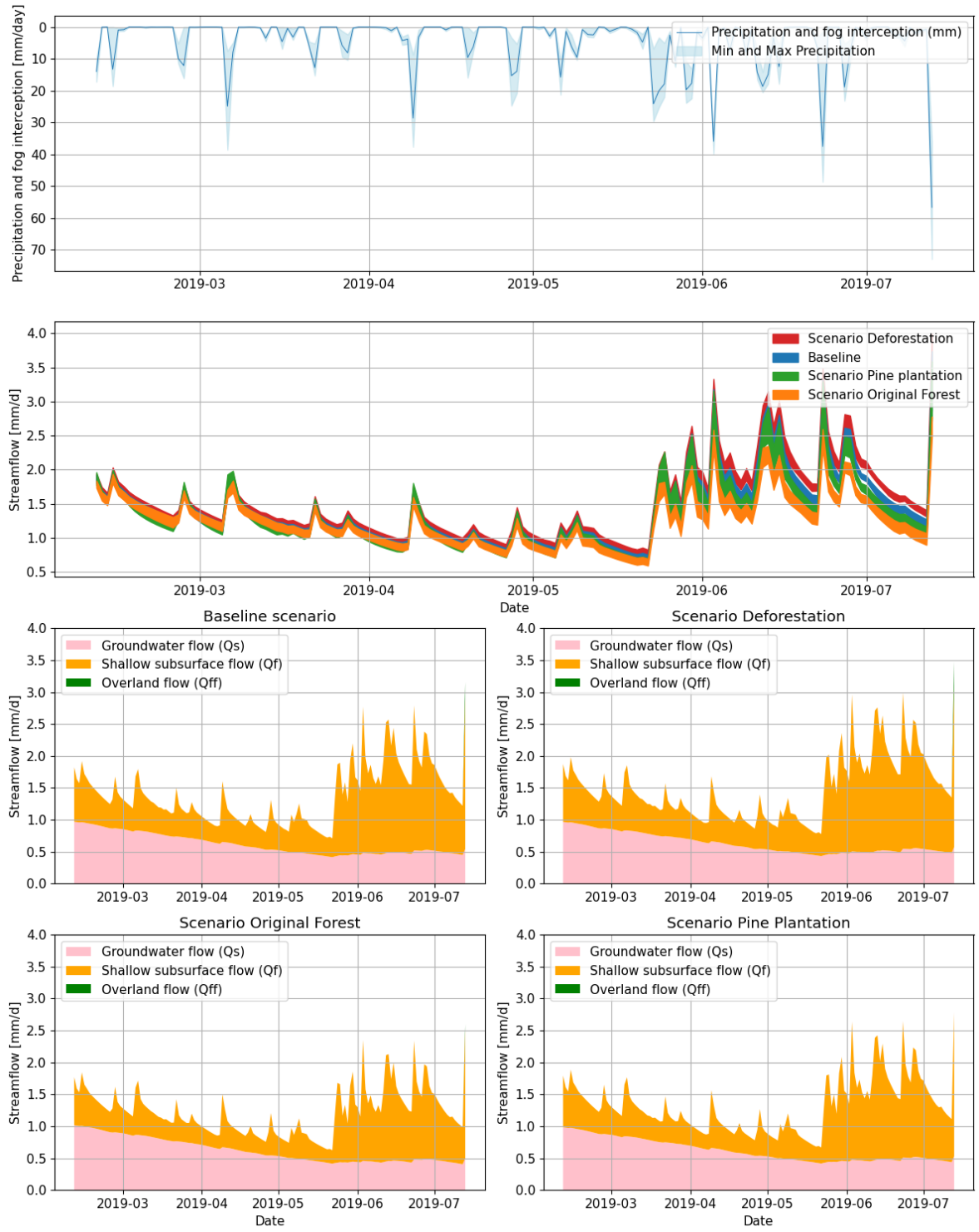

Figure C.6: Streamflow and it different flow contributions to streamflow shown for the different scenarios for very low flow conditions. Including an overview of the fog and precipitation inputs (top) and overall streamflow compared for each scenario (middle)

C.1. Flow components
C.2. Quantiles

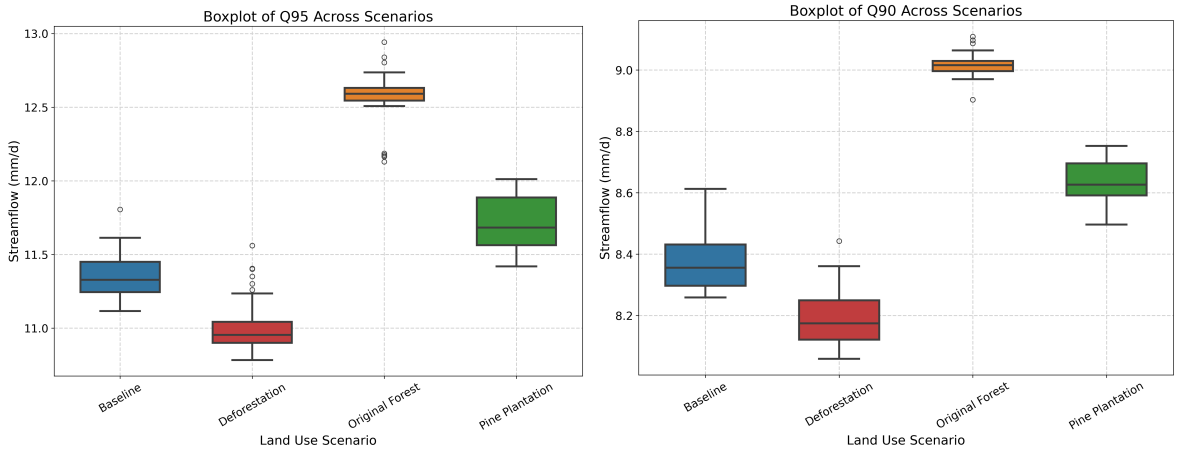

(a) Boxplot 95th percentile of flows

(b) Boxplot 90th percentile of flows

Figure C.7: Boxplots of the Q90 and Q95 quantiles for different land use scenarios, representing high flows. Boxplots are developed with all parameter sets results.

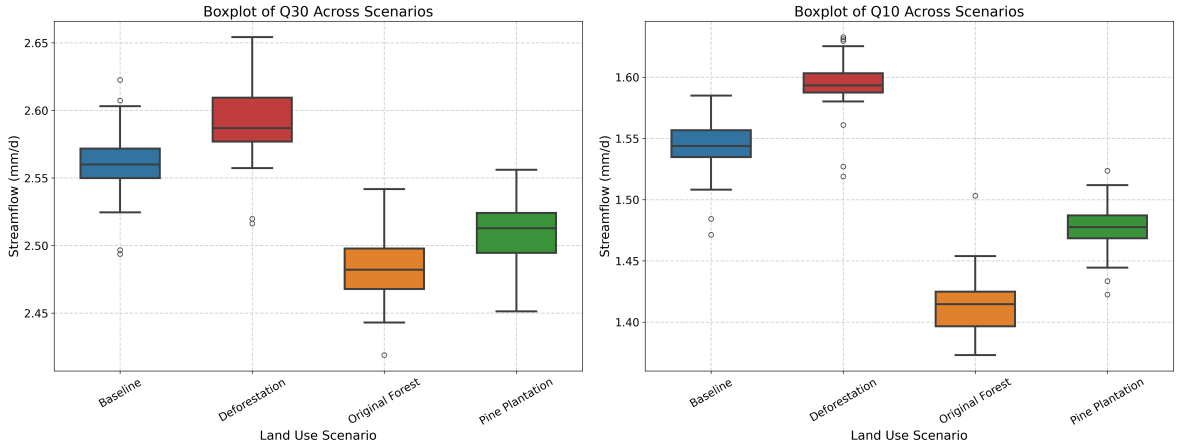

(a) Boxplot 30th percentile of flows

(b) Boxplot 10th percentile of flows

Figure C.8: Boxplots of the Q30 and Q10 quantiles for different land use scenarios, representing low to median flows. Boxplots are developed with all parameter sets results.